CHARACTERIZATION OF HYDRO-TREATED VEGETABLE OIL COMBUSTION BEHAVIOR AND PARTICLE EMISSION

SIPPAKORN RUNGSRITANAPAISAN

A THESIS REPORT SUBMITTED IN PARTIAL FULFILLMENT
OF THE REQUIREMENTS FOR THE DEGREE OF
MASTER OF ENGINEERING IN AUTOMOTIVE ENGINEERING
INTERNATIONAL COLLEGE
KING MONGKUT'S INSTITUTE OF TECHNOLOGY LADKRABANG
ACADEMIC YEAR 2018
KMITL-2018-IC-M-004-005

CHARACTERIZATION OF HYDRO-TREATED VEGETABLE OIL COMBUSTION BEHAVIOR AND PARTICLE EMISSION NANOSTRUCTURE

SIPPAKORN RUNGSRITANAPAISAN

A THESIS REPORT SUBMITTED IN PARTIAL FULFILLMENT
OF THE REQUIREMENTS FOR THE DEGREE OF
MASTER OF ENGINEERING IN AUTOMOTIVE ENGINEERING
INTERNATIONAL COLLEGE
KING MONGKUT'S INSTITUTE OF TECHNOLOGY LADKRABANG
ACADEMIC YEAR 2018
KMITL-2018-IC-M-004-005

THESIS TITLE	Characterization of Hydro-treated Vegetable Oil Combustion Behavior and Particle Emission Nanostructure
STUDENT NAME	Mr. Sippakorn Rungsritanapaisan
STUDENT ID	59610033
DEGREE	Master of Engineering
PROGRAME	Automotive Engineering
ADVISOR	Asst.Prof.Dr.Preechar Karin
CO-ADVISOR	Dr.Nuwong Chollacoop
CO-ADVISOR	Prof.Dr.Hidenori Kosaka

ABSTRACT

This research investigates the effects of Hydrotreated vegetable oil (HVO) and commercial diesel to combustion characteristics under low temperature and various ambient density conditions. Combustion characteristics were investigated by using heat release rate analysis, two color method and soot concentration measurement. The experiments were carried out on a rapid compression expansion machine to simulate the condition of a CI engines as compression stroke at TDC. Various temperature and ambient density at BDC were simulated as different pressure condition in actual engine. And compare with actual small CI engine. Particle emission and nanostructure were investigated by using scanning electron microscope (SEM), transmission electron microscope (TEM) and investigated by image processing.

Soot can be reduced by using Hydrotreated vegetable oil without the need of engine and control modification. HVO is a second-generation biofuel that produce from vegetable oil by using hydrotreating process to remove oxygen from structure. HVO can be a candidate to replace diesel. It can be produced from various many kind of vegetable oil without compromising fuel quality. HVO has a similar viscosity, density and heating value as diesel. The high cetane number of HVO decreases HC emissions and fuel consumption by increasing the advanced heat release rate and

shortening ignition delay. Other advantages of using HVO include advanced combustion phase, shortened combustion duration, and improved thermal efficiency. HVO has almost the same heating value with diesel fuel, while its H/C ratio is higher due to the molecular structure of paraffinic hydrocarbon. However, HVO still has limitations in the CI engine due to its low lubricity and poor low-temperature flow properties.

Keywords: Hydrotreated vegetable oil, Combustion characteristics, Two color method, Particulate matter, Nanostructure

ACKNOWLEDGEMENT

Without the contribution of many people, this thesis would not have been existed. It owes the existence to the supports and inspirations from a lot of people.

Initially, I would like to express, first and foremost, to my advisor Asst. Prof. Dr. Preecha Karin and Prof. Dr. Hidenori Kosaka for their spacious advice, guidance and encouragement throughout my thesis.

I am extremely grateful to thank National Science and Technology Development Agency (NSTDA), THAILAND for the financial and measuring equipment support in my research and Science Technology Engineering and Mathematics (STEM) for scholarship which support my research and daily life.

I would like to sincerely thank to Prof. Dr. Hidenori Kosaka and Assoc. Prof. Dr. Susumu Sato who has given a chance to perform the experiment in their laboratory. I have learned many things under his kind guidance during I spent my special time in Tokyo Institute of Technology.

I wish to express my gratitude to all lecturers for your support and guidance to me for the whole two years. Also, I would like to thank all my senior, junior and friends at KMITL automotive laboratory, Mr. Settavit Sirivarocha, Mr. Phyo Zin Ko Ko, Mr. Ekkawut Saenkhumvong, Mr. Park Watanawongskorn and Mr. Jiramed Boonsakda for their sincere advice and technical support such as the electronic program, equipment some comment and suggestion.

I also wish to express my gratitude to assistance from my senior, junior and friends at Tokyo Institute of Technology Advance Thermo-Fluid Dynamics Laboratory, Mr. Pop-Paul Ewphun, Mr. Jaeok Bae, Mr.Jaehoon Jeong for their sincerely support during my experiment in Tokyo Institute of Technology.

I also wish to thank Bangchak Corporation, PTT Research & Technology Institute for test fuels.

Finally, I must express my very greatest gratitude to my parents and all relatives for providing me with unfailing support and continuous motivation throughout my years of study. This accomplishment would not have been possible without them.

Sippakorn Rungsritanapaisan

TABLE OF CONTENTS

LIST OF TABLES

Table **Page**

LIST OF FIGURES

Figure **Page**

CHAPTER 1

INTRODUCTION

1.1 Research Background

Currently, the world is faced with fossil fuel depletion and numerous environmental problems. Many researchers are trying to develop new, clean energy sources for vehicles such as electricity, fuel cell, etc. Unfortunately, it is difficult to replace conventional vehicles due to cost, energy sources, distance between refueling and vehicle performance. Internal combustion and hybrid engines will likely play a role in powering light-duty vehicles at least until 2050 (Fulton,2013).

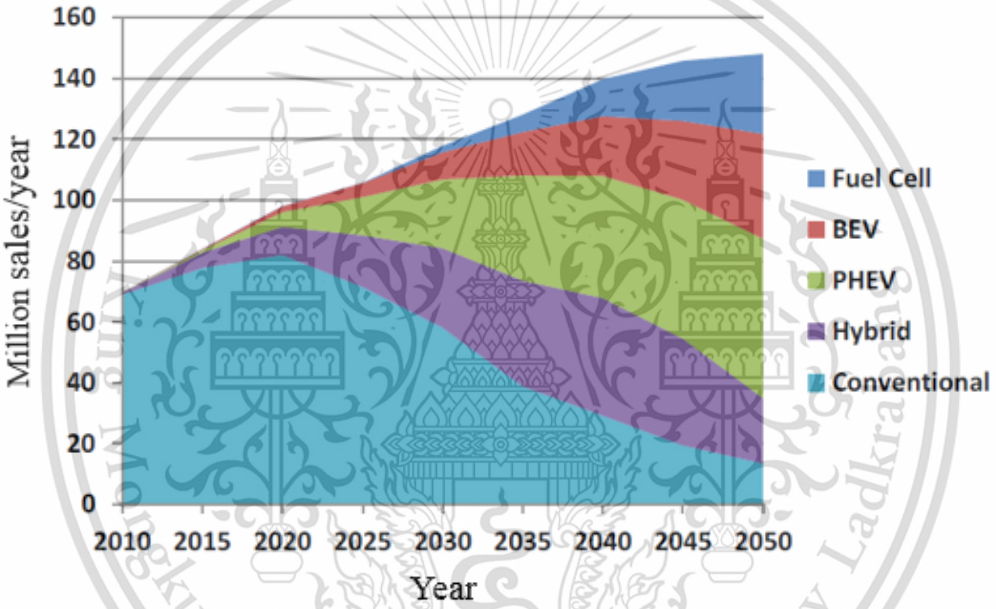

Figure 1.1 Life cycle of technology vehicle, Views to year 2050

Source: Fulton, L., Lah, O. and Cuenot, F. (2013). Transport pathways for light duty vehicles: Towards a 2° scenario. Sustainability 5, 5, 1863−1874.

and the energy from oil is 36 % of global energy using which the biggest factor (Coley,2008). Thus, the finding for using worthy or renewable energy is the way to solve this crisis. One of this is the using of high efficiency engine. Compression ignition (CI) engines provide higher thermal efficiency compared to other internal combustion engines (Kosaka,2015). However, large amounts of soot are produced during combustion. The pollutants should be removed from exhaust gas because of their effects on environment and human health, such as lung cancer.

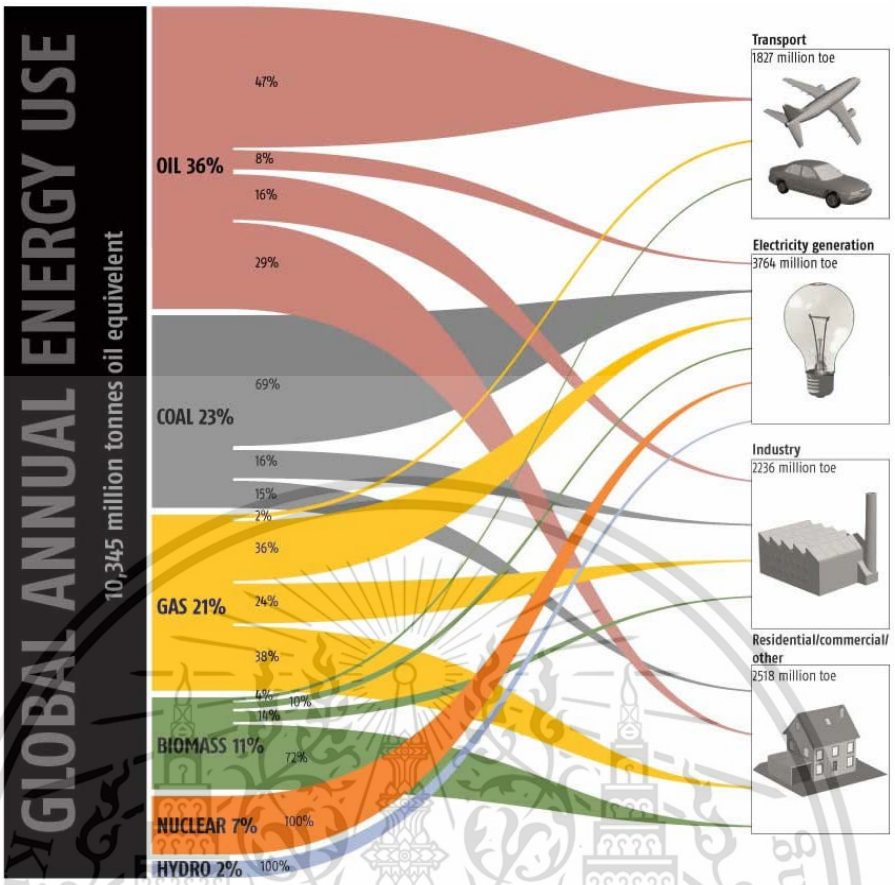

Figure 1.2 World energy use and the sectorial split of fuel use

Source: Coley, D. "Energy and Climate Change Creating a Sustainable Future, John Wiley & Sons, Ltd. 2008.

The biofuel such as biodiesel diesel is the good option to substitute for fossil fuel. Because biofuel can be made from biomass and can re-produce faster than fossil fuel. Therefore, Thailand government promotes the using of biodiesel to Thai people. Due to, biodiesel can be produced in country with the domestic

Biodiesel which is a first generation of biofuel can be produced by transesterification process. Biodiesel have been widely used, as it can be directly used or blending used with diesel in the engines without no modification. However, it still has some disadvantages to the engines such as low heating value (Qi,2010) and high density and viscosity that make larger droplet size distribution, poor fuel-air mixing processes and mixture formation (Gao,2009).

Hydrotreated vegetable oil (HVO) is a second generations biofuel that produce from many kind of vegetable oil and have benefited in emission reduction. Using hydrotreating process its similar physical properties to diesel fuel (Atola,2008).

HVO has a similar viscosity, density and heating value as diesel (Rantanen,2005) using hydrotreating process to remove oxygen from structure. HVO can be a candidate to replace diesel. It can produce from various many kind of vegetable oil without compromising fuel quality, difference form FAME (fatty acid methyl ester) that can produce from limit (Atola,2008). The high cetane number of HVO decreases HC emissions and fuel consumption by increasing the advanced heat release rate and shortening ignition delay (Sugiyama,2011). Other advantages of using HVO include advanced combustion phase, shortened combustion duration, and improved thermal efficiency (Jaroonjitsathian,2008).

1.2 Objectives

1.2.1 Investigation the effects of Hydrotreated vegetable oil and commercial diesel combustion characteristics by using rapid compression expansion machine (RCEM) and small CI engine

1.2.2 Physical characterization on nanostructure of Hydrotreated vegetable oil and commercial diesel particulate matter (PM)

1.3 Scope of work

1.3.1 Fuel properties test

These fuel samples will be tested fuel properties such as density, surface tension, viscosity, cetane number, heating value.

1.3.2 Combustion characteristic experiment

In this experiment was investigated combustion characteristics using pressure volume diagram, heat release rate analysis, ignition delay, two color method, soot concentration measurement under various temperature and ambient density by using RCEM and using small CI engine under various engine rpm and engine load conditions.

1.3.3 Soot morphology and Nano structure experiment

Study of soot formation inside HVO and commercial diesel by using two color method and high speed digital camera photographs. Study nanostructure with scanning electron microscope (SEM), transmission electron microscope (TEM) and image processing program.

CHAPTER 2

LITERATURE REVIEW

2.1 Diesel engine

A conventional internal combustion diesel engine works on “Diesel Cycle”. In the simple diesel engines, an injector injects diesel into the combustion chamber above the piston directly. Diesel engines are also commonly known as Compression-Ignition engines. The ‘Diesel Cycle’ does not use an external mechanism such as a spark-plug to ignite the air-fuel mixture. The principle of diesel cycle can be divided in to 4 stoke.

Diesel engine is internal combustion engine that use the heat of compression to start combustion process. Fuel was injected into the combustion chamber during the final steps of compression stroke. It was developed by Rudolf Diesel in 1897 based on Carnot's cycle, which was invented by Sardis Sardi Carnot. Diesel engine is different from the gasoline engine that used spark plug to ignite. Diesel engine ignite by compressed of air and fuel under high pressure and temperature (Pulkrabek,2014).

2.1.1 Diesel engine operation

Principle of the diesel engine is compress air to a higher temperature then inject fuel. Rapidly compression made pressure and temperature increased without heat loss (Adiabatic compression). The fuel is injecting in to combustion chamber then vaporizes and the mixture ignites by itself. Pressure rise from combustion transfer to piston and connecting rod made crack shaft rotated.

Diesel engine is a compression ignition engine of a two or four stroke type. However, in automotive application, diesel engines are four stroke type. The 4 cycle consists of, intake, compression, power, and exhaust as show in Figure 2.1.

1. Intake stroke: Piston move down from top dead canter (TDC) to bottom dead canter (BDC) during intake valve open and exhaust valve close. The fresh air is drawn in to cylinder.

2. Compression stroke: Piston move up from BDC. In this timing both intake valve and exhaust valve are close. The cylinder pressure and temperature increase corresponding to compression.

3. Power stroke: Piston moves up almost TDC. At the end of the compression stroke fuel is injected into the combustion chamber. In this timing both intake valve

and exhaust valve are close. The cylinder pressure increased from combustion is converted into mechanical energy through the piston to the crankshaft.

4. Exhaust stroke: Piston move up from BDC to TDC during intake valve close and exhaust valve open. The exhaust is push out of cylinder.

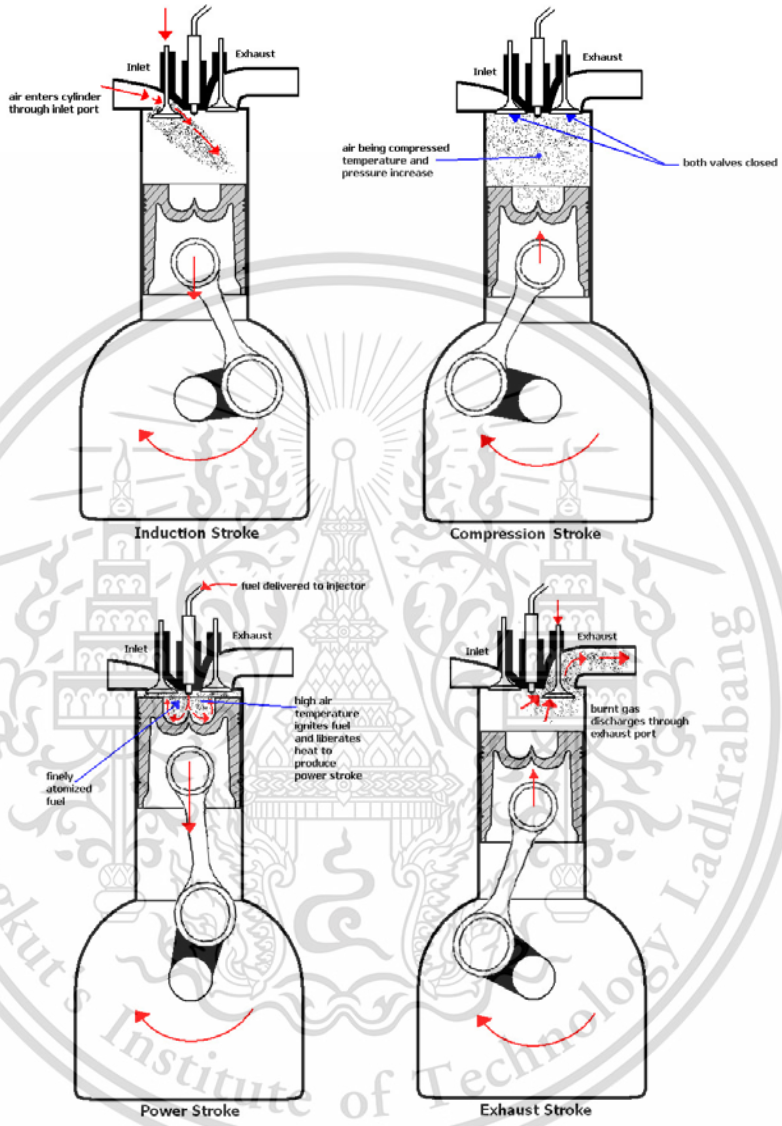

Figure 2.1 Four stroke operating diesel cycle

Source: "https://willycar.com/2014/06/08/perbedaan-direct-dan-indirect-injection/ci-engine-cycle-4-stroke-square/"

2.2 Diesel combustion process

In diesel engine, fuel is injected directly into combustion chamber at TDC. However, the fuel will not immediately combustion. Mixing time of fuel and air mixture is require. Figure 2.2 shows the relationship between heat release rate from start of injection (SOI) to end of combustion.

Ignition delay (a to b) is the period between the start of fuel injection into the combustion chamber and start of combustion. Specifically, the point that heat release rates curves recovers from negative value due to evaporation of fuel into the hot environment.

Premixed combustion (b to c). In this phase combustion of the fuel which already mixed with air during the ignition delay period occurs rapidly in a short time. The burning mixture is added to fuel that ready for burning and burns during this phase, the high heat release rate characteristic of this phase result.

Mixing controlled combustion (c to d). When fuel and air that mixed during the ignition delay have been consumed, the heat release rate is controlled by the rate at which mixture becomes available for burning. While several processes are involved liquid fuel atomization, vaporization, mixture formation, chemical reaction the rate of burning is controlled in this phase primarily by the mixture of fuel and air. The heat release rate may or may not reach a second peak in this phase; it decreases as this phase progresses.

Late combustion (d to e). Heat release continues at lower rate. There are several reasons for this phenomenon. A small fraction of the fuel may not yet have burned. A fraction of the fuel energy present in soot and fuel rich combustion product. The cylinder charge mixing in this period promotes more complete combustion and less dissociated gases. The kinetics of the final burnout process become slower as the temperature of the cylinder gases fall.

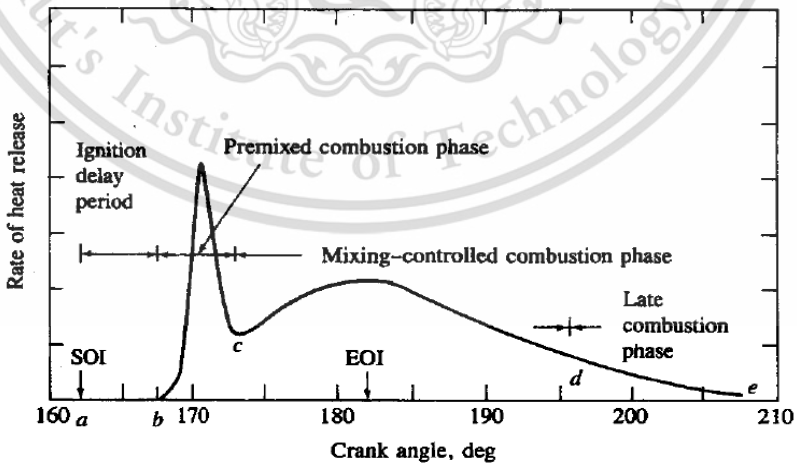

Figure 2.2 Stage of heat release rate

Source: Heywood, J. B. (1988). Internal Combustion Engine Fundamentals. 2nd edition. McGraw-Hill. New York, USA.

2.3 Emission of diesel engine

Diesel engines convert the chemical energy contained in the fuel into mechanical power. Diesel fuel is injected under pressure into the engine cylinder where it mixes with air and where the combustion occurs. The exhaust gases which are discharged from the engine contain several constituents that are harmful to human health and to the environment. By the emission of diesel engine consist of CO, HC, NOx, SO2 and particulate matter as shown on equation 2.1 and Figure 2.3 shown the combustion phenomena in combustion chamber.

$$C_xH_y + AIR \rightarrow aCO_2 + bH_2O + cCO + dC_{(s)} + mHC_{(l)} + nNO_x \quad (2.1)$$

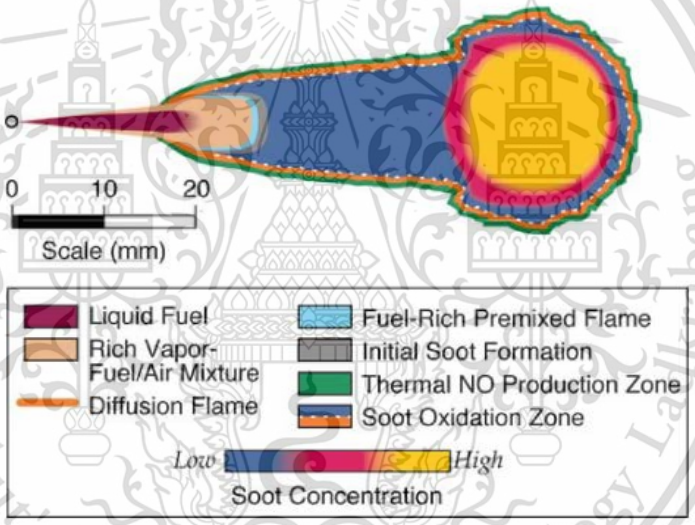

Figure 2.3 Diesel combustion flame zone

Source: Dec, J. (1997). A conceptual model of DI diesel combustion based on laser-sheet imaging. SAE Paper No. 970873.

Carbon monoxide (CO), hydrocarbons (HC), and aldehydes are generated in the exhaust as the result of incomplete combustion of fuel. A significant portion of exhaust hydrocarbons is also derived from the engine lube oil. When engines operate in enclosed spaces, such as underground mines, buildings under construction, tunnels or warehouses, carbon monoxide can accumulate in the ambient atmosphere and cause headaches, dizziness and lethargy. Under the same conditions, hydrocarbons and aldehydes cause eye irritation and choking sensations. Hydrocarbons and

aldehydes are major contributors to the characteristic diesel smell. Hydrocarbons also have a negative environmental effect, being an important component of smog.

Nitrogen oxides (NO_x) are generated from nitrogen and oxygen under the high pressure and temperature conditions in the engine cylinder. NO_x consists mostly of nitric oxide (NO) and a small fraction of nitrogen dioxide (NO_2). Nitrogen dioxide is very toxic. NO_x emissions are also a serious environmental concern because of their role in the smog formation.

Sulfur dioxide (SO_2) is generated from the sulfur present in diesel fuel. The concentration of SO_2 in the exhaust gas depends on the sulfur content of the fuel. Low sulfur fuels of less than 0.05% sulfur are being introduced for most diesel engine applications. Sulfur dioxide is a colorless toxic gas with a characteristic, irritating odor. Oxidation of sulfur dioxide produces sulfur trioxide which is the precursor of sulfuric acid which, in turn, is responsible for the sulfate particulate matter emissions. Sulfur oxides have a profound impact on environment being the major cause of acid rains.

Particulate matter (PM) is a complex aggregate of solid and liquid material. Its origin is carbonaceous particles generated in the engine cylinder during combustion. The primary carbon particles form larger agglomerates and combine with several other, both organic and inorganic, components of diesel exhaust.

2.4 Particulate matter

Particulate matter is the most characteristic of diesel emissions which responsible for the black smoke traditionally associated with diesel powered vehicles. The diesel particulate matter emission is usually abbreviated as PM or DPM. Particulate matter was divided into three characteristic ranges of size: nucleation mode, accumulation mode and coarse mode. The nucleation-mode particles are more arcane: most are probably formed from nucleated volatiles, Accumulation mode particles are constructed from a solid core of carbonaceous building blocks called ‘spherules’, together forming ‘agglomerates’ within the range of 60–100 nm. Spherules are fairly uniform in size, i.e. mostly 20–50 nm. The coarse-mode particles are solid and are formed from the other two modes through a process of storage and release in the exhaust system, or through material disintegration. Composition-wise, there are five distinct ‘fractions’: ash, carbonaceous, organic, sulphate and nitrate as

shown Figure 2.4. The diesel particulate matter has a complicated physical and chemical structure.

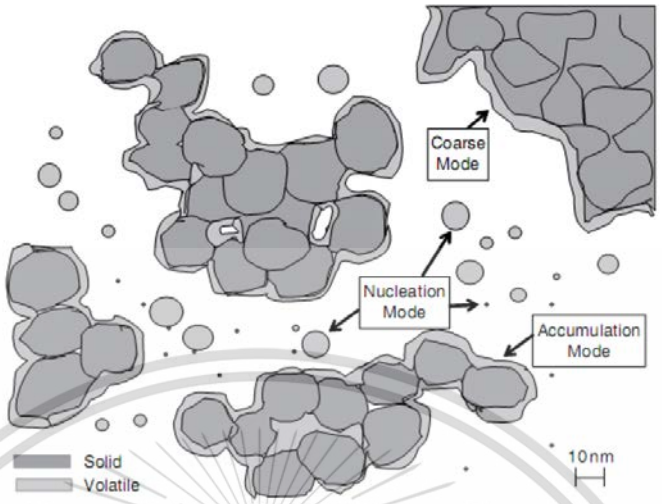

Figure 2.4 Depicted schematically of particulate matter: coarse mode (largest, shown in part), nucleation mode (smallest); accumulation mode (middling)

Source: Majewski, W.A., (2001). Diesel Particulate Filters. www.DieselNet.com. Copyright © Ecopoint Inc. Revision 2001.07b.

Two main elements of diesel particulate matter are Solid Organic Fraction (SOL), consisting of carbon and metallic ash, and the Soluble Organic Fraction (SOF), consisting of hydrocarbon. Figure 2.5 is also illustrated the definition of size of atmosphere particles: PM10, D (diameter) < 10 μm; fine particles, D < 2.5 μm; ultrafine particles, D < 0.10 μm; and nano - particles, D < 0.05 μm or 50 nm.

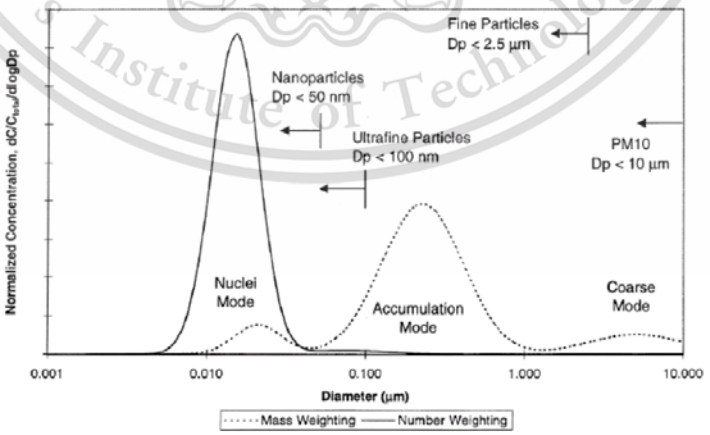

Figure 2.5 Particle size distribution of soot from a diesel engine

Source: Kittelson, D.B. (1998). Engines and nanoparticles: a review. Journal of Aerosal Science. 29: p. 575-588.

2.5 Hydrotreated vegetable oil

Hydrotreated vegetable oil (HVO) can be produced from many kinds of vegetable oils and fats. This includes triglycerides and fatty acids from vegetable oils, (e.g. rapeseed, soybean and corn oil), tall oil, (a co-product from the pulp and paper industry) in addition to the use of animal fats. HVO is produced through the hydrotreating of oils, in which the oils (triglycerides) are reacted with hydrogen under high pressure in order to remove oxygen. The hydrocarbon chains produced are chemically equivalent to petroleum diesel fuel. Propane is typically produced as a by-product. Investment costs are much higher for HVO than biodiesel production, which requires large scale production plants to allow the production to be economic. Production may be carried out in stand-alone plants producing only HVO or in integrated plants together with fossil fuels. HVO is the second generation biofuel the triglyceride is hydrogenated in the first step and broken down into various intermediates, mainly monoglycerides, diglycerides, and carbonxylic acids. These intermediates are then converted into alkanes by different pathways: decarboxylation, decarbonylation (both removing a carbon atom from the initial intermediate), and hydrodeoxygenation (with no carbon removal) at the temperatures at temperature above 300–360 ^{o}C and pressure at least 3 MPa. Propane, water, carbon monoxide and carbon dioxide are produced as side-products. HVO is a mixture of normal paraffin and iso-paraffin with shorter chain-length. However, there are some disadvantages that may limit to use HVO from previous study such as poor low-temperature properties, as displayed by cloud point, pour point and cold filter plugging point (CFPP) (No,2014). Therefore, an improvement process as isomerization process is can be used to solve that problem then HVO would be iso-HVO.

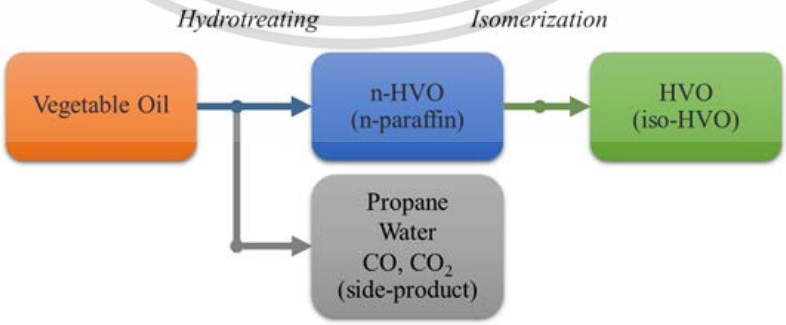

Figure 2.6 HVO production process

Source: No, S. (2014). Application of hydrotreated vegetable oil from triglyceride-based biomass to CI engines – A review. Fuel, 115, 88−96.

HVO can be a candidate to replace diesel. It can produce from various many kind of vegetable oil without compromising fuel quality, difference form FAME (fatty acid methyl ester) that can produce from limit feedstocks as show in Table 2.1 (Atola,2008).

Large scale production	Process	Product	Feedstocks: Volume availability and price	Product quality	Production plant investments
≈ 1995 …	Esterification	Biodiesel Ester FAME	-	-	+
2007 …	Hydrotreating	Renewable diesel C_nH_{2n+2} HVO	+	+ + +	-
≈ 2015 …	Gasification + Fischer-Tropsch	Renewable diesel C_nH_{2n+2} FT-BTL	+ + +	+ + +	- - -

C_nH_{2n+2} is a general formula for paraffinic hydrocarbons. + sign indicates benefit, - sign indicates disadvantage

Table 2.1 Comparison between FAME and HVO production

Source: Dec, J. (1997). A conceptual model of DI diesel combustion based on laser-sheet imaging. SAE Paper No. 970873.

HVO has a similar viscosity, density and heating value as diesel as show in Table 2.2

FUEL PROPERTIES *)	NExBTL biodiesel	GTL diesel	FAME (RME)	EN590 /2005
Density @15°C [kg/m3]	775...785	770....785	≈ 885	≈ 835
Viscosity @40°C [mm2/s]	2.9...3.5	3.2...4.5	≈ 4.5	≈ 3.5
Cetane number	84...99 **)	73...81	≈ 51	≈ 53
Distillation 10 vol% [°C]	260...270	≈ 260	≈ 340	≈ 200
Distillation 90 vol% [°C]	295...300	325...330	≈ 355	≈ 350
Cloud point [°C]	- 5...- 30	0...- 25	≈ - 5	≈ - 5
Lower heating value [MJ/kg]	≈ 44	≈ 43	≈ 38	≈ 43
Lower heating value [MJ/litres]	≈ 34	≈ 34	≈ 34	≈ 36
Polyaromatics [wt%]	0	0	0	≈ 4
Oxygen [wt%]	0	0	≈ 11	0
Sulfur [mg/kg]	≈ 0	< 10	< 10	< 10

Table 2.2 HVO (NEx BTL) properties in comparison with different fuel

Source: Rantanen, L., Linnaila, R., Aakko, P. and Harju, T. (2005). Hydrotreated NExBTL-Biodiesel fuel of the second generation. SAE Paper No. 2005-01-3771.

2.6 Technical analysis

2.6.1 Scanning electron microscope

The scanning electron microscope (SEM) uses a focused beam of high-energy electrons to generate a variety of signals at the surface of solid specimens. The signals that derive from electron-sample interactions reveal information about the sample including external morphology (texture), chemical composition, and crystalline structure and orientation of materials making up the sample. In most applications, data are collected over a selected area of the surface of the sample, and a 2-dimensional image is generated that displays spatial variations in these properties. Areas ranging from approximately 1 cm to 5 microns in width can be imaged in a scanning mode using conventional SEM techniques (magnification ranging from 20X to approximately 30,000X, spatial resolution of 50 to 100 nm). The main SEM components include: Source of electrons, Column down which electrons travel with electromagnetic lenses, Electron detector, Sample chamber and Computer and display to view the images as shown in Figure 2.7. Electrons are produced at the top of the column, accelerated down and passed through a combination of lenses and apertures to produce a focused beam of electrons which hits the surface of the sample. The sample is mounted on a stage in the chamber area and, unless the microscope is designed to operate at low vacuums, both the column and the chamber are evacuated by a combination of pumps. The level of the vacuum will depend on the design of the microscope. The position of the electron beam on the sample is controlled by scan coils situated above the objective lens. These coils allow the beam to be scanned over the surface of the sample. This beam scanning, as the name of the microscope suggests, enables information about a defined area on the sample to be collected. As a result of the electron-sample interaction, a number of signals are produced. These signals are then detected by appropriate detectors.

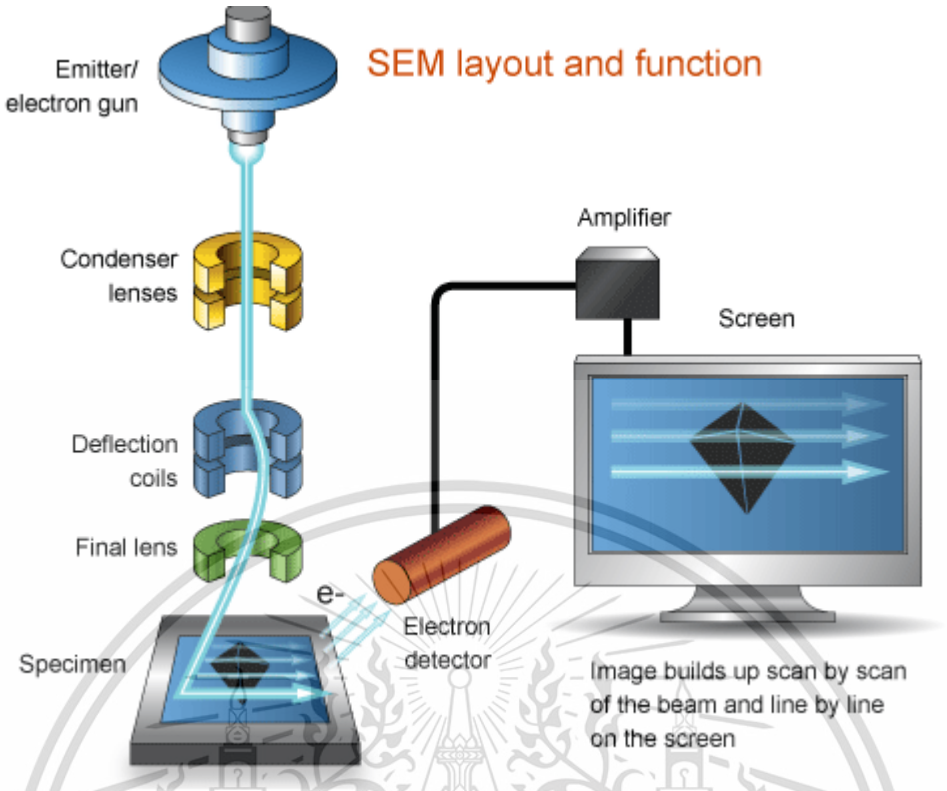

Figure 2.7 Schematics of scanning electron microscopy operation

Source: http://li155-94.members.linode.com/myscope/sem/practice/principles/layout.php

2.6.2 Transmission electron microscope

The transmission electron microscope (TEM) is a very powerful tool for material science. A Figure 2.8 shown schematic of transmission electron microscopy operation by a high energy beam of electrons is shone through a very thin sample, and the interactions between the electrons and the atoms can be used to observe features such as the crystal structure and features in the structure like dislocations and grain boundaries. Chemical analysis can also be performed. TEM can be used to study the growth of layers, their composition and defects in semiconductors. High resolution can be used to analyze the quality, shape, size and density of quantum wells, wires and dots. The TEM operates on the same basic principles as the light microscope but uses electrons instead of light. Because the wavelength of electrons is much smaller than that of light, the optimal resolution attainable for TEM images is many orders of magnitude better than that from a light microscope. Thus, TEMs can reveal the finest details of internal structure - in some cases as small as individual atoms.

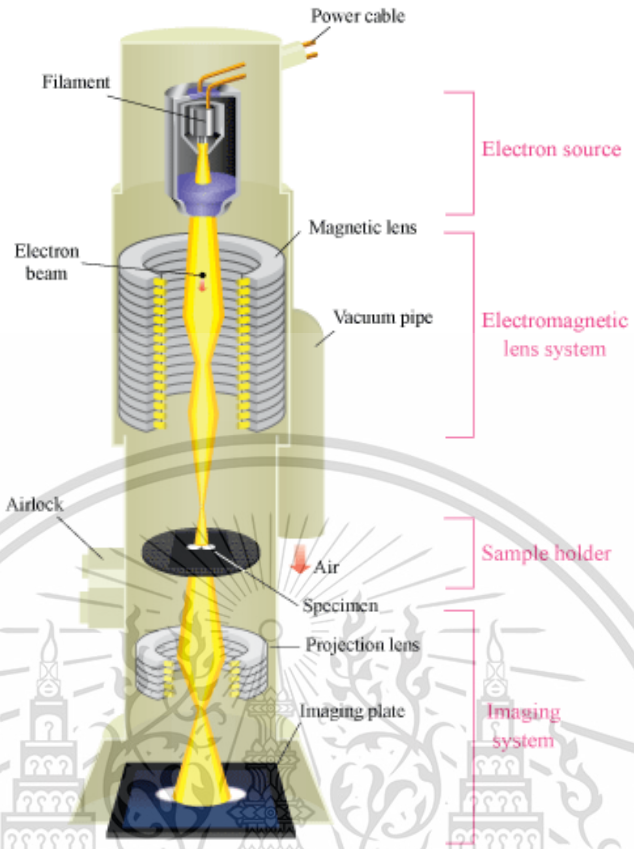

Figure 2.8 Schematics of transmission electron microscopy operation

Source: http://www.hk-phy.org/atomic_world/tem/tem02_e.html

In the TEM, when a beam of electrons of high energy strikes a thin sample then most of the electrons pass through it. These are called transmitted electrons and include both undeflected and deflected electrons. The beam of electrons which passes through the sample without any deflection from its original direction is focused at the back focal plane (BFP) of the objective lens parallel to the optical axis and is called direct beam as shown in Figure 2.9 (Akhtar,2012). The other electrons which are scattered at certain angles are focused off-axis at the BFP of the lens and they are called diffracted beams.

In order to form images in the TEM from transmitted electrons, either the central bright spot, or some or all of the scattered electrons can be used. Electrons scattered at a specific angle can thus be selected by inserting an aperture into the BFP of the objective lens. This aperture is called the objective aperture. If the direct beam is selected, the resultant image is called bright-field (BF) image, and if scattered

electrons are selected then the micrograph is called dark-field (DF) image. Typical magnification ranges of these modes are 25,000x-100,000x.

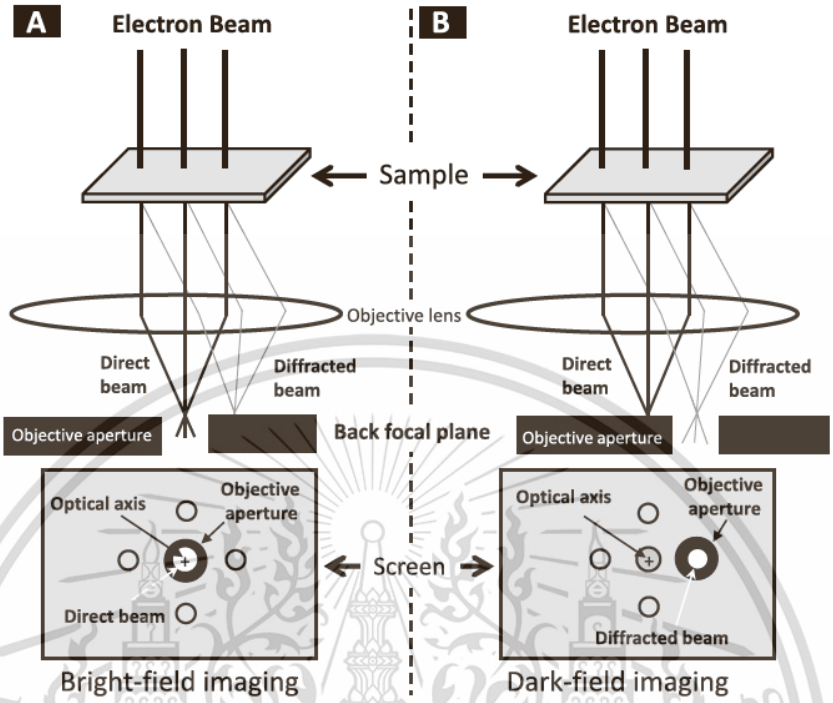

Figure 2.9 Schematics of how the direct and diffracted beams can be selected to form an image on TEM

Source: Akhtar, S. (2012). Transmission Electron Microscopy of Graphene and Hydrated Biomaterial Nanostructures. Uppsala. Acta Universitatis Upsaliensis.

2.7 Research gap

From alternative biofuel HVO might be beneficial to reduce exhaust emissions, particulate matters and improve thermal efficiency from CI engine.

To date, no study performed on the effect of HVO as an alternative biofuel on small CI engine and combustion characteristic under low temperature and high ambient density.

CHAPTER 3

RESEARCH METHODOLOGY

3.1 Experimental apparatus

3.1.1 Diesel engine specification

The small diesel engine was used for produce particulate matter in condition of diesel and HVO fuel is “KUBOTA RT140 DI plus ES” which picture and specification shown in Figure 3.1 and Table 3.1 respectively. This engine was used for combustion characteristic experiment. The engine was operated and controlled on eddy current dynamometer. This engine was fitted with pressure sensor on a cylinder head to measure the pressure in the combustion chamber.

Figure 3.1 Diesel Engine Picture for Combustion Characteristic Experiment

Source: http://www.siamkubota.co.th/en/product/diesel-engine/250-RT-Di-Plus-Powerfully-responsive-Durable-Tough-Fuel-saving

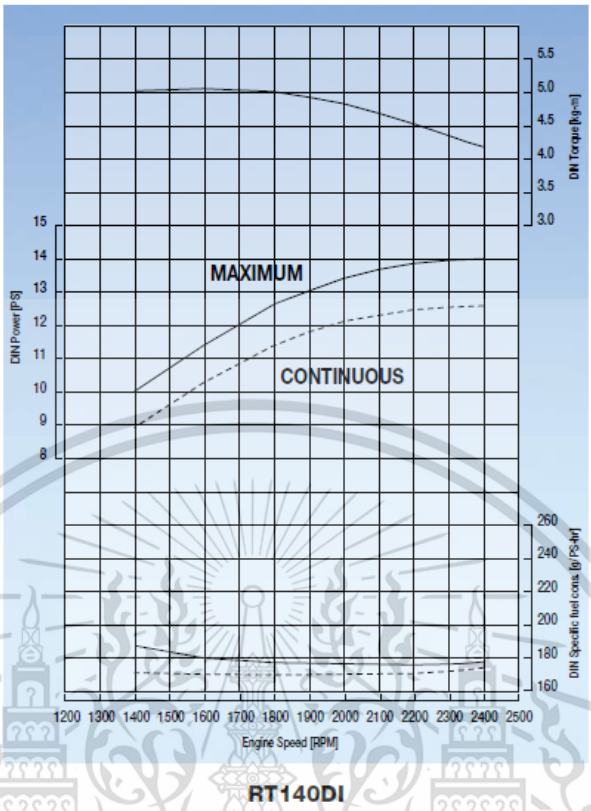

Model	KUBOTA RT140 DI Plus ES
Type	diesel, 4 stroke, 1 cylinder, water cooled
Injection type	direct injection
Bore x stroke	97x96
Displacement	709cc
Maximum power	14hp/2400rpm
Maximum torque	5kg-m/1600rpm
Continuous power	12.5hp/2400rpm
Compression ratio	18:01

Table 3.1 Diesel Engine Specification for Combustion Characteristic Experiment

Source: http://www.siamkubota.co.th/en/product/diesel-engine/250-RT-Di-Plus-Powerfully-responsive-Durable-Tough-Fuel-savin

3.1.2 Eddy current engine dynamometer

The engine dynamometer, Tokyo Plant model ED-60-LC, was used in the experiment for applying a load on the tested engine and also measuring force, moment of force (torque) and power that the tested engine can produce against the load. The type of the engine dynamometer is Eddy current with external water cooling systems. Eddy current dynamometer can provide a quick load change rate for rapid load setting. Eddy current dynamometer consists of an electrically conductive core moving across a magnetic field to produce resistance to brake the movement. The magnetic field is generated by using variable electromagnets that can change the magnetic field strength to control the amount of braking. The electromagnet voltage is control by a desktop computer, using changes in the magnetic field to match the power output.

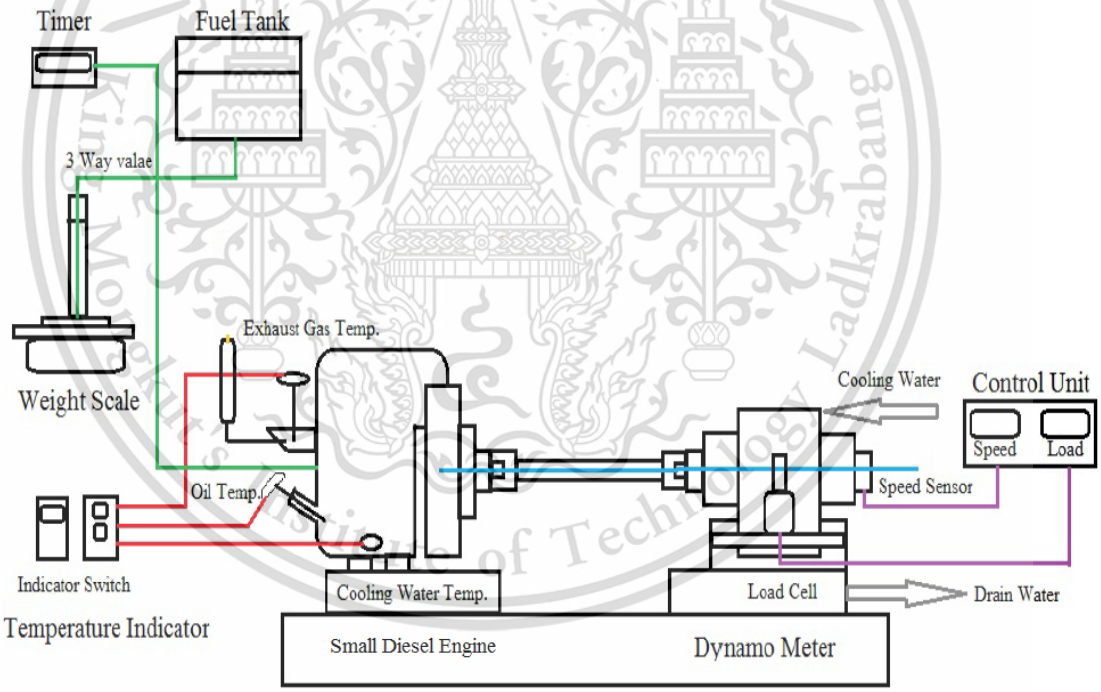

Figure 3.2 Schematic diagram of engine dynamometer

3.1.3 Black smoke meter

Particulate matter emitted from engine combustion is measured in black smoke percentage. The smoke meter is applied to measure the concentration between particulate matter in exhaust gas before the filter and remaining after trapping in

particulate filter by light emitting method. The zero-percentage black smoke mean that is no particulate on filter and the other hand 100 percentage is mean the filter is covered by particulate all of area. This smoke meter percentage can be summarized that the filtration efficiency of particulate filter. However, the smoke meter, Okuda DSM - 240, is shown in Figure 3.3 which is used in investigation of particulate matter concentration and particulate filter efficiency.

Figure 3.3 Smoke meter and filter paper

3.1.4 Pressure sensor

To measure the pressure in the combustion, chamber this research choose “Kistler 6052C31” which can measure up to 250 bars mounted on the cylinder head. This sensor is piezoelectric crystal which achieves high sensitivity.

Figure 3.4 Pressure sensor

3.1.5 Crank encoder

Tracing the position of crank angle by using an optical crankshaft encoder is cost-efficient and convenient, as long as the signal is well calibrated. Nowadays, this type of shaft encoder usually generates at least two different signals: one is position identifying normally with a frequency of one pulse per revolution; the other one is the crank-angle marking signal.

To measure crankshaft position for calculate combustion chamber volume, "CA-RIE-360" encoder was chosen and mounted on the end of brake shaft for serviceability. 360 pulses per revolution so the resolution is 1 degree. The function is based on transmission light principle. An infrared beam is emitted and received at the sensor unit. The customized marker disk (with slits) is mounted in-between the sensors gate. The slits will interrupt the infrared beam, the receiver transforms the light to voltage signal.

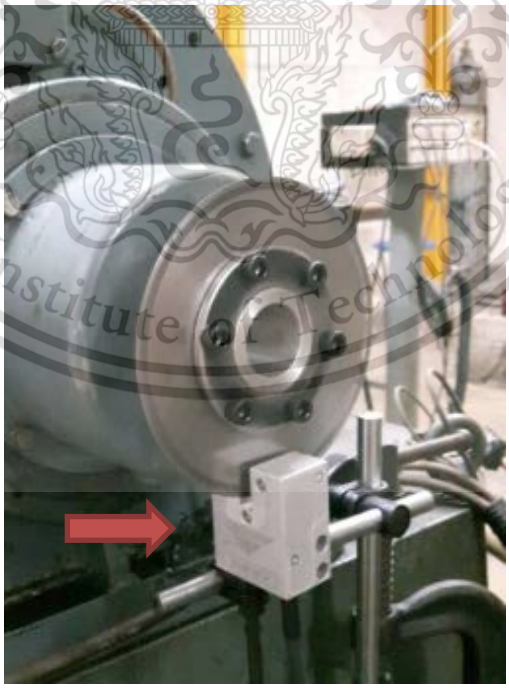

Figure 3.5 Crank encoder

3.1.6 Data acquisition system

For understanding the combustion inside an engine cylinder, many researchers work on either experimental tests or computer model simulations. Because of booming computing technology and growing hardware ability, mathematic simulations methods have become increasingly popular and economic. However, an experimental result is the fundamental validation measure for complex mathematic models, hence it is necessary and needs to be accurate and reliable, moreover, easy and efficient.

The pressure in combustion chamber and crank angle position data was kept by data acquisition system. The hardware which used in the experiment were SIRIUSi Custom with CHG and CHG+ as shown in Figure 3.7. And the software was DEWESoft X2 SP8 as shown in Figure 3.8 which can calculate many parameter in real time such as combustion chamber volume in that moment, heat release rate, IMEP, PMEP, and etc.

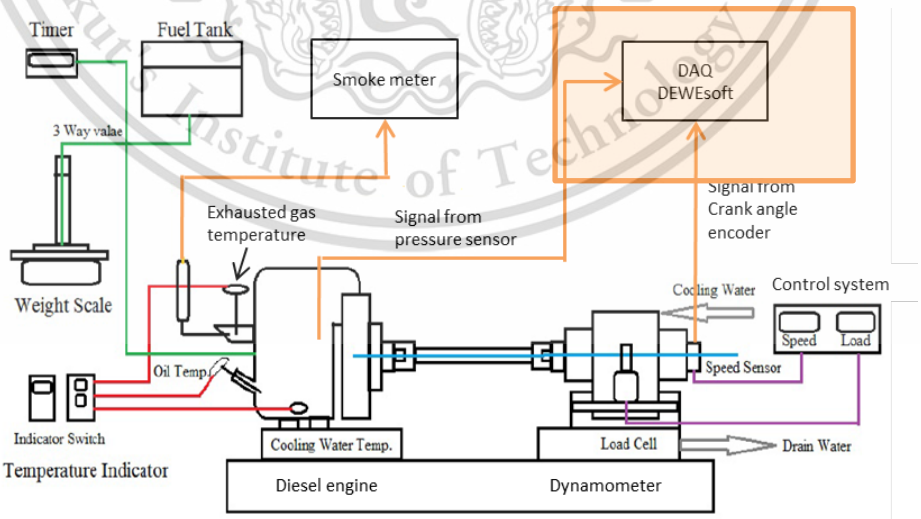

Figure 3.6 Schematic diagram of data acquisition unit connected to Pressure and Crank angle encoder

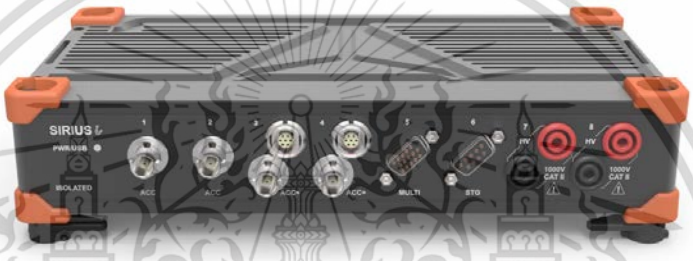

Figure 3.7 Data acquisition hardware

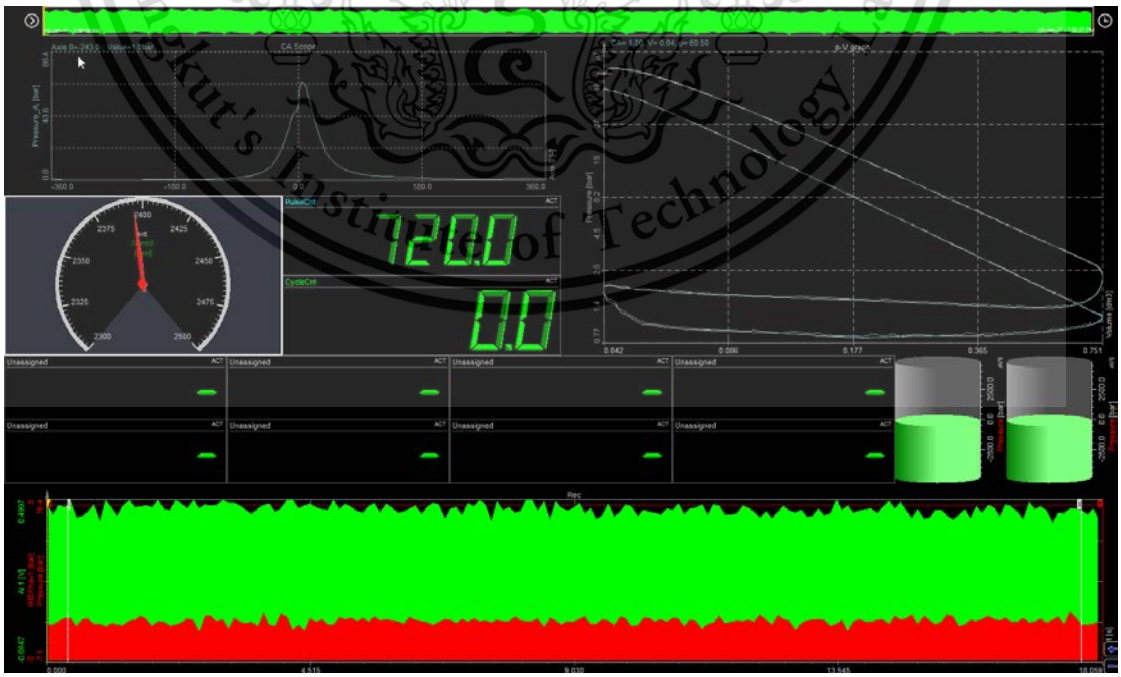

Figure 3.8 DEWESoft X2 software

3.1.7 Rapid compression expansion machine (RCEM)

Rapid compression expansion machine (RCEM) (Kobori,1995) shown in Figure 3.9. The RCEM combustion chamber has 86.0 mm bore with a 151.5 mm diameter. Ambient pressure was arrived at by mixing O_2 and N_2 in a mixing tank at 453K, then filling synthetic gas into the combustion chamber until the setting pressure. It was then compressed by piston from BDC to TDC within 30 ms and kept at TDC for 150 ms to provide a constant volume condition. A single hole 0.2 mm diameter exit orifice was equipped with solenoid injector to injected test fuel with 100 MPa into the combustion chamber. A static pressure transducer was installed to measure ambient pressure at BDC. Pressure increase from combustion was measured by a piezoelectric dynamic pressure transducer (AVL GU22CK) and amplified by charge amplifier (Kistler 5011B). The pressure increase from the injected fuel was recorded by oscilloscope (YOKOGAWA DL750) with a sampling rate of $1x10^6$ sampling/sec. The flame image was captured by high speed camera (NAC GX-1) with lens (Nikkor 55 mm f/2.8) at 10,000 frames per second (fps) and 464x464 pixels. Soot concentration was measured by passing through exhaust gas from combustion to filter paper in order to collect soot emissions. It was then measured by smoke meter (SOKKEN GSM-3).

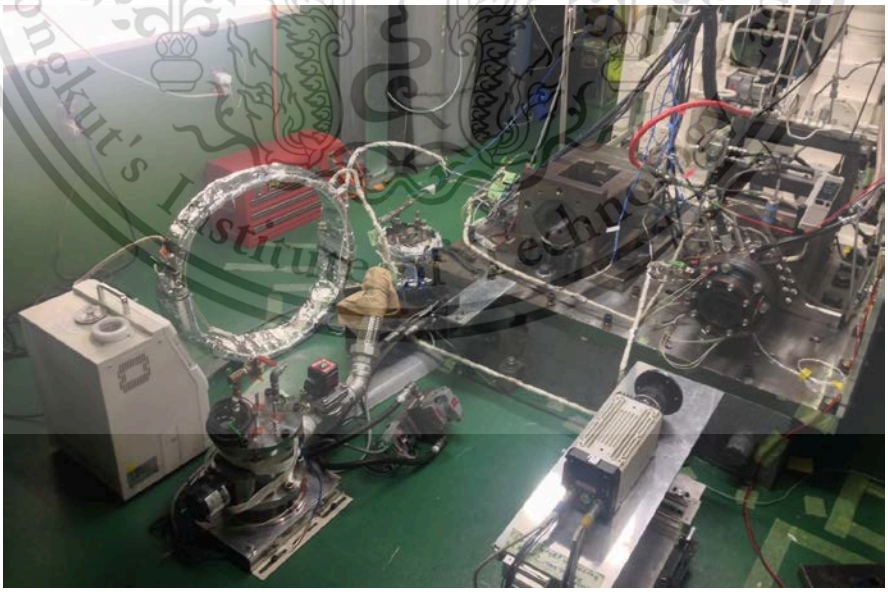

Figure 3.9 Combustion characteristic experimental equipment

3.2 Experiment condition

Table 3.2 shows test conditions in RCEM. The experiment was conducted using two different fuels- commercial diesel and HVO. Other conditions were a nozzle exit orifice diameter of 0.2 mm. solenoid injector 2.0 ms energizing time, to reduce the effect of transient opening and closing. 100 MPa injection pressure, to avoid cavitation and vary ambient density were used to simulate the effect of supercharge under naturally aspirated conditions. For ambient temperature of 650, 700 and 750 kelvin the effect was investigated of low temperature concentrations at ambient pressure under a constant equivalent ratio. All tests were repeated 5 times for each test condition.

Parameter	Conditions
Test fuel	Diesel, HVO
Nozzle orifice diameter	Single hole 0.2mm
Energizing time	2.0 ms
Injection pressure	100 MPa
Ambient gas temperature	650, 700 and 750 K
Oxygen concentration	21%
Ambient Density	16, 24 and 32 kg/m^3
Repeat	5 Times / Condition

Table 3.2 Test conditions of Rapid compression expansion machine

Table 3.3 shows test conditions in small CI engine. The experiment was conducted using two different fuels- commercial diesel and HVO. Other conditions were engine load using 20, 50, 80 and 100 %. Engine speed 1600, 2000 and 2400 rpm. All tests were repeated 5 times for each test condition.

Parameter	Conditions
Test fuel	Diesel, HVO
Engine load	20, 50, 80 and 100 %
Engine speed	1600, 2000 and 2400 rpm
Repeat	5 Times / Condition

Table 3.3 Test conditions of Small CI engine

3.3 Experiment procedure

3.3.1 Small CI engine combustion analysis

The raw data from data acquisition start from pressure at each crank angle. It's collect 720 engine cycles for each engine condition and then calculate to find the average pressure of each crank angle.

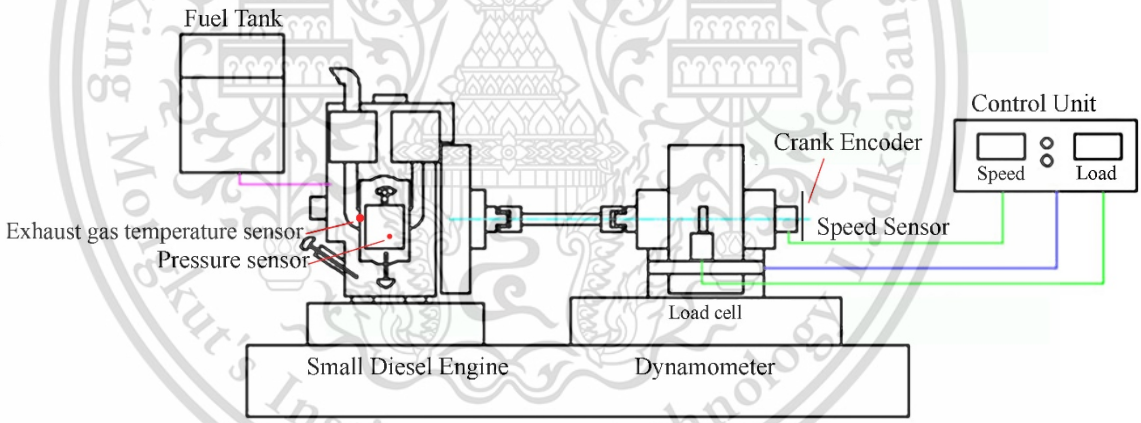

Figure 3.10 Schematic diagram of tested small CI engine operation on dynamometer for combustion characteristic

3.3.2 RCEM combustion analysis

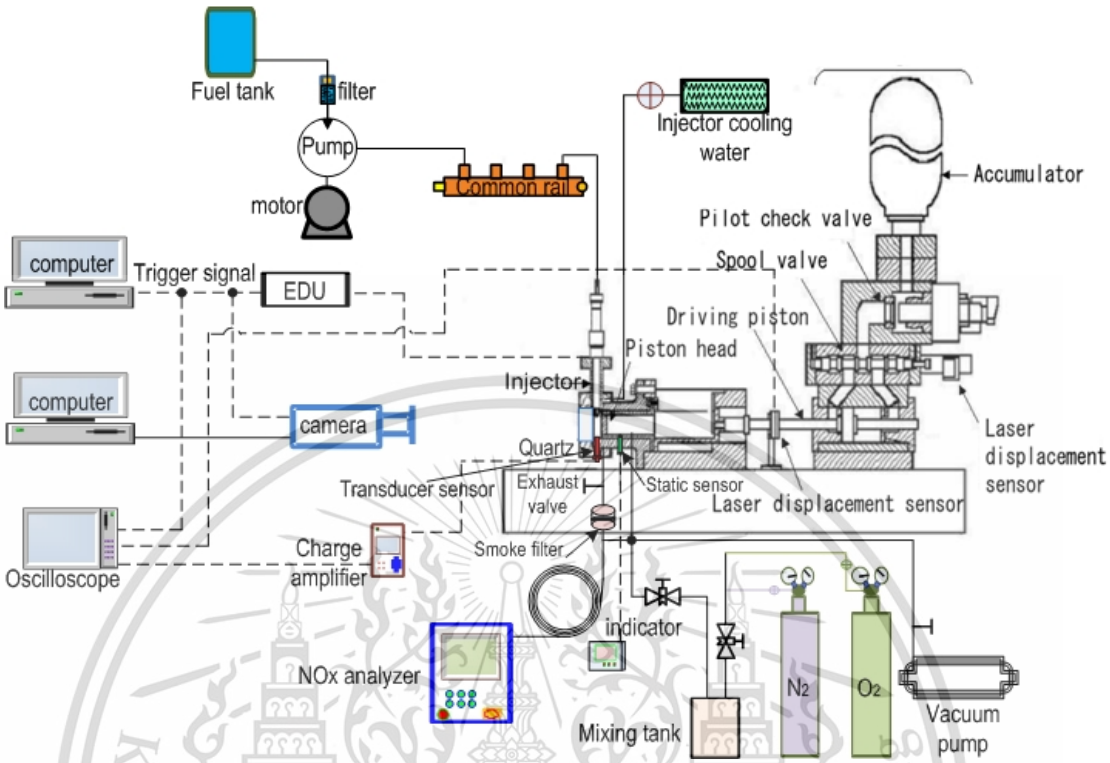

Figure 3.11 Schematic diagram of tested rapid compression expansion machine for combustion characteristic

3.3.3 Particulate matter quantities

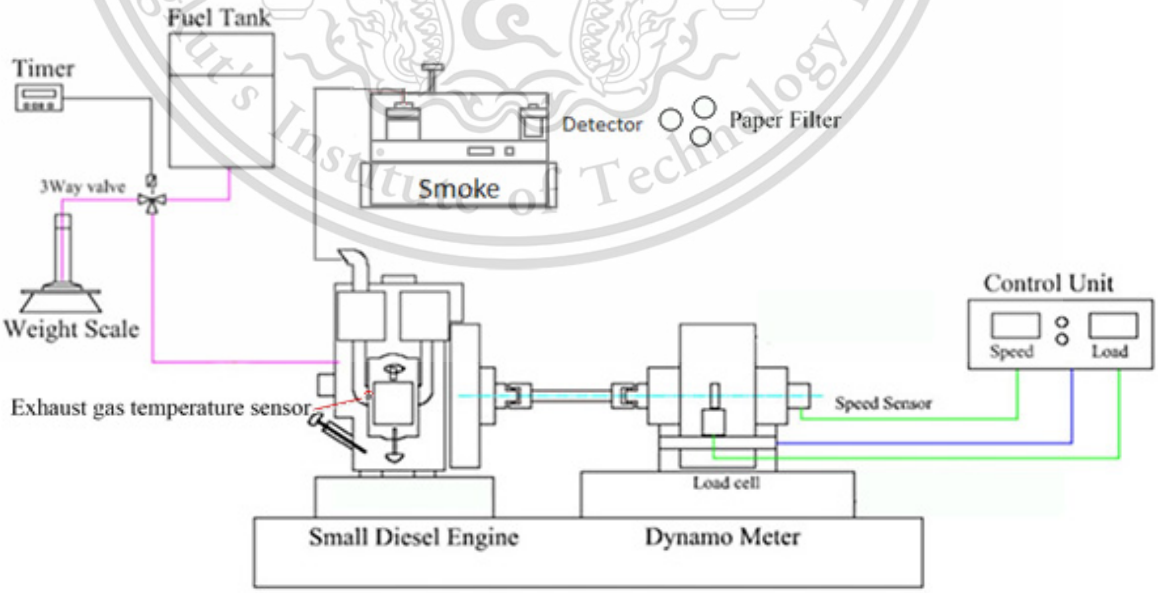

Figure 3.12 Schematic diagram of particulate matter quantity measurement

3.3.4 Particulate matter size distribution

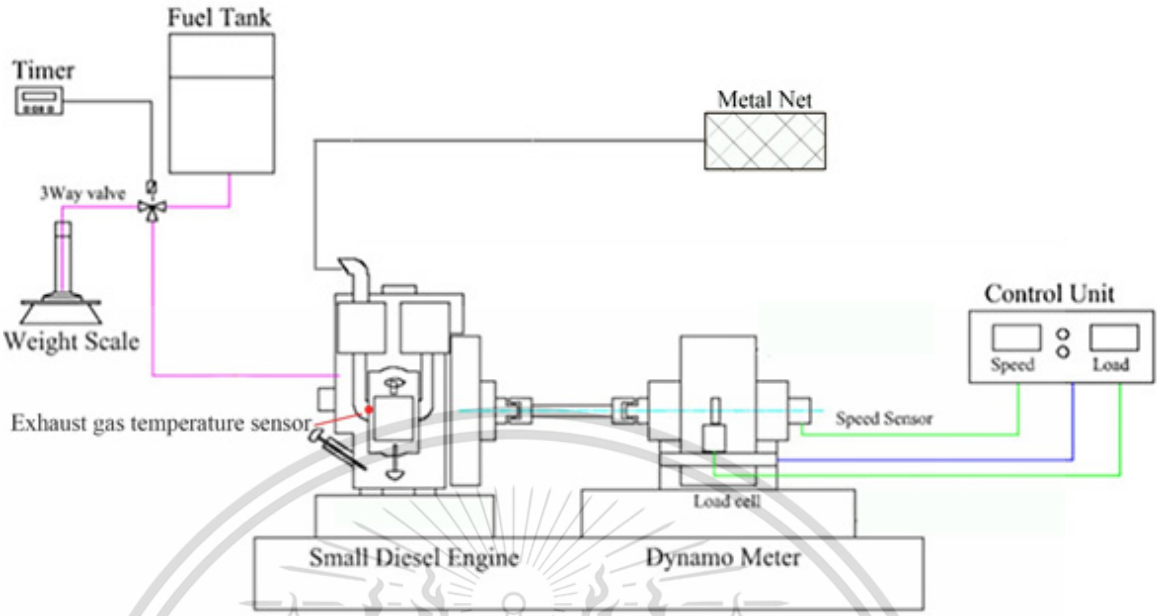

Figure 3.13 Schematic diagram of particulate matter trapping

3.4 Methods of combustion experiment

Ignition delay is defined as the interval between the start of injection (SOI) and the start of combustion (SOC). Specifically, the point that heat release rate curves recovers from negative value due to evaporation of fuel into the hot environment (Heywood,1988) as show in Fig. 3.14.

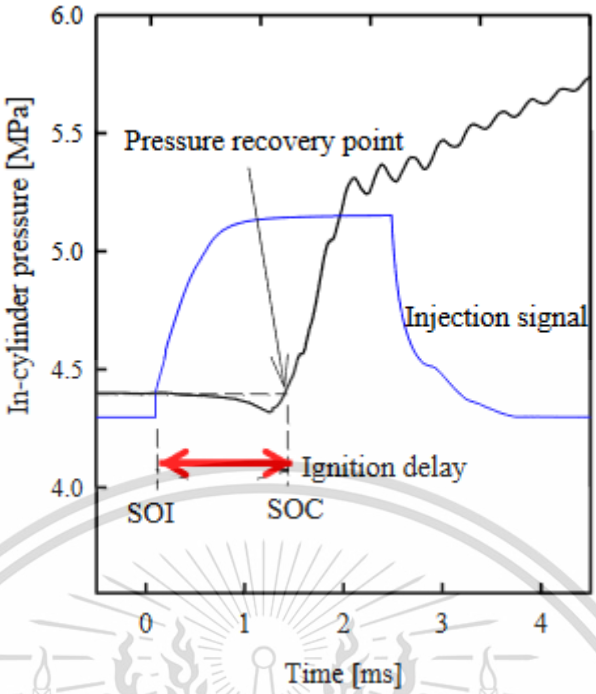

Figure 3.14 Definition of ignition delay by combustion pressure and injection signal

Source: Munsin, R., Laoonual, Y., Jugjai, S., Matsuki, M. and Kosaka, H. (2012). Investigation of effects of ignition improvers on ignition delay time of ethanol combustion with rapid compression and expansion machine. SAE Paper No. 2012-01-0854.

Heat release rate was calculated from combustion pressure rise after fuel injection by applying the first law of thermodynamics (Heywood,1988), as shown in Equation (1) where γ is the specific heat ratio, P is the chamber pressure, dV/dt is the rate of volume change in chamber and dP/dt is the rate of pressure change in chamber.

$$\frac{dQ}{dt} = \frac{\gamma}{\gamma - 1} \cdot P \cdot \frac{dV}{dt} + \frac{1}{\gamma - 1} \cdot V \cdot \frac{dP}{dt} \qquad (1)$$

Heat release is calculated by integration under the curve area of heat release rate from the start of combustion to the point at which the heat release rate decreases to a negative value.

Flame temperatures were measured by the two color method based on thermal radiation of soot particle in two different wave lengths (Matsui,1979). Monochromatic radiation from non-black body, explained by Equation (2) where ε is the emissivity, λ is the wavelength, C_1 is the first Planck constant, C_2 is the second Planck constant and T flame is the flame temperature.

$$I_{(\lambda,T)} = \varepsilon_\lambda \frac{C_1}{\pi\lambda^5} exp^{(-C_2/\lambda T)} \qquad (2)$$

The monochromatic radiant intensity can also be explained in terms of the apparent temperature (T_a), as shown in Equation (3).

$$I_{(\lambda,T)} = \frac{C_1}{\pi\lambda^5} exp^{(-C_2/\lambda T_a)} \qquad (3)$$

Monochromatic radiant intensity in Equation (2) and (3) are equal. By replacing $\varepsilon\lambda$ from Equation (2) with Equation (3), Equation (4) is obtained.

$$\varepsilon_\lambda = 1 - exp^{(-KL/\lambda)} \qquad (4)$$

The measurement of soot particle radiations in two wavelengths enables solution for *KL* and *T*, based on Equation (5) where *K* is the absorption coefficient and *L* is the path.

$$KL = -\lambda^a \ln\left[1 - exp\left\{\frac{C_2}{\lambda}\left(\frac{1}{T_a} - \frac{1}{T}\right)\right\}\right] \qquad (5)$$

Before the two color method can be applied to measure flame temperature, it is necessary to calibrate high speed camera for flame brightness measurement. Black body furnace and pyrometer are used to accurately determine the reference temperature. Distance between black body furnace and highspeed camera was set same as measurement distance used in the experiment. The visible light can be converted by CCD detector in the highspeed camera into three color bands, red, green and blue. Any two of the three color bands can be used for the calculation of temperature and KL factor. Two wavelengths that used in this experiment are blue (501 nm) and red (612 nm). Then flame temperature can be calculated by using MATLAB base on Equation (5).

Soot concentration is determined by passing exhaust gas from a combustion unit chamber to filter paper to collect soot emissions. It is then measured with a smoke meter.

CHAPTER 4

RESULTS AND DISCUSSIONS

4.1 RCEM Combustion characteristic

In this experiment was conducted using two different fuels- HVO and conventional diesel. Other conditions were a nozzle exit orifice diameter of 0.2 mm, solenoid injector 2.0 ms energizing time, to reduce the effect of transient opening and closing; 100 MPa injection pressure, to avoid cavitation; and vary ambient density were used to simulate the effect of supercharge under naturally aspirated conditions. For ambient temperature of 650, 700 and 750 kelvin, the effect was investigated of low temperature concentrations at ambient pressure under a constant equivalent ratio. All tests were repeated 5 times for each test condition. Result of combustion characteristics experimental are present in terms of heat release rate, ignition delay, heat release, flame temperature, soot concentration

4.1.1 Pressure

From the experimental results, the pressure of Diesel and HVO are nearly identical to those of temperature 750K and 700K, while 650K shows a different result as shown in Figure 4.1. At temperature 650K as shown in Figure 4.1 has the most rapid pressure rise because the longest ignition delay of this condition allows more time for the better fuel-air mixing leading to a strong pre-mixed combustion, the steep pressure rise and the large heat release during the premixed combustion phase then turned to premixed charge compression ignition (PCCI). The strong pre-mixed combustion could increase the possibility of engine wear and combustion noise in CI engines, commonly referred to as diesel knocking (Heywood,1988). However, pressure during the premixed combustion phase can be reduced by using HVO fuels with a shorter ignition delay and smaller pressure rise. The shorter ignition delays of 750 K and 700 K of HVO fuel result in the earlier and longer mixing-controlled combustion phase as shown in Figure 4.2 and 4.3.

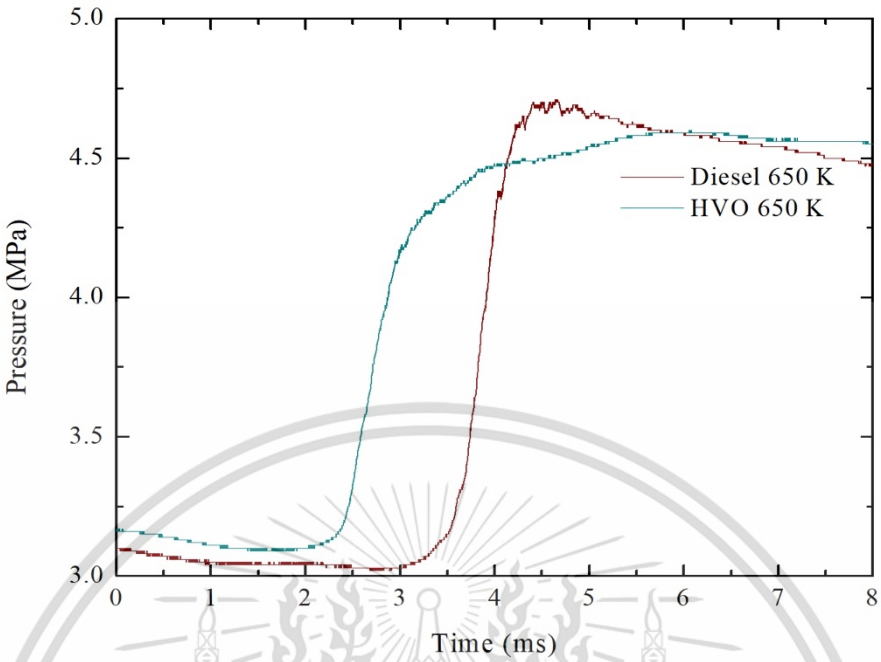

Figure 4.1 Pressure of 650 K condition

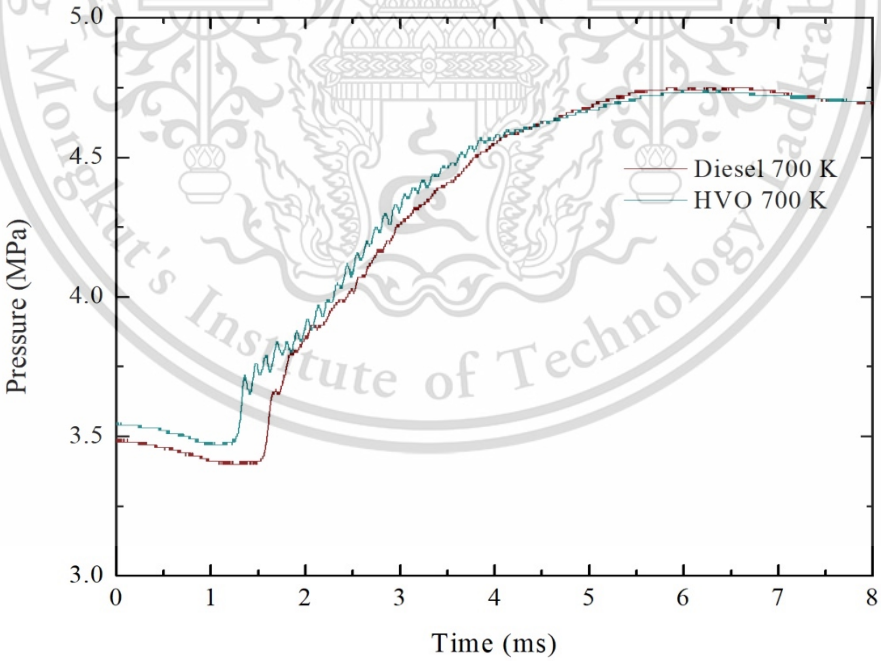

Figure 4.2 Pressure of 700 K condition.

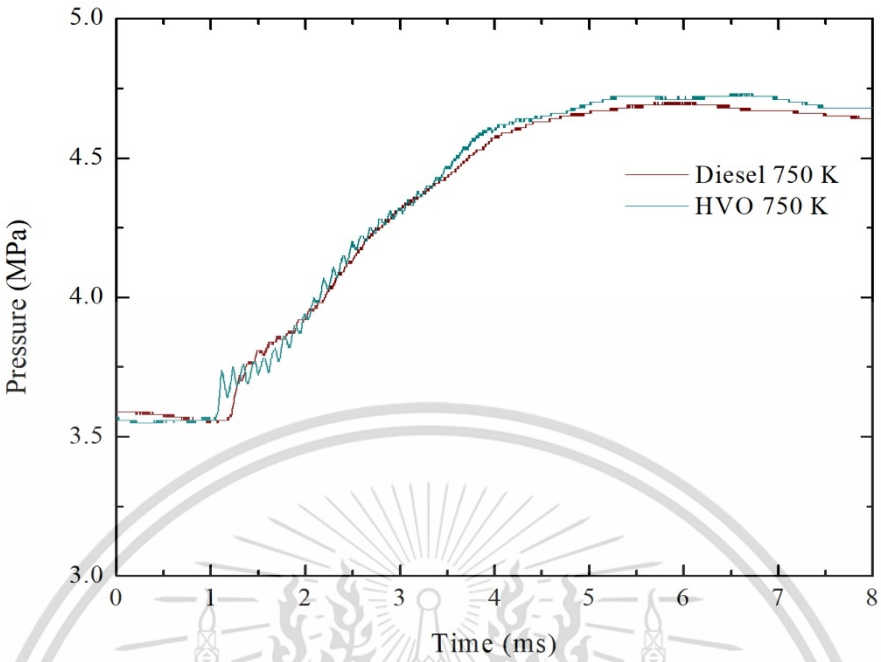

Figure 4.3 Pressure of 750 K condition.

4.1.2 Heat release rate

Figure 4.4, 4.5 and 4.6 shows heat release rates of diesel and HVO as representative. Heat release rates are calculated from pressure rise after injected fuel by using Equation (1). In both after injection the evaporation of fuel into the hot environment causes a dramatically reduce to negative value in the heat release rates curves (Heywood,1988). And the lowest ambient temperature 650 K condition in both fuels show effect of longer ignition delay making more premixed combustion occurred in the chamber and turned to premixed charge compression ignition (PCCI) also had the effect of making the heat release rate higher compared to higher temperature.

HVO shows a lower heat release rate curve compared to diesel in all test conditions due to a higher cetane number making ignition delay shorter. HVO made more premixed combustion occurred in the chamber also had the effect of making the heat release rate more gradual. and lower peak heat release rate curve during lower ambient temperature condition compared to diesel fuel. Higher ambient density resulted in higher and increase peak pressure value. And also resulted in a shorter ignition delay.

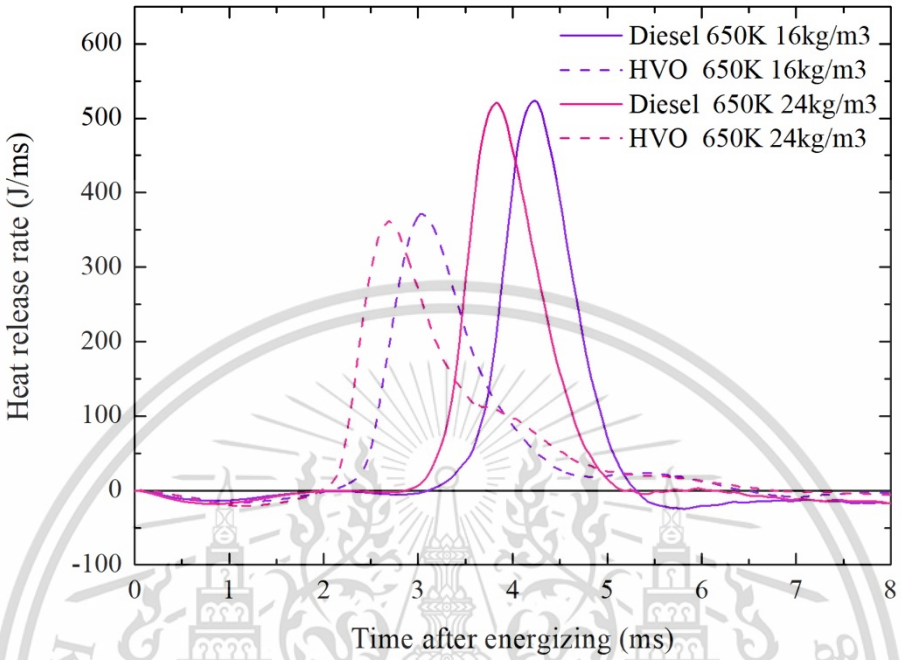

Figure 4.4 Heat release rate of 650 K condition

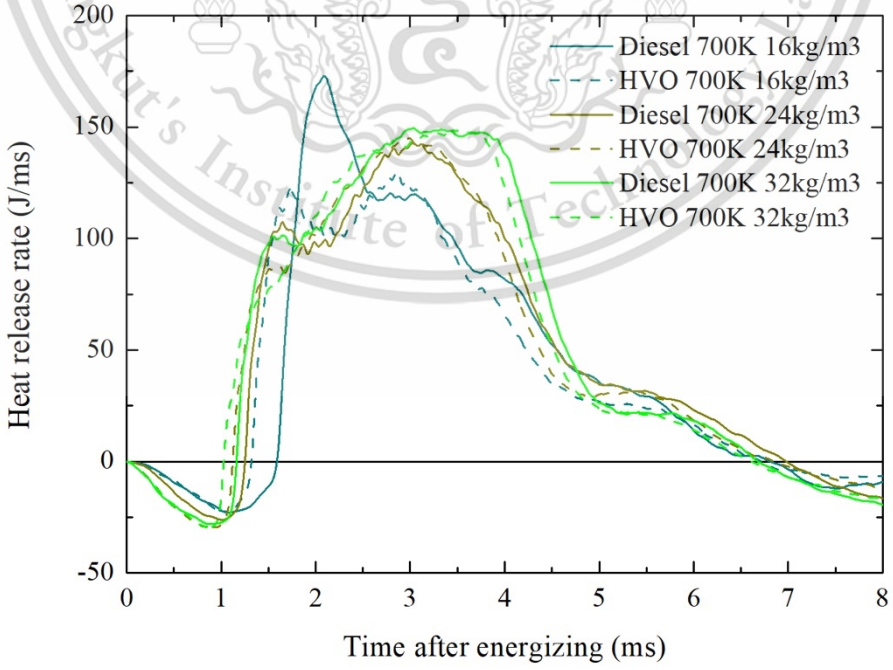

Figure 4.5 Heat release rate of 700 K condition

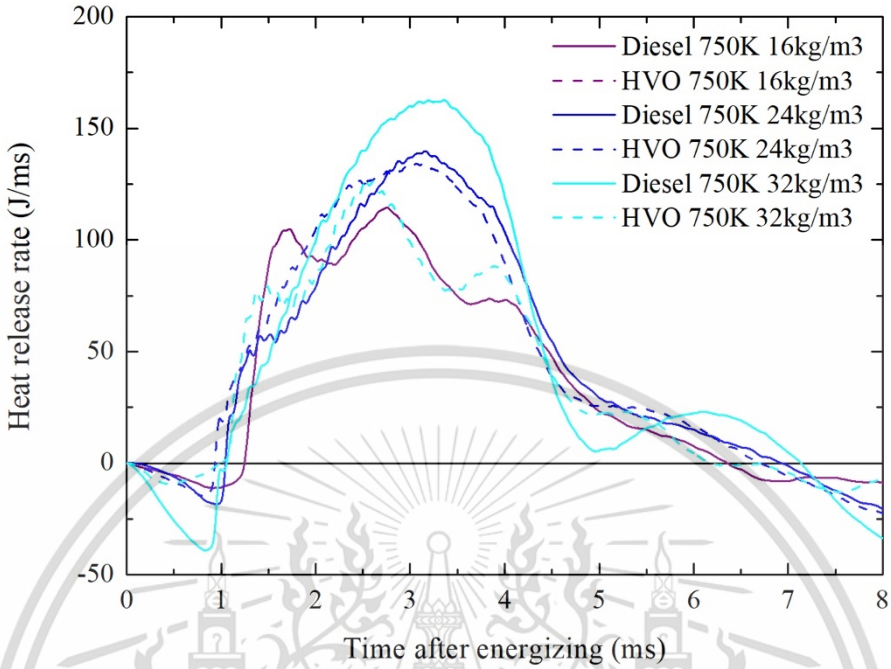

Figure 4.6 Heat release rate of 750 K condition

4.1.3 Ignition delay

Figure 4.7 and 4.8 shows ignition delay. Ignition delay is mainly dependent on the fuel cetane number (Jung,2010). HVO shows shorter ignition delays compared to diesel and show significantly shorter ignition delay in lower ambient pressure and lower temperature condition

Figure 4.9 shows the effects of ambient temperature under constant ambient density on ignition delay. HVO also shows shorter ignition delays compared to diesel 20.69 % at an ambient temperature 750 K, 16.92 % at ambient temperature 700 K and 30.34 % at ambient temperature 650 K. The highest ambient temperature in both fuels show the shortest ignition delay compared to other cases. Increasing ambient temperature with constant ambient density improves mixture formation also decreases ignition delay. However, shorter ignition delay of HVO is the lower distillation temperature which make its faster evaporation with surrounding air in the chamber, and it might contribute to small droplet size distribution (Oo,2015) (No,2014), which is related to a better mixture formation.

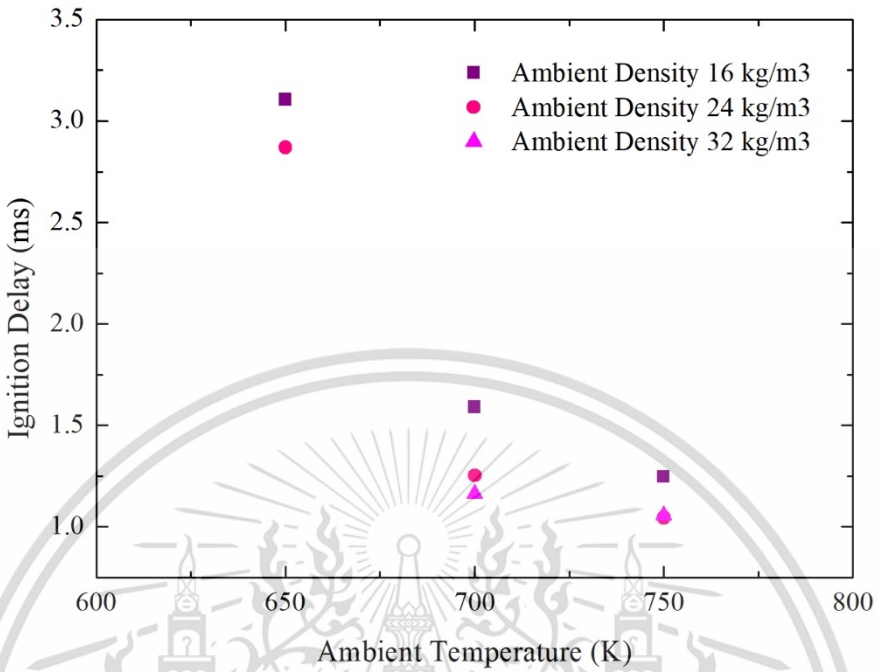

Figure 4.7 Ignition delay of diesel fuel

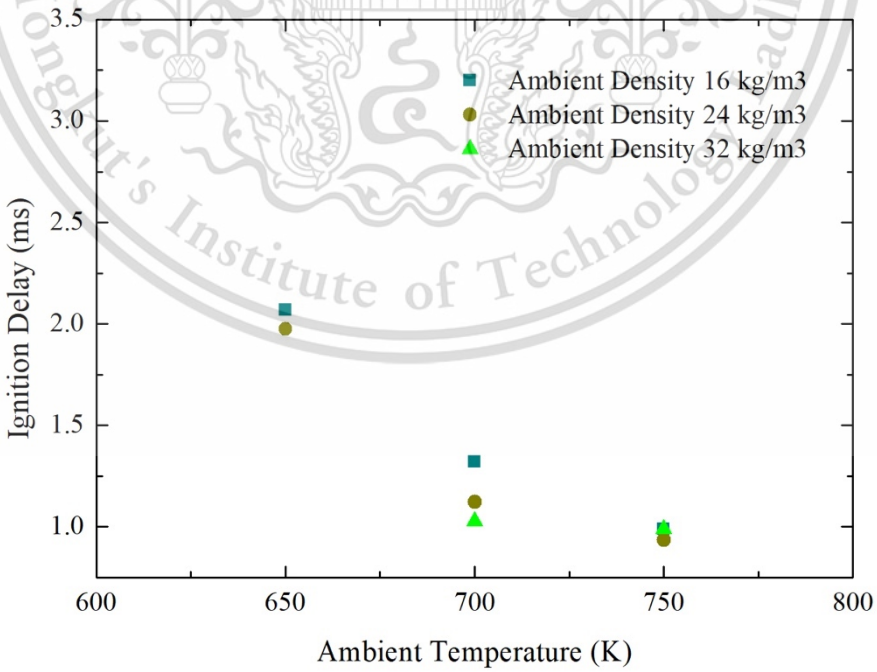

Figure 4.8 Ignition delay of HVO fuel

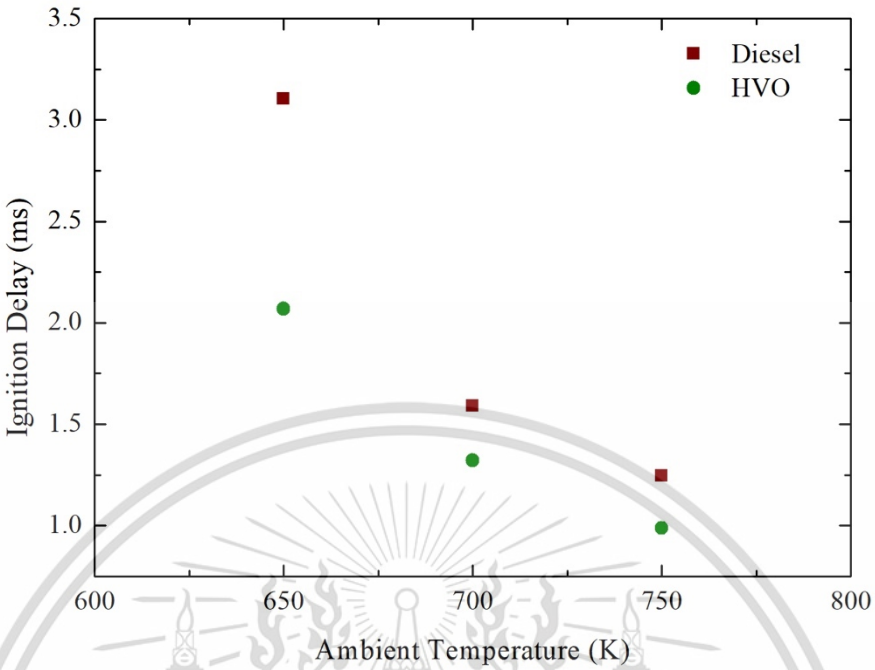

Figure 4.9 Ignition delay under constant density

4.1.4 Integral heat release

Figure 4.10 and 4.11 shows the effects of ambient temperature on heat release. Significant differences between the integral heat release rate of diesel and HVO at ambient 16, 24 and 32 kg/m^3 condition. HVO showed a lower integral heat release compared to diesel respectively. The primary reason for a decrease in integral heat release is the changing fuel cetane number, which shortens the ignition delay. That results in the formation of a less combustible mixture, and the extra reactions do not have a chance to occur- especially at low oxygen concentrations (Kook,2005) (Azimov,2009). Another effect of increasing the pressure rate was an increased heat capacity of ambient gas making a lower integral heat release (Pierpont,1995).

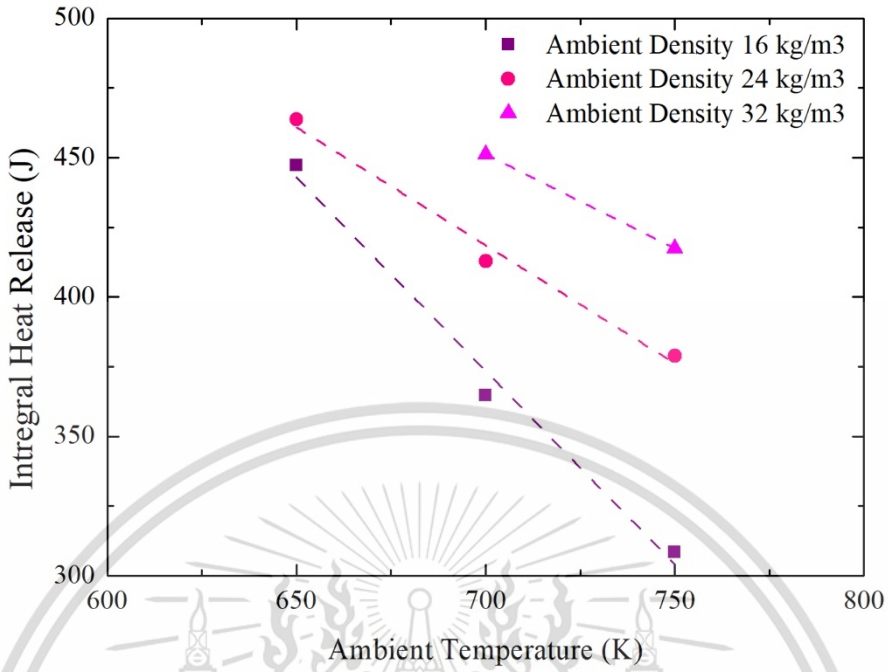

Figure 4.10 Integral heat release of Diesel fuel

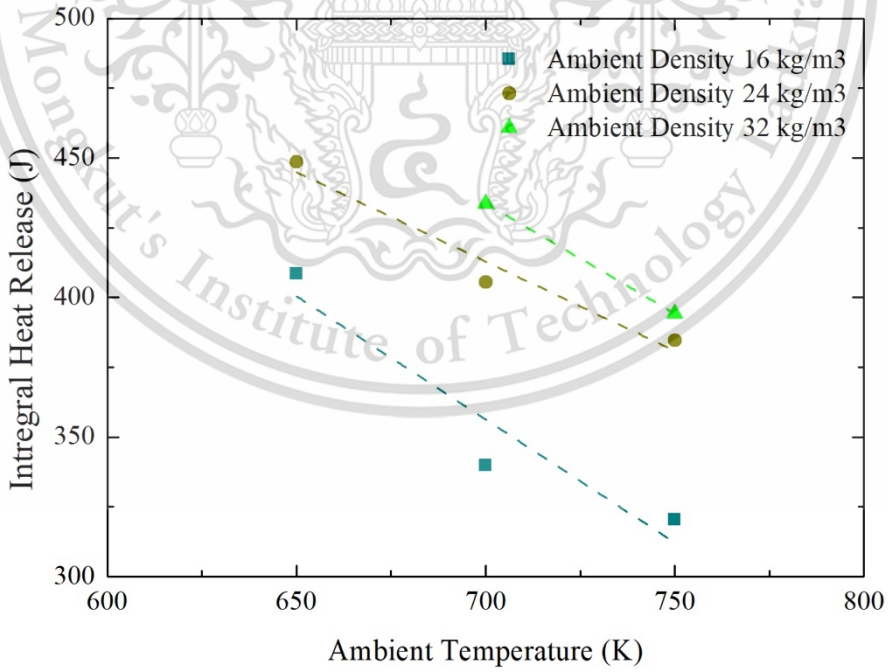

Figure 4.11 Integral heat release of HVO fuel

4.1.5 Flame temperature

Table 4.1 show combustion image of HVO and diesel before calculated by two color method table 4.2 show flame temperature image calculated by the two color method of diesel and HVO as representative.

HVO shows slightly lower flame temperature compared to diesel. This is due to a higher cetane number. HVO shows slightly wider flame image under ambient condition O_2 21% at 16 kg/m^3 during 2.5 to 3.5ms after energizing. This is due to a wider spray angle (Hulkkonen,2011). The lower viscosity of HVO increases turbulence at the nozzle exit making a wider spray angle (Dernotte,2012). Also contributing to making the flame image of HVO wider than diesel, is a lower distillation temperature which results in better vaporization and mixture formation at the flame border. Both diesel and HVO at O_2 21% at 16 kg/m^3 was the conditions that show flame temperature image at 1.5 ms. At ambient condition, O_2 21% at 16 kg/m^3 shows the highest flame temperature among other ambient conditions from 1.5 to 7.0 ms after energizing. Increasing ambient pressure promoted oxygen enhancement in spray volume improve mixture formation, thus better combustion, result flame temperature was increased.

Ambient condition	Fuel	1.5 ms	2.0 ms	2.5 ms	3.5 ms	5.0 ms	7.0 ms
$O_2$21% 16 kg/m^3	Diesel						
	HVO						

Table 4.1 Combustion image of HVO and Diesel fuel

Ambient condition	Fuel	1.5 ms	2.0 ms	2.5 ms	3.5 ms	5.0 ms	7.0 ms
$O_2$21% 16 kg/m^3	Diesel	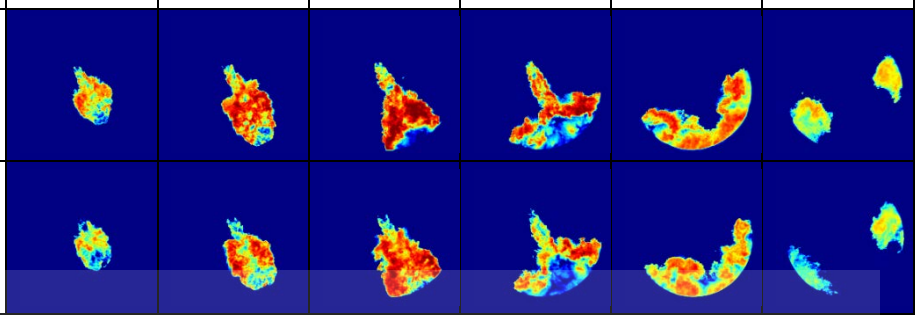					
	HVO						

Table 4.2 Flame temperature image of HVO and Diesel fuel

Figure 4.12 show average flame of diesel and HVO as representative. Average flame temperature is calculated by summarizing the flame temperature of each pixel in the flame area and dividing by the total pixels (Munsin,2015). HVO shows significant lower soot concentration compared to diesel, with ambient condition O 21 % at ambient density 16 kg/m3.

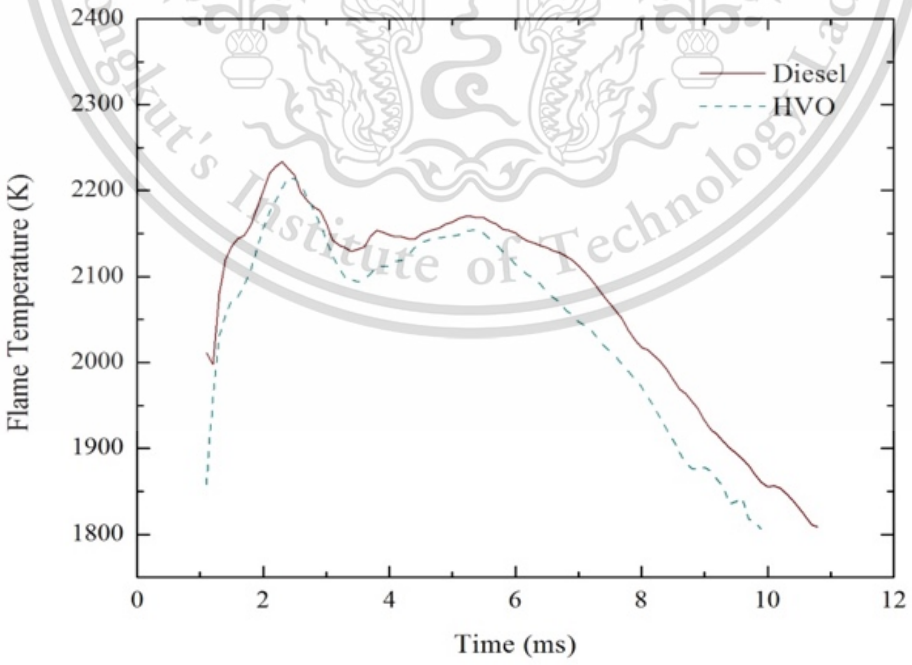

Figure 4.12 Flame temperature of ambient condition

4.2 RCEM soot morphology and nanostructure

The particulate matter from HVO and Diesel combustion was investigated for PM morphology and nanostructure in RCEM experiment. Results were also to be compared with small CI engine experiment. PM morphology and nanostructure can be analyzed via images derived from modern electron microscopes i.e. Scanning Electron Microscope (SEM) and Transmission Electron Microscope (TEM) techniques.

In RCEM experiment was collected only soot from a paper filter that consisted of many single nanoparticles as shown in Figure 4.13. And appropriate to investigated by Scanning Electron Microscope (SEM).

For SEM images, PMs with a level of agglomerated particles can be investigated. Figure 4.13, 4.14, 4.15, 4.16, 4.17 and 4.18 show samples of SEM images of PM derived from 650 K, 700 K and 750 K from HVO and diesel fuel respectively. They are composed of groups of agglomerated particles gathered on paper filter. Sizes of these agglomerated particle groups vary from hundreds of nanometers to few microns. Fine particles or PM2.5 as shown on Figure 4.14a, 4.15a, 4.16a, 4.17a, 4.18a and 4.19a can be observed. Bigger groups or PM10 is also shown in Figure 4.14b, 4.15b, 4.16b, 4.17b, 4.18b and 4.19b However, relationships between particle's size, appearance, and combustion of each type of fuel cannot be found in the agglomerated level.

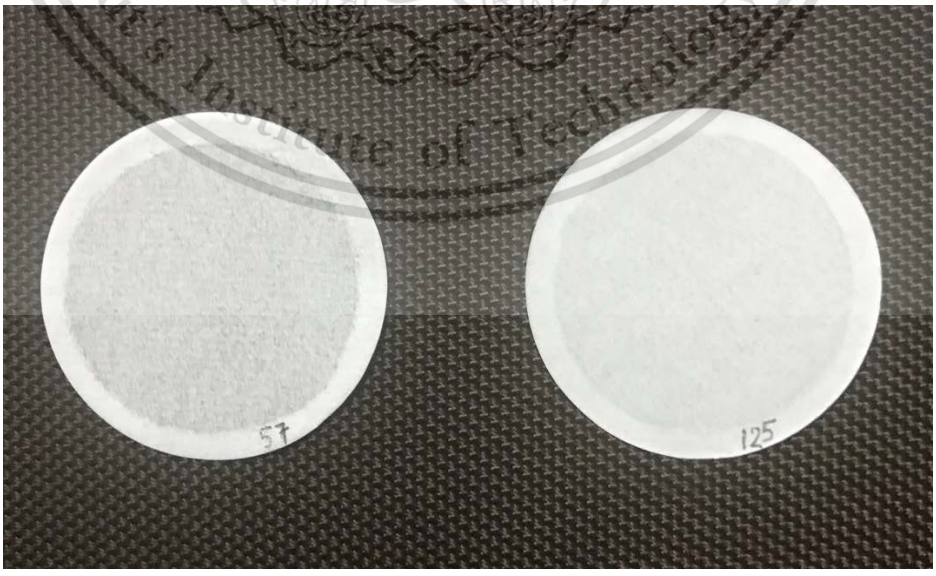

Figure 4.13 Filter papers of HVO and diesel from RCEM experiment

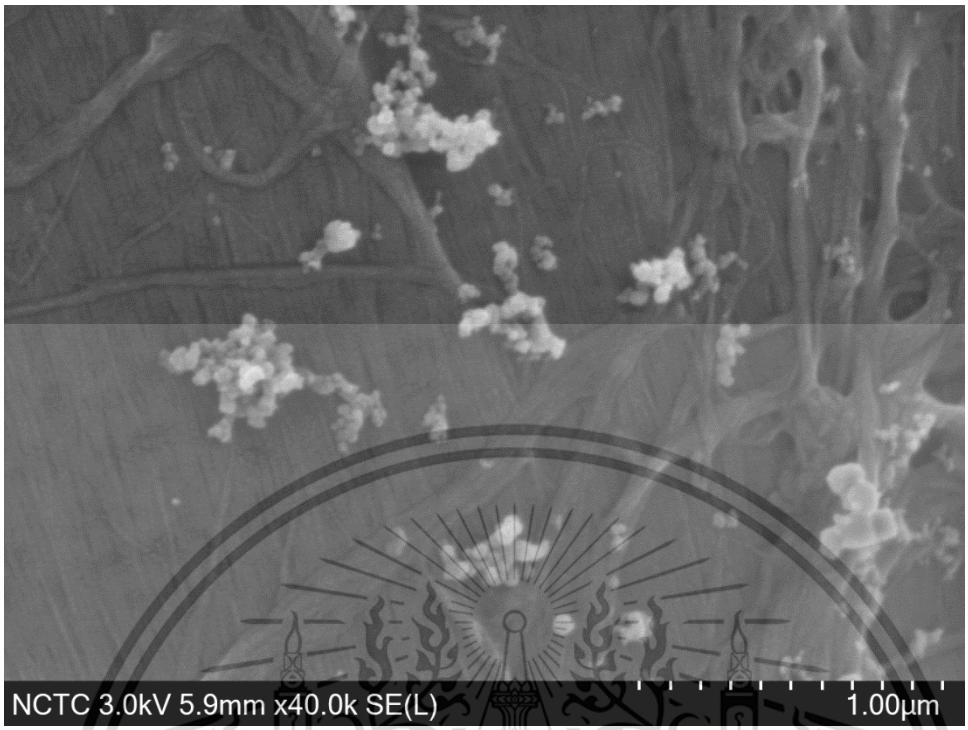

Figure 4.14a SEM images of diesel particulate matter at 650 K condition

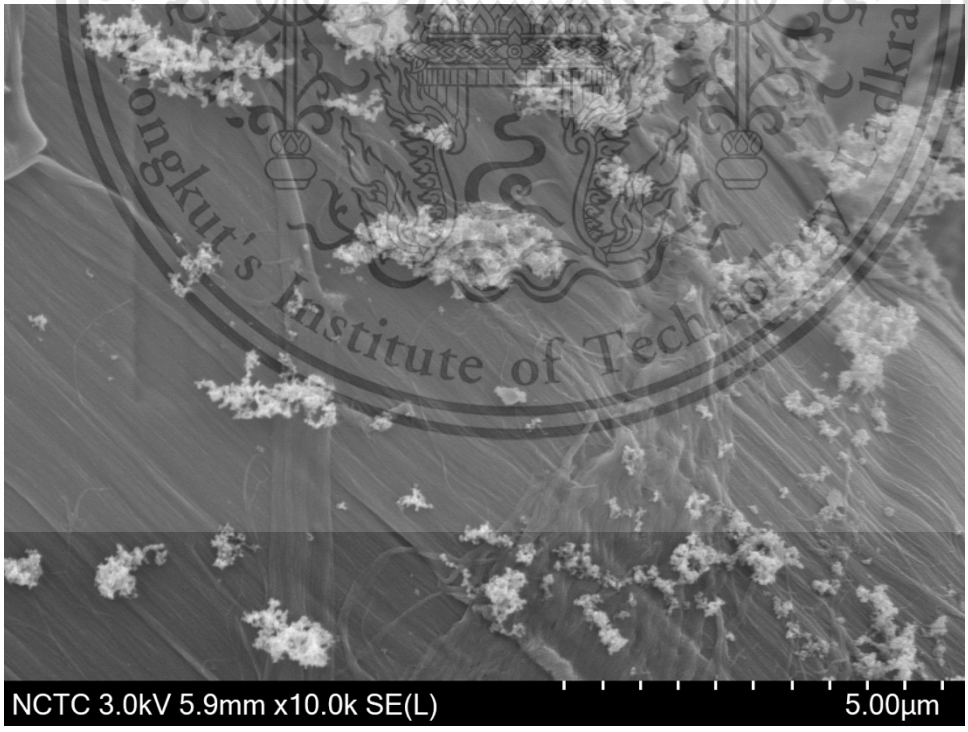

Figure 4.14b SEM images of diesel particulate matter at 650 K condition

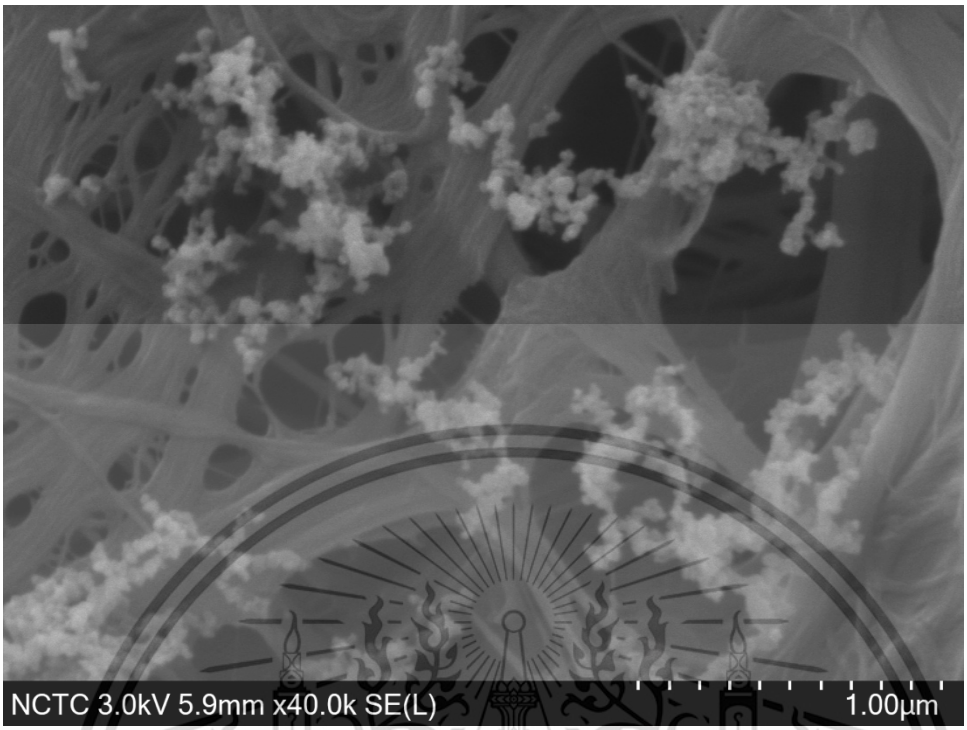

Figure 4.15a SEM images of diesel particulate matter at 700 K condition

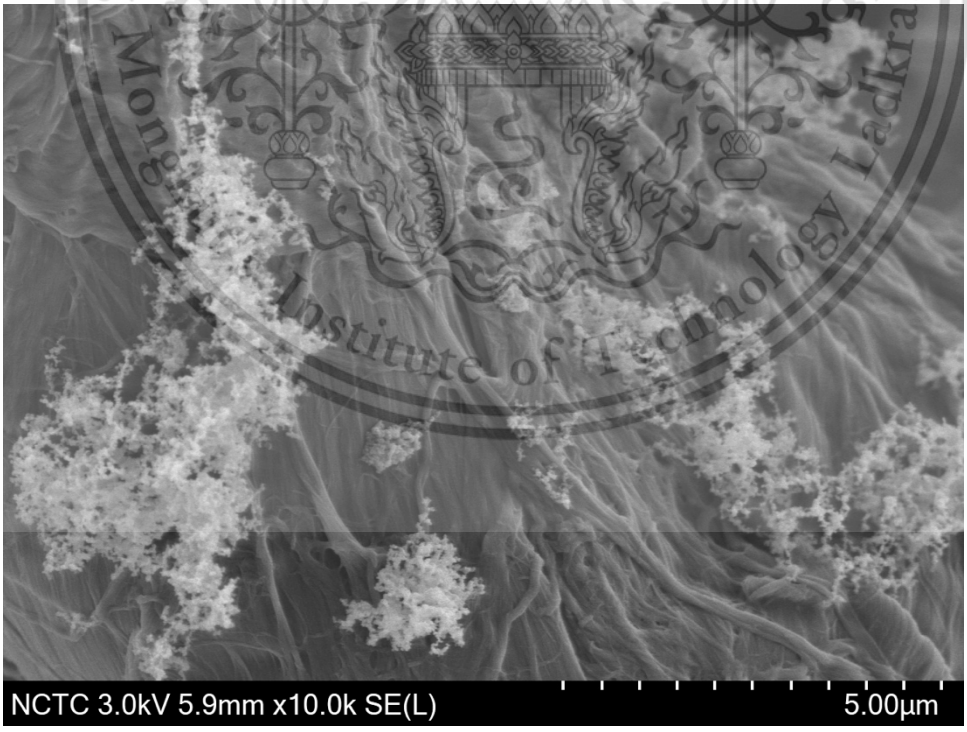

Figure 4.15b SEM images of diesel particulate matter at 700 K condition

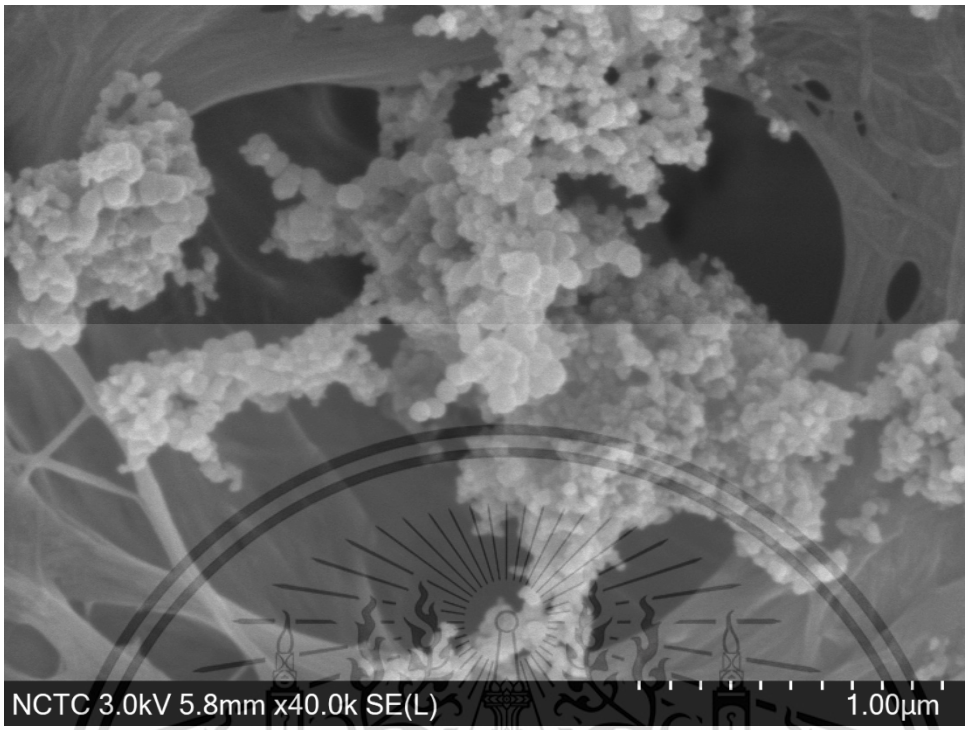

Figure 4.16a SEM images of diesel particulate matter at 750 K condition

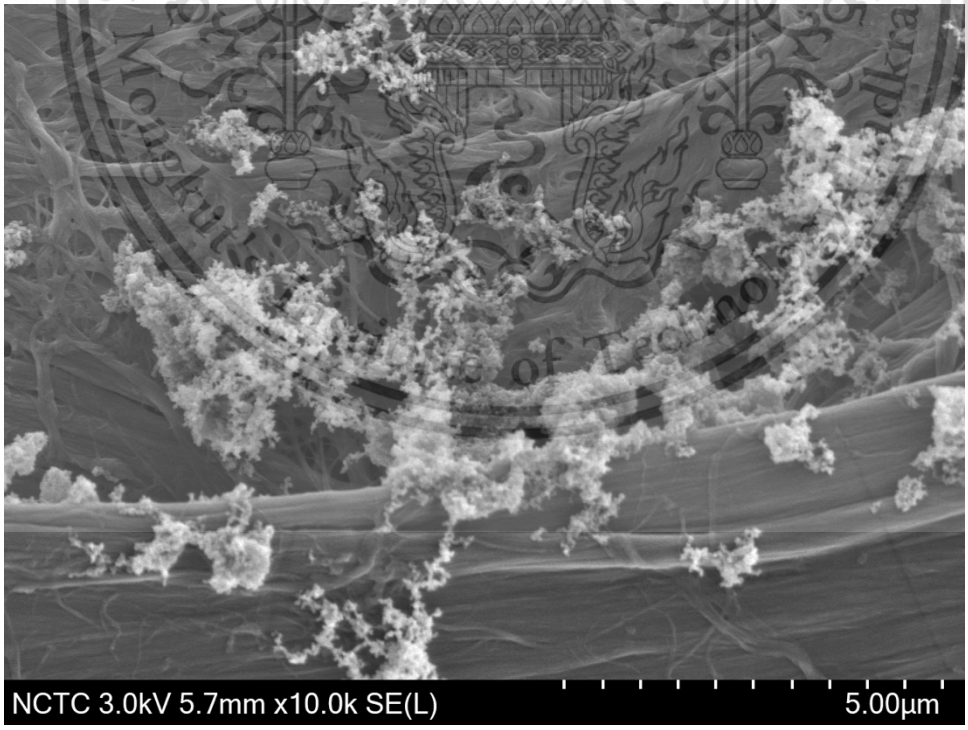

Figure 4.16b SEM images of diesel particulate matter at 750 K condition

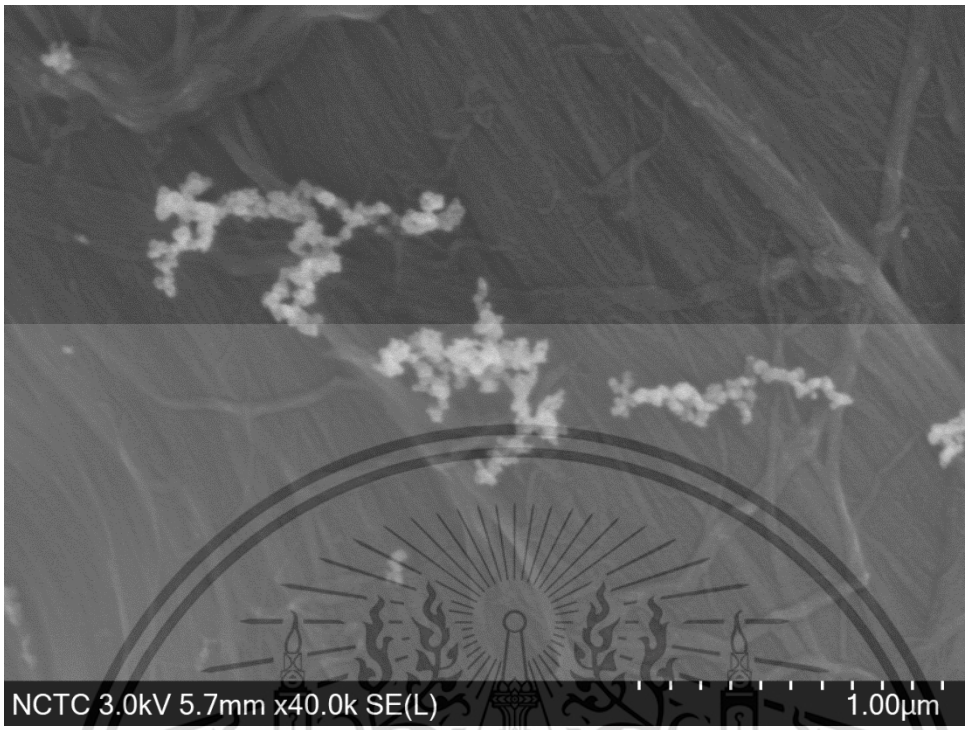

Figure 4.17a SEM images of HVO particulate matter at 650 K condition

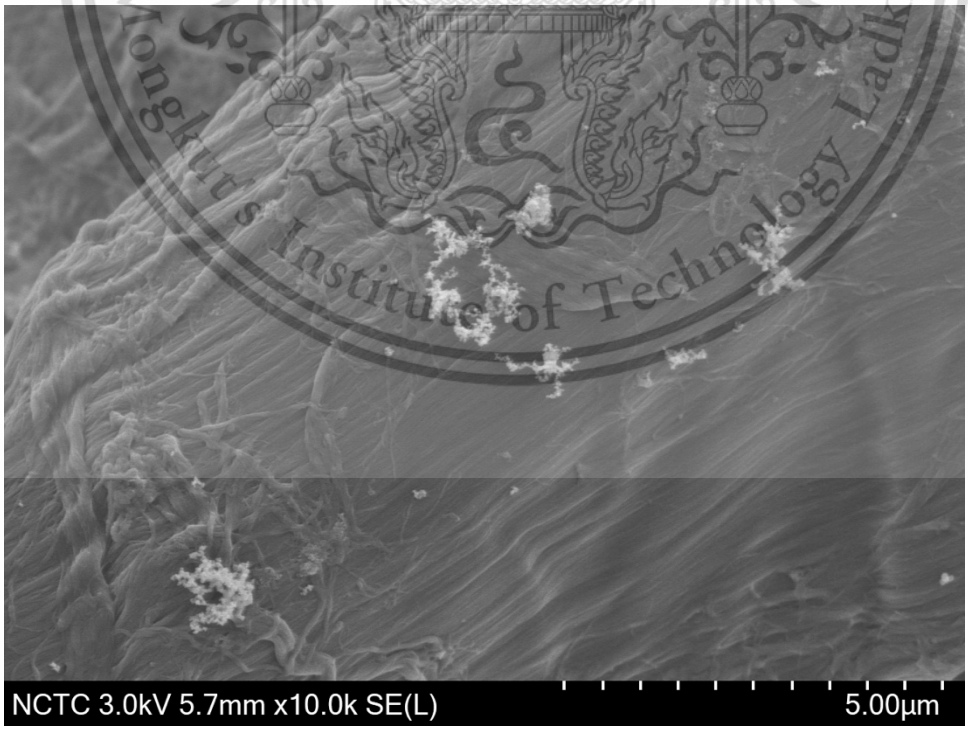

Figure 4.17b SEM images of HVO particulate matter at 650 K condition

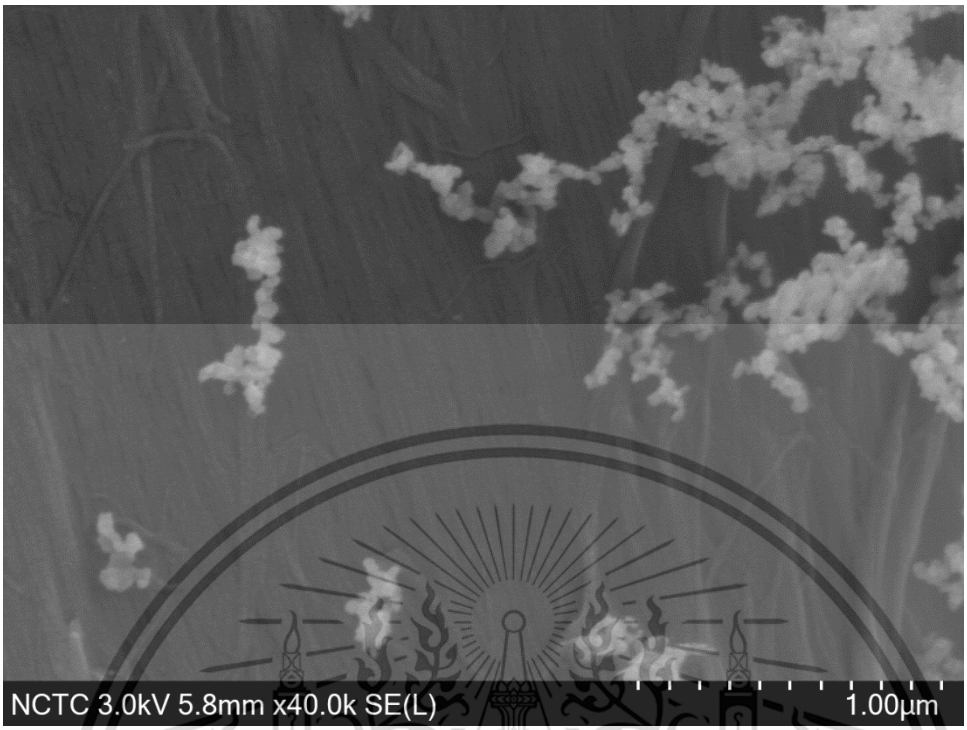

Figure 4.18a SEM images of HVO particulate matter at 700 K condition

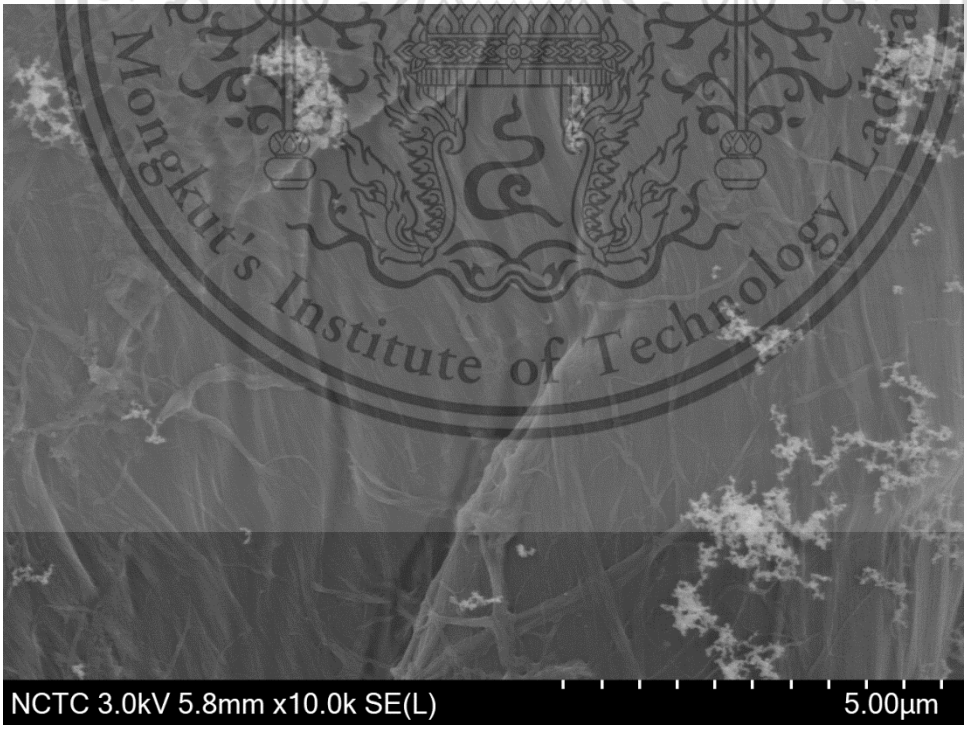

Figure 4.18b SEM images of HVO particulate matter at 700 K condition

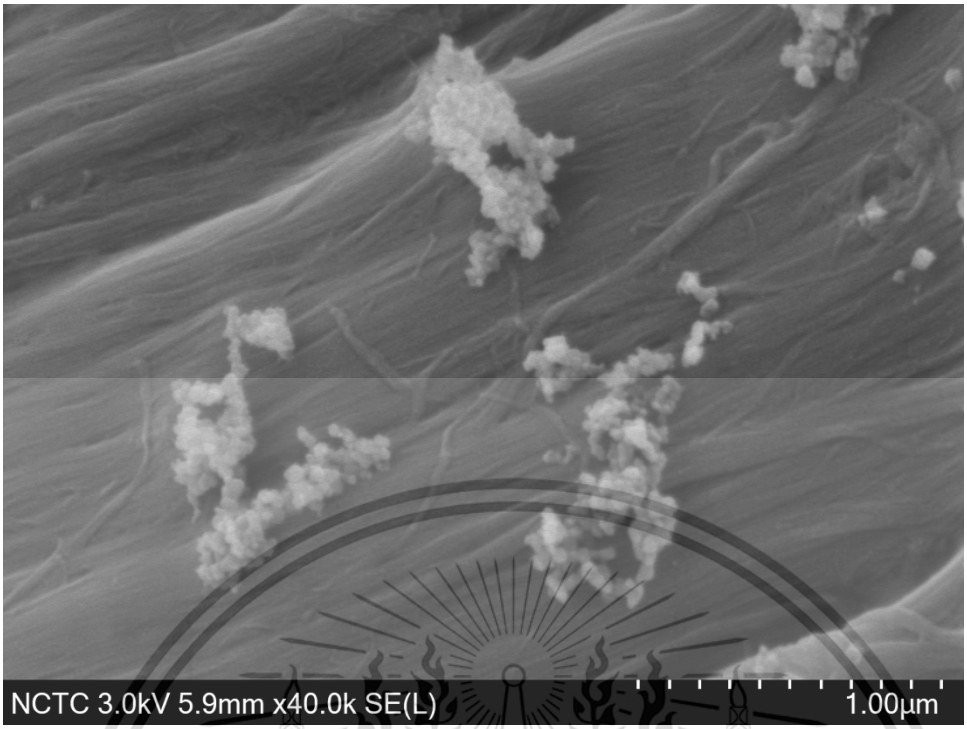

Figure 4.19a SEM images of HVO particulate matter at 750 K condition

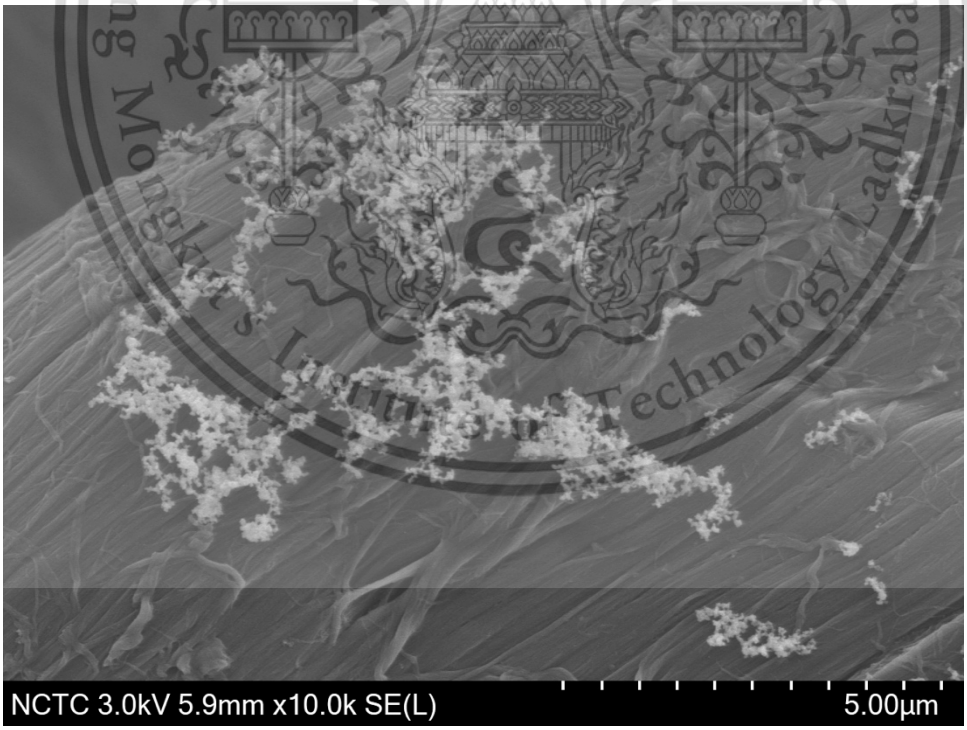

Figure 4.19b SEM images of HVO particulate matter at 750 K condition

However, detailed morphology and nanostructure were to be analyzed by image processing with software called Image J to measure quantitative data of particles such as particle's size, particle's surface, or graphitic structure Moreover, SEM image is used for numerate area of particulate matters from focused area, after post processing of two colors from the two colors images, the area of the PM were measured by image processing program. were measured for the black area in the image to be a PM. The estimated of area of conventional diesel and HVO in 650 K, 700 K and 750 K condition are shown in Figure 20, 21, 22, 23, 24 and 25.

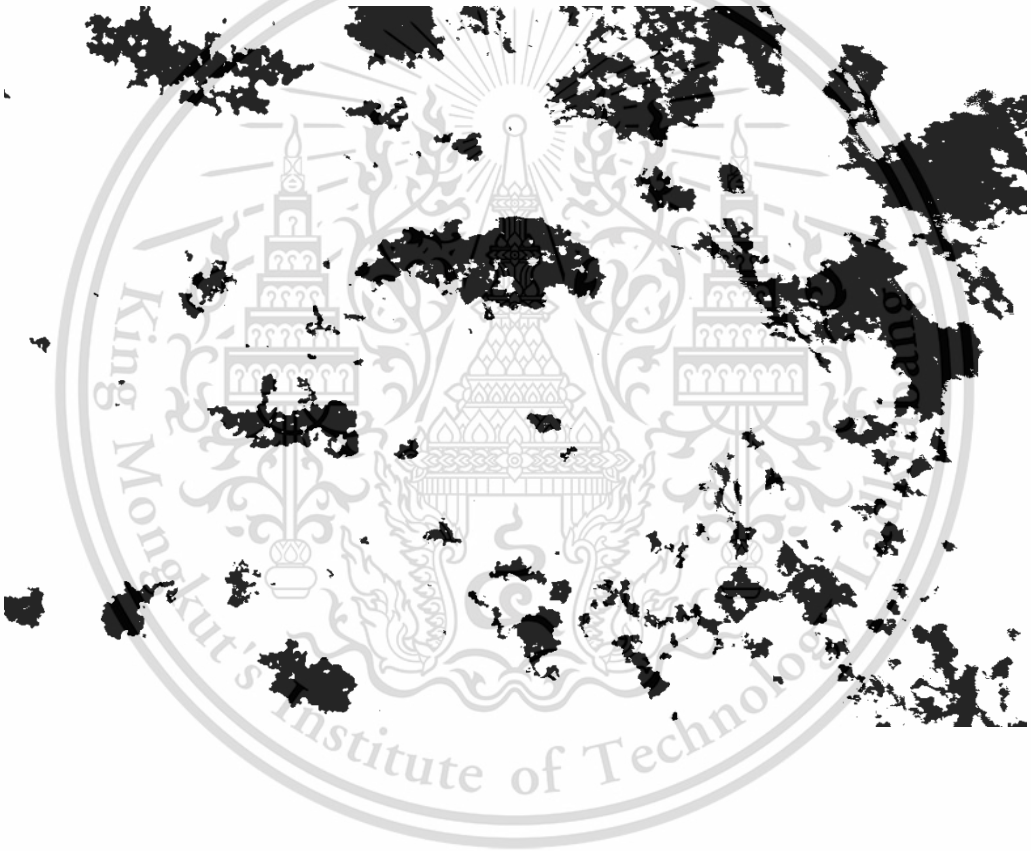

Figure 4.20 Two colors SEM images post process in 650 K condition of diesel

Figure 4.21 Two colors SEM images post process in 700 K condition of diesel

Figure 4.22 Two colors SEM images post process in 750 K condition of diesel

Figure 4.23 Two colors SEM images post process in 650 K condition of HVO

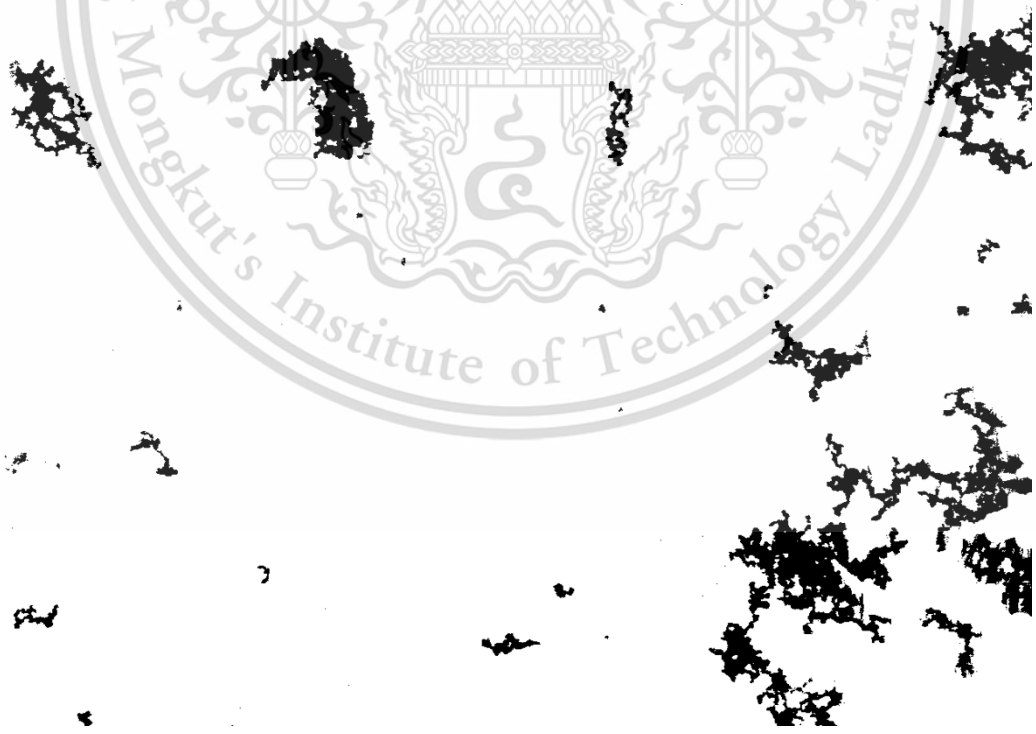

Figure 4.24 Two colors SEM images post process in 700 K condition of HVO

Figure 4.25 Two colors SEM images post process in 750 K condition of HVO

After passed calculation process. The result shown that HVO fuel was significant lower average PM per focus area than conventional diesel fuel in all test condition as show in table 4.3.

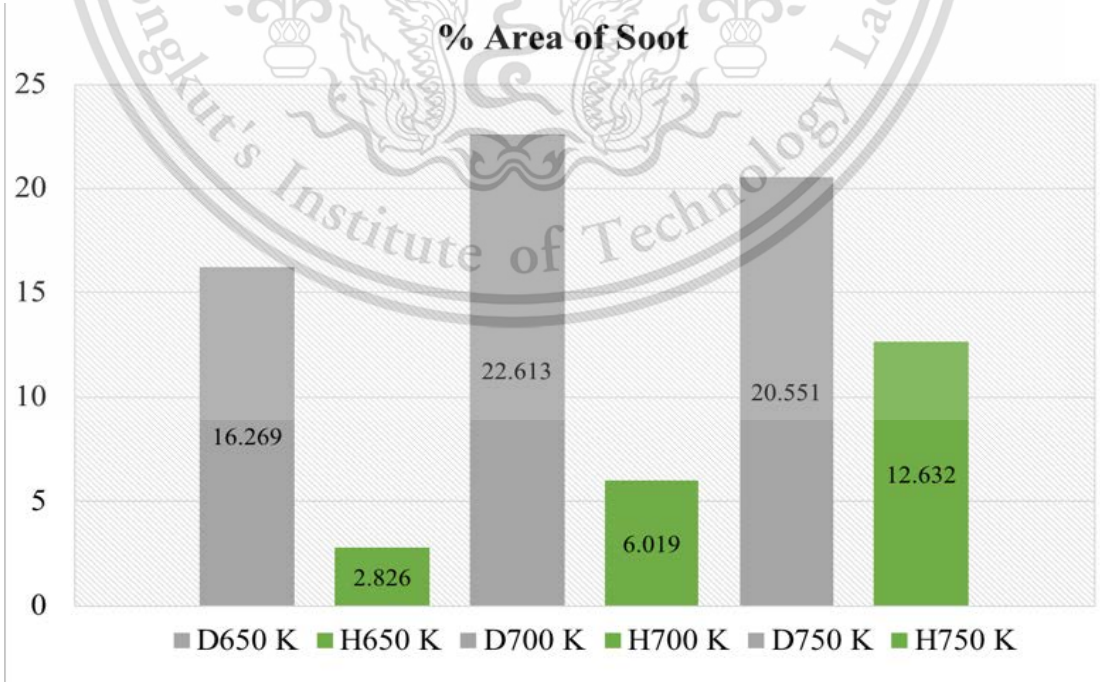

Table. 4.3 Percent area of soot on focus area from SEM image

4.3 CI Small engine Combustion characteristic

4.3.1 Engine Performance

The engine performance curve of HVO and commercial diesel is plotted in Figure 4.26. Engine load drops as increasing engine speed for all fuels. The HVO fuel produces lower load due to lower heating value and worse air fuel mixing than diesel as well as lower stoichiometric air-fuel ratio with higher viscosity i.e. leaner combustion compared with diesel. The engine load shows significant drop at higher speed.

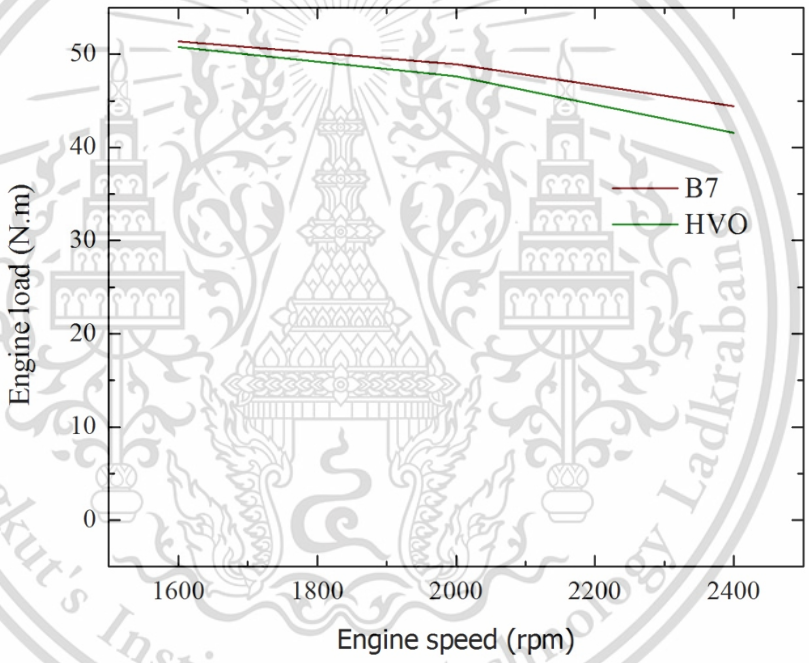

Figure 4.26 Engine performance curve

4.3.2 Pressure

For the engine combustion characteristics, in-cylinder pressure variation with respect to crank angle is shown in Figure 4.27-4.30. And engine pressure-volume diagram as shown in Figure 4.31-4.34. The engine load was varied in the range of 20%, 50%, and 80% load at constant engine speed of 2400 rpm. Peak pressures of all fuels increase with the increasing engine load. Considering at the HVO fuel, the peak pressure lower than commercial diesel because of longer mixing-controlled combustion phase from shorten ignition delay resulted in small pressure rise as well as RCEM experiment.

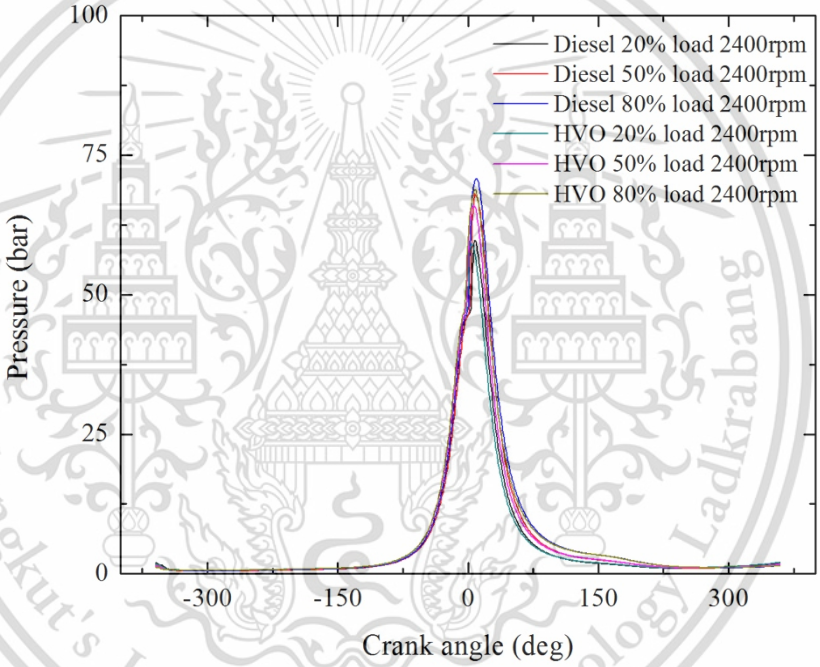

Figure 4.27 Pressure-crank angle graph on different engine load

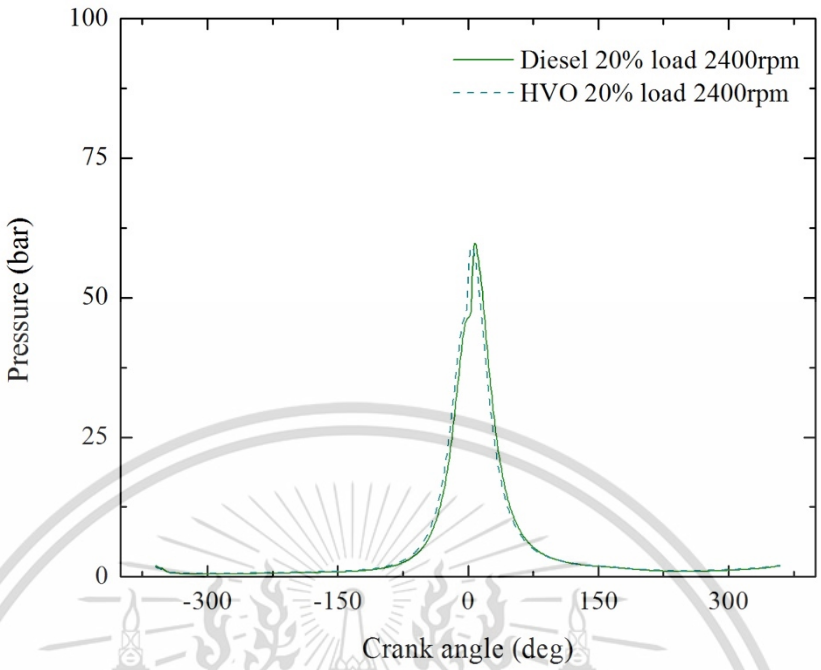

Figure 4.28 Pressure-crank angle graph on 20% engine load

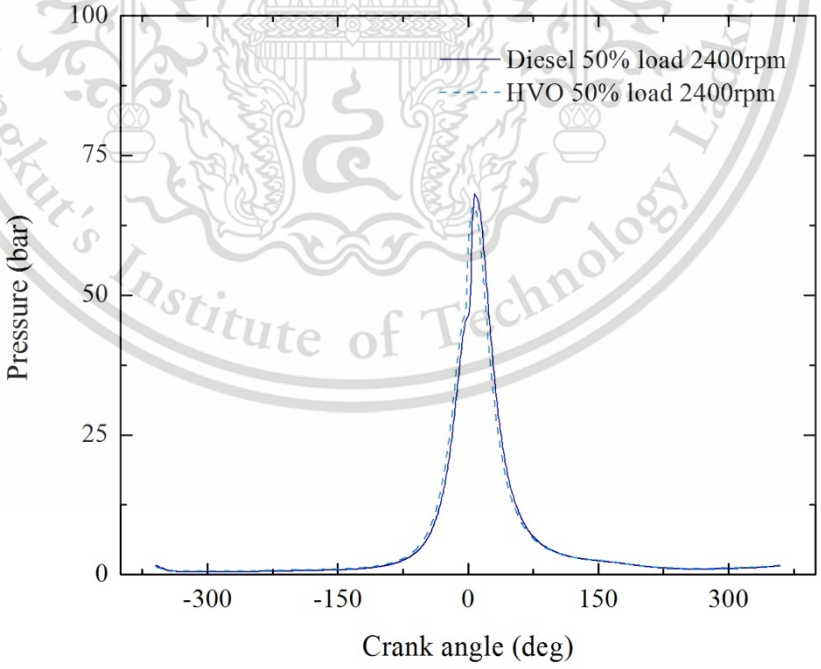

Figure 4.29 Pressure-crank angle graph on 50% engine load

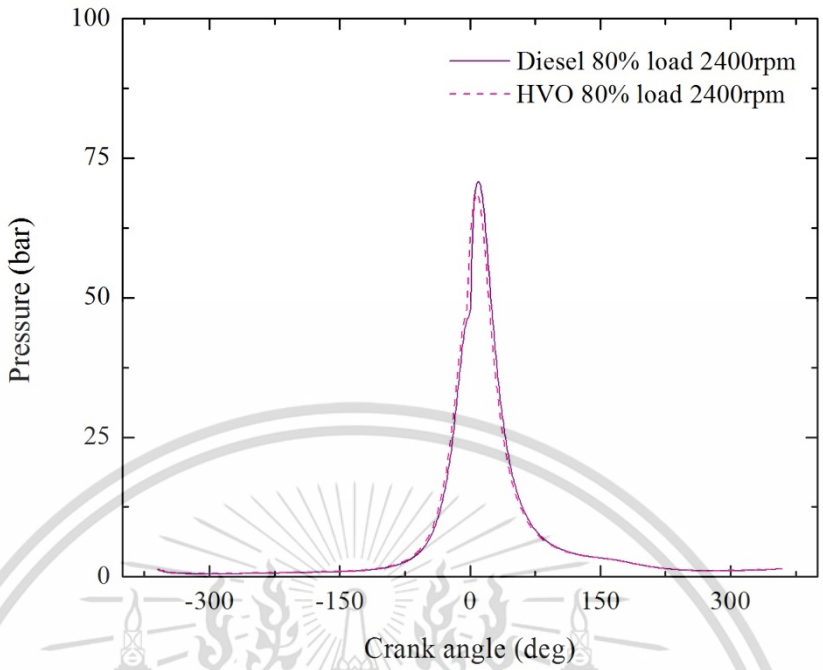

Figure 4.30 Pressure-crank angle graph on 80% engine load

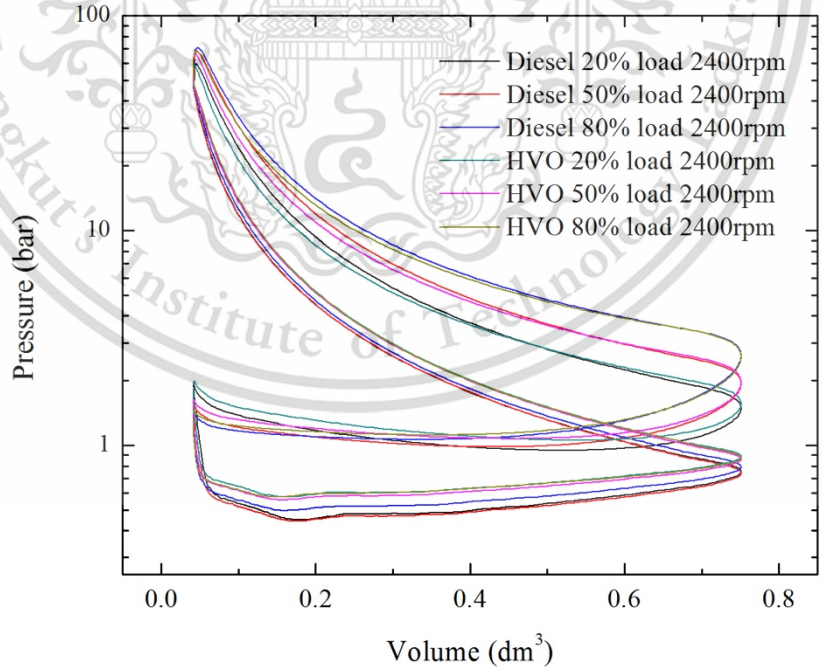

Figure 4.31 Pressure-volume diagram on different engine load

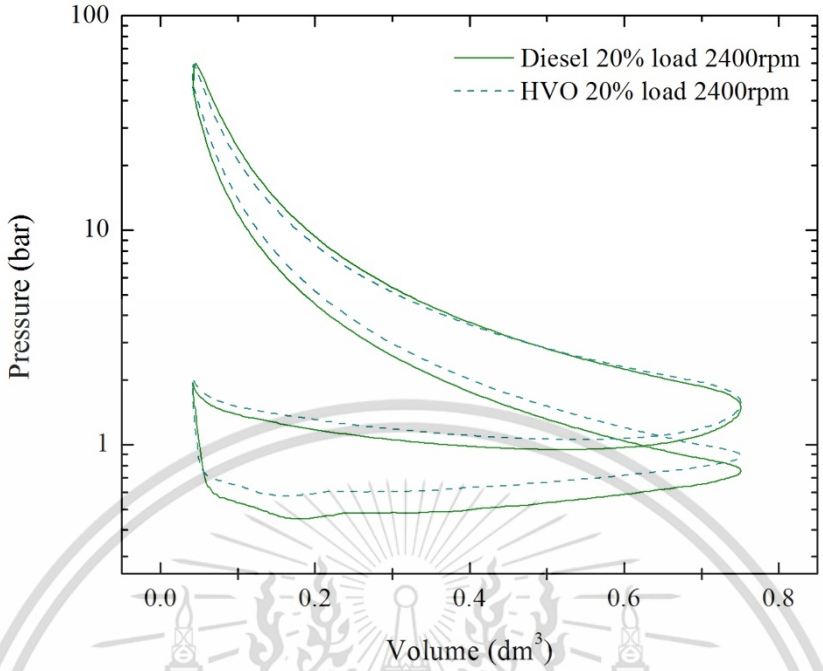

Figure 4.32 Pressure-volume diagram on 20% engine load

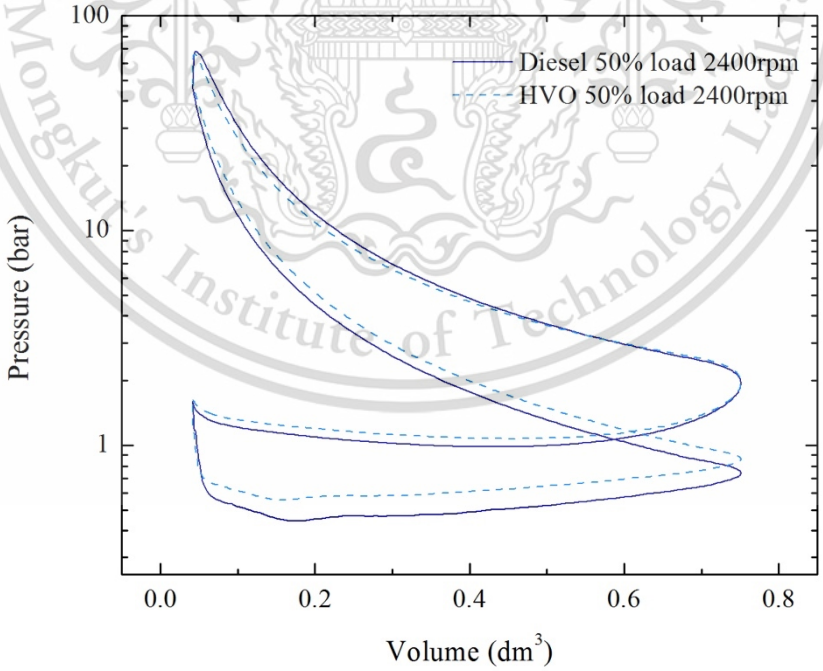

Figure 4.33 Pressure-volume diagram on 50% engine load

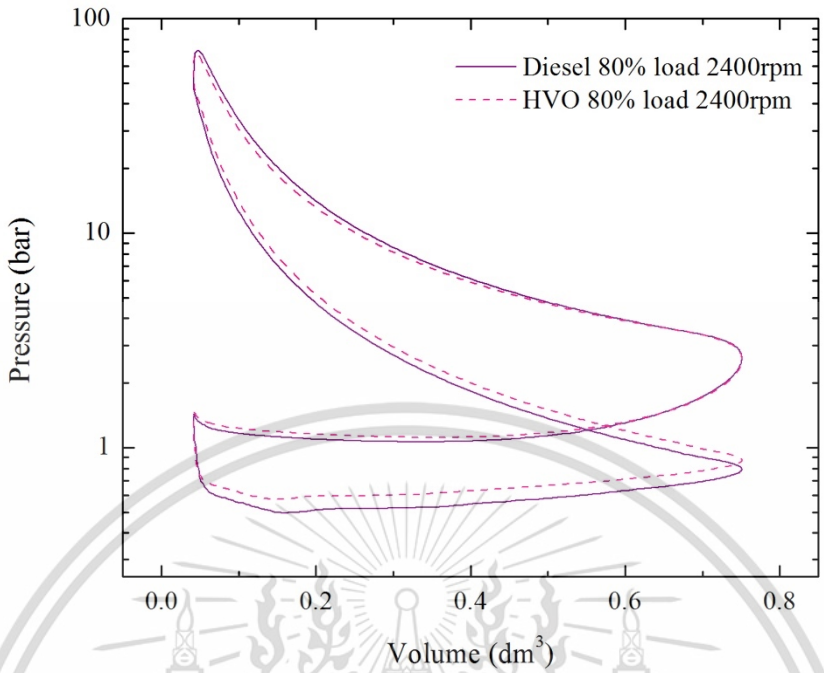

Figure 4.34 Pressure-volume diagram on 80% engine load

4.3.3 Het release rate

Heat release rate plots in Figure 4.35-4.38. show that combustion processes of all fuels start with premixed combustion phase followed by diffusion combustion phase. HVO tends to start combustion before commercial diesel 3-5 degrees crank angle, while a higher peak of the heat release HVO lower than commercial diesel in all test condition. The reason can be explained as; a higher cetane number making ignition delay shorter, lower distillation temperature resulted in better vaporization and mixture formation. Therefore, HVO need more time for fuel atomization. After enough fuel atomization and mixing with oxygen, HVO fuel tends to promote rapid combustion with producing high peaks of heat release rate. At the lower engine speed as shown in Figure 4.36, increasing time for makes better fuel vaporization and fuel atomization as well. The result showed that HVO fuels become stronger premixed combustion and lead to higher peak of heat release rate than higher engine speed.

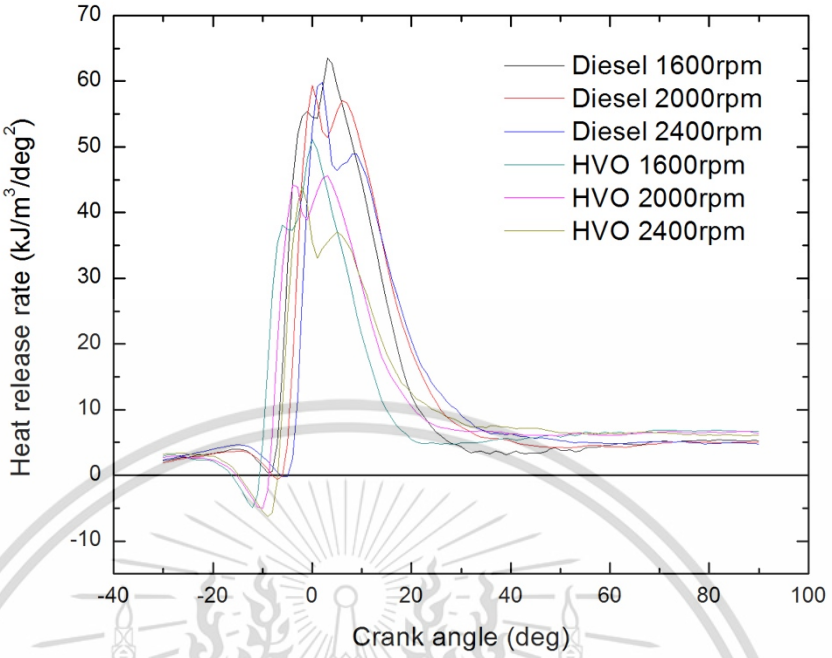

Figure 4.35 Heat release rate on different engine speed

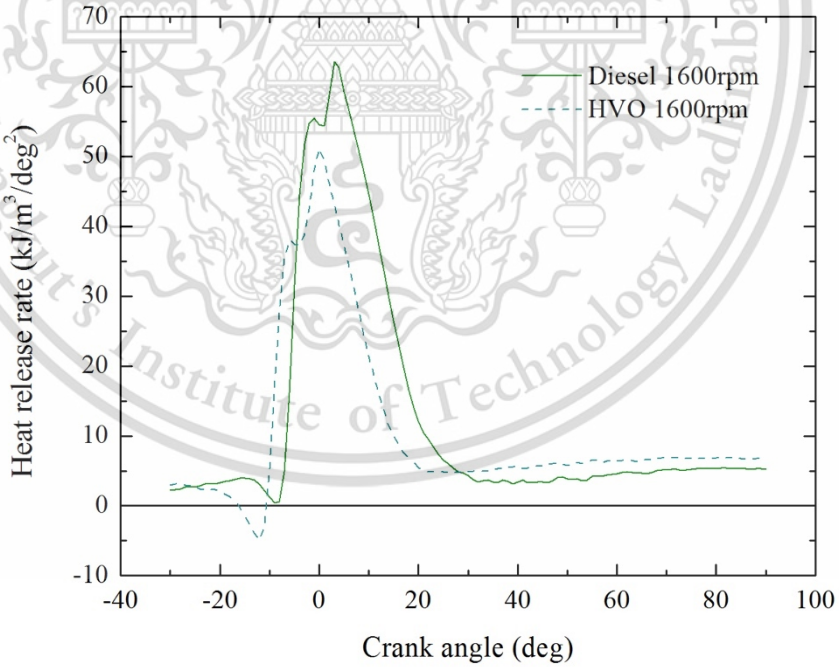

Figure 4.36 Heat release rate on 1600 rpm engine speed

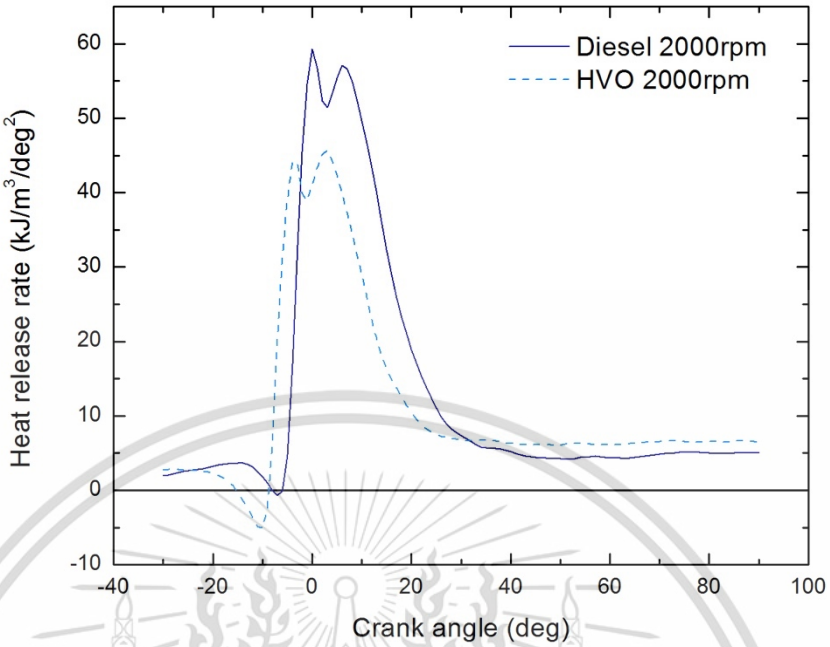

Figure 4.37 Heat release rate on 2000 rpm engine speed

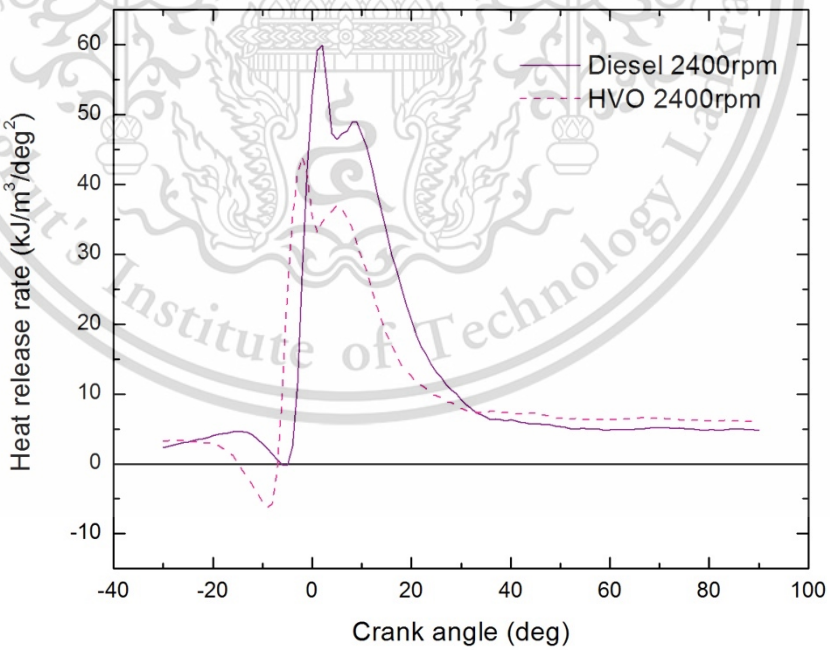

Figure 4.38 Heat release rate on 2400 rpm engine speed

4.3.4 Smoke intensity

Figure 4.39 shows a result of the previous research in smoke intensity comparison between biodiesel and diesel combustion. The study was found that the intensity be strongly dependent on the engine load. The more engine load, the greater smoke intensity due to more fuel supply for combustion. Biodiesel emits approximately 50% smoke intensity less than diesel combustion in overall operating conditions. The reason was referred as oxygen fraction in biodiesel's fuel molecules which promotes complete combustion. Surely, the smoke intensity measurement can express trends of smoke quantity, however it is difficult to interpret accurate PM's quantity since it is possible that PM covered by colorless volatile or hydrocarbon might not reflect actual measurement result.

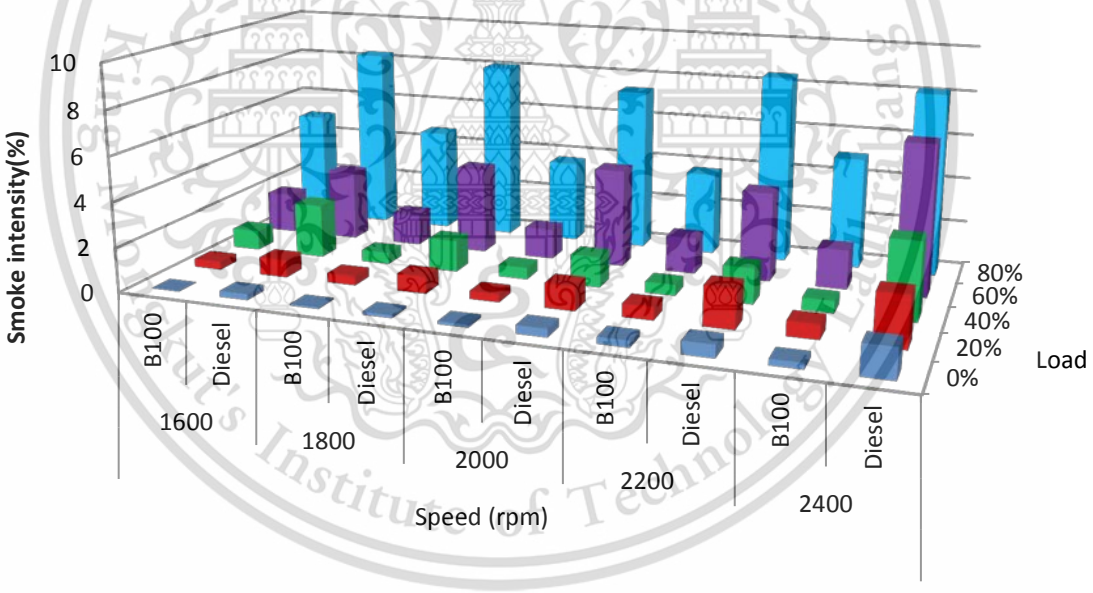

Figure 4.39 Smoke intensity comparison between diesel and biodiesel combustion (**Previous research**)

In this research, comparison of smoke intensity between HVO fuels and commercial diesel is shown as Figure 4.40 aimed to see effects of smoke intensity emission. HVO fuels produced less smoke at almost all engine operating conditions compared with commercial diesel. Average smoke reduction for HVO was approximately 50% lower than commercial diesel. It can be explained into 2 main aspects. First reason which is similar to the research in Fig. 4.39 is that more oxygen fraction in HVO plays a key role in promoting complete combustion. Second, better vaporization and mixture formation of the HVO provide enough time for better fuel atomization as well as high peak of heat release contributes better fuel-oxygen's reactivity i.e. more complete combustion.

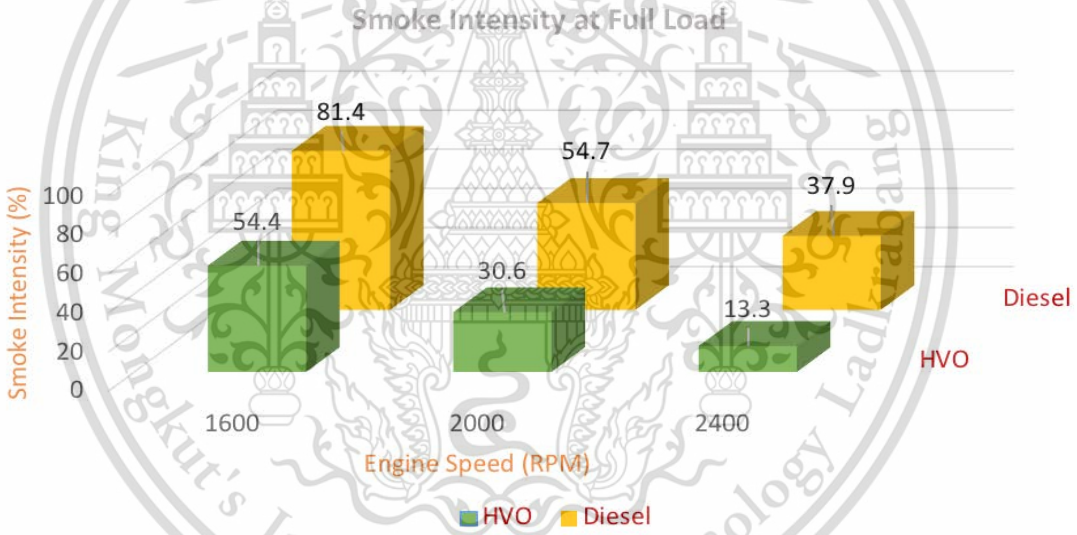

Figure 4.40 Smoke intensity comparison between diesel and HVO on different engine speed

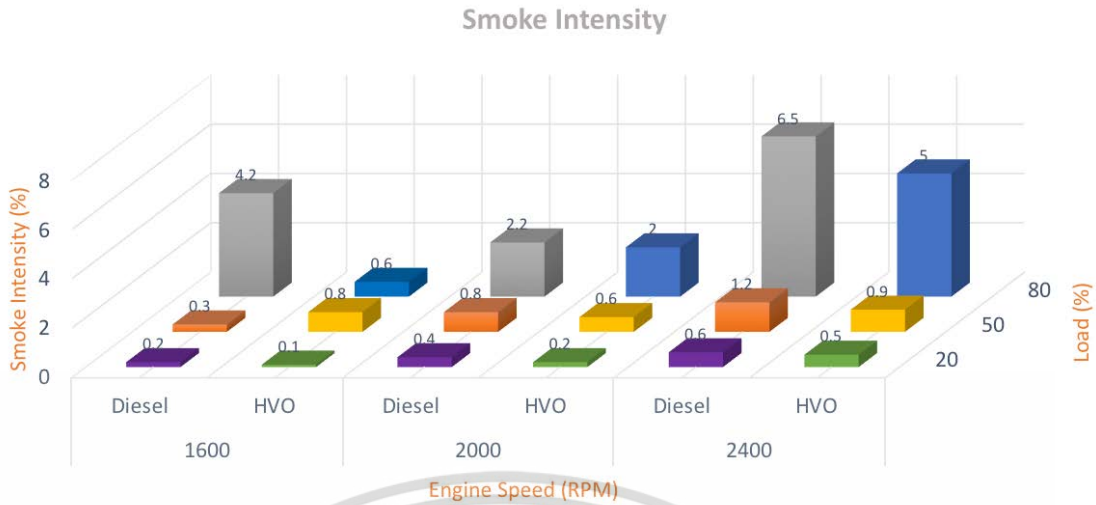

Figure 4.41 Smoke intensity comparison between diesel and HVO combustion

smoke intensities of each fuel, engine load, and engine speed. Commercial diesel emitted the highest amount of smoke. The PM reduced by HVO due to oxygenate fuel. It was clearly observed that HVO engine's particulate matter was approximately a half of conventional diesel engine's particulate matter. When increase engine load, smoke intensity increased because more fuel was supplied to the engine. For engine speed it has a little different amount of smoke due to the engine efficiency of each engine speed. The lowest amount of smoke in each engine load usually occurs around 1800-2000rpm.

In addition, when operating at high engine speed, particulate matter was increase because of shorter oxidation time in combustion period.

CHAPTER 5

CONCLUSIONS AND RECOMMENDATIONS

This research investigates the effects of Hydrotreated vegetable oil and diesel to combustion characteristics under low temperature and various ambient density conditions. A single hole injector was tested with different fuels conventional diesel and HVO. The research were carried out on a rapid compression expansion machine to simulate the condition of a CI engines as compression stroke at TDC. And investigates the effects of Hydrotreated vegetable oil and diesel to combustion characteristics with small CI engine under high, middle and low load with various engine rpm.

In a viewpoint of combustion, HVO fuel is quite compatible with diesel fuel usage for overall performance except a little performance drop at high speed and more fuel consumption. However, unique fuel properties of HVO in lower viscosity, lower surface tension, and higher heat of vaporization effect on better fuel atomization. Moreover, more oxygen content promotes more complete combustion. As a result, Smoke or PM emission from HVO can be reduced more than 50% compared with conventional diesel combustion in full load condition.

5.1 RCEM Combustion characteristic conclusions

5.1.1 Peak HVO heat release rate was lower than diesel in all test conditions due to a higher cetane number which shortened ignition delay. Decreasing ambient temperature resulted in an extended ignition delay and more premixed combustion. Increasing ambient pressure resulted in increasing the heat release rate during the diffusion combustion phase.

5.1.2 Ignition delay decreased by increasing the cetane index number. Decreasing the ambient temperature had the effect of increasing ignition delay due to. Increasing ambient pressure decreased ignition delay from oxygen entrainment due to increasing ambient density.

5.1.3 Heat release increase due to increased ambient pressure made shortens the ignition delay. This results in less combustible mixture formation, which means that the extra reactions do not have a chance to occur. Decreasing the ambient Temperature made more premixed combustion occurred in the chamber also had the effect of making the heat release rate more gradual.

5.1.4 Flame temperatures of HVO are lower than diesel in all test condition due to smaller molecular weight, lower surface tension and viscosity promote more complete combustion and effect on heat transfer of soot radiation.

5.1.5 Soot concentration decreased with HVO due to an increased cetane number. This lead to a reduction in the unburned fractions. A low distillation range of HVO improved fuel evaporation and mixing with the surrounding gas. In addition, the aromatic compounds which represent to the soot precursor are absent in HVO.

5.2 CI small engine Combustion characteristic conclusions

5.2.1 Engine Performance engine load drops as increasing engine speed for all fuels. The HVO fuel produces lower load due to lower heating value and worse air fuel mixing than diesel as well as lower stoichiometric air-fuel ratio with higher viscosity

5.2.2 Pressure and peak pressures of all fuels increase with the increasing engine load. Considering at the HVO fuel, the peak pressure lower than commercial diesel because of longer mixing-controlled combustion phase from shorten ignition delay resulted in small pressure rise as well as RCEM experiment.

5.2.3 Heat Release rate of HVO lower than commercial diesel in all test condition. The reason can be explained as; a higher cetane number making ignition delay shorter, lower distillation temperature resulted in better vaporization and mixture formation. Therefore, HVO need more time for fuel atomization.

5.2.4 Smoke intensity HVO fuels produced less smoke at almost all engine operating conditions compared with commercial diesel. Average smoke reduction for HVO was approximately 50% lower than commercial diesel.

5.3 PM morphology and Nano structure

SEM image from RCEM, The result shown that HVO fuel was significant lower average PM per focus area than conventional diesel fuel in all test condition approximately 10%

REFERENCES

Akhtar, S. (2012). Transmission Electron Microscopy of Graphene and Hydrated Biomaterial Nanostructures. Uppsala. Acta Universitatis Upsaliensis.

Atola, H., Larmi, M., Sarjovaara, T. and Mikkonen, S. (2008). Hydrotreated vegetable oil (HVO) as a renewable diesel fuel: Trade-off between NO , particulate emission, and fuel consumption of a heavy duty engine. SAE Paper No. 2008-01-2500.

Azimov, U. B., Kim, S. K., Jeong, D. S. and Lee, Y. G. (2009). Evaluation of low-temperature diesel combustion regimes with n-Heptane fuel in a constant-volume chamber. Int. J. Automotive Technology 10, 3, 265−276.

Coley, D. (2008). "Energy and Climate Change Creating a Sustainable Future, John Wiley & Sons, Ltd.

Dec, J. (1997). A conceptual model of DI diesel combustion based on laser-sheet imaging. SAE Paper No. 970873.

Dernotte, J., Hespel, C., Houille, C., Foucher, F. and Mounaim-Rousselle, C. (2012). Influence of fuel properties on the diesel injection process in nonvaporizing conditions. Atomization and Spray 22, 6, 461−492.

Diesel Engine Picture for Combustion Characteristic Experiment. Website: http://www.siamkubota.co.th/en/product/diesel-engine/250-RT-Di-Plus-Powerfully-responsive-Durable-Tough-Fuel-saving

Four stroke operating diesel cycle. Website: https://willycar.com/2014/06/08/perbedaan-direct-dan-indirect-injection/ci-engine-cycle-4-stroke-square/

Fulton, L., Lah, O. and Cuenot, F. (2013). Transport pathways for light duty vehicles: Towards a 2° scenario. Sustainability 5, 5, 1863−1874.

Gao, Y., Deng, J., Li, C., Dang F., Liao, Z., Wu, Z. and Li, L. (2009). Experimental study of the spray characteristics of biodiesel based on inedible oil, Biotechnology Advances, vol. 27, pp. 616-624.

Heywood, J. B. (1988). Internal Combustion Engine Fundamentals. 2nd edition. McGraw-Hill. New York, USA.

Hulkkonen, T., Hillamo, H., Sarjovaara, T. and Larmi, M. (2011). Experimental study of spray characteristics between hydrotreated vegetable oil (HVO) and crude oil based EN 590 diesel fuel. SAE Paper No. 2011-24-0042.

Jaroonjitsathian, S., Saisirirat, P., Sivara, K., Tongroon, M. and Chollacoop, N. (2014). Effects of GTL and HVO blended fuels on combustion and exhaust

emissions of a common-rail DI diesel technology. SAE Paper No. 2014-01-2763.

Jung, S., Ishida, M., Yamamoto, S. and Sukaguchi, D. (2010). Enhancement of NO - PM trade-off in a diesel engine adopting bio-ethanol and EGR. Int. J. Automotive Technology 11, 5, 611−615.

Kittelson, D.B. (1998). Engines and nanoparticles: a review. Journal of Aerosal Science. 29: p. 575-588.

Kobori, S. and Kamimoto, T. (1995). Development of a rapid compression-expansion machine simulating diesel combustion. SAE Paper No. 952514.

Kook, S., Bae, C., Miles, P., Choi, D. and Pickett, L. M. (2005). The influence of charge dilution and injection timing on low-temperature diesel combustion and emissions. SAE Paper No. 2005-01-3837.

Kosaka, H. (2015). Lecture slide Advance of Internal combustion engine for TAIST Automotive Engineering Course, NSTDA, Thailand.

Majewski, W.A. (2001). Diesel Particulate Filters. www.DieselNet.com. Copyright © Ecopoint Inc. Revision 2001.07b.

Mohan, B., Yang, W., Tay, K.L. and Yu, W. (2014). Experimental study of spray characteristics of biodiesel derived from waste cooking oil, Energy Conversion and Management, vol.88, pp. 622-632.

Munsin, R., Laoonual, Y., Jugjai, S., Matsuki, M. and Kosaka, H. (2012). Investigation of effects of ignition improvers on ignition delay time of ethanol combustion with rapid compression and expansion machine. SAE Paper No. 2012-01-0854.

Nguyen, D.N., Ishida, H., and Shioji, M. (2010). Ignition and Combustion Characteristics of Gas-to-Liquid Fuels for Different Ambient Pressures.

No, S. (2014). Application of hydrotreated vegetable oil from triglyceride-based biomass to CI engines – A review. Fuel, 115, 88−96.

Oo C.W., Shioji, M., Nakao, S., Dung, N.N., Reksowardojo, I., Roces, S.A. and Dugos, N.P. (2015). Ignition and combustion characteristics of various biodiesel fuels (BDFs), Fuel, vol. 158, pp. 279-287.

Pulkrabek, W. (2014). Engineering fundamentals of the internal combustion engine. 2nd edition. Pearson education limited. London.

Qi, D.H., Chen H., Geng L.M., and Bian, Y. ZH. (2010). Experimental studies on the combustion characteristics and performance of a direct injection engine fueled

with biodiesel/diesel blends, Energy Conversion and Management, vol. 51, pp. 2985-2992.

Rantanen, L., Linnaila, R., Aakko, P. and Harju, T. (2005). Hydrotreated NExBTL-Biodiesel fuel of the second generation. SAE Paper No. 2005-01-3771.

Sugiyama, K., Goto, I., Kitano, K., Mogi, K. and Honkanen, M. (2011). Effects of hydrotreated vegetable oil (HVO) as renewable diesel fuel on combustion and exhaust emissions in diesel engine. SAE Paper No. 2011-01-1954.

Oo C.W., Shioji, M., Nakao, S., Dung, N.N., Reksowardojo, I., Roces, S.A. and Dugos, N.P. (2015). Ignition and combustion characteristics of various biodiesel fuels (BDFs), Fuel, vol. 158, pp. 279-287.

Nguyen, D.N., Ishida, H., and Shioji, M. (2010). Ignition and Combustion Characteristics of Gas-to-Liquid Fuels for Different Ambient Pressures.

Pierpont, D., Montgomery, D. and Reitz, R. (1995). Reducing particulate and NO using multiple injections and EGR in a D.I. diesel. SAE Paper No. 950217.

APPENDIX A

EXPERIMENTAL PRESSURE SENSOR SPECIFICATION

Pressure

KISTLER
measure. analyze. innovate.

Miniature Measuring Probe

Type 6053CC...

for Non-Cooled Cylinder Pressure Measurement, M5 Thread

Patent No. US 6,105,434

The miniature measuring probe with very small dimensions and M5x0,5 mounting thread is particularly suitable for direct installation in small-capacity combustion engines with more than two valves per cylinder. The measuring element is identical to the standard sensor Type 6052C... .

- Good temperature stability of the sensitivity
- Acceleration-compensated
- Needs only 6 mm mounting bore
- Low thermal shock error and long life thanks to the front seal
- Very high sensitivity

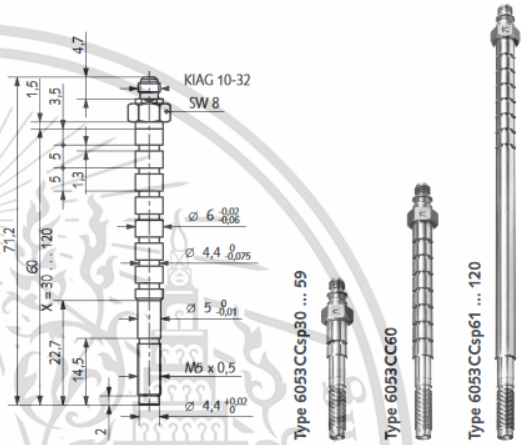

Description

Type 6053CC... uses a new type of PiezoStar® crystal which achieves high sensitivity in conjunction with an extremely small sensor structure. The sensitivity drifts by a maximum of ±0,5 % over the temperature range of 200 ±50 °C. The passive acceleration compensation patented by Kistler keeps the influence of engine vibrations to a minimum.

The front seal allows very good heat dissipation and thus briefly a maximum operating temperature of 400 °C. The diaphragm, optimized by finite element calculation, produces good measuring results and ensures a long service life.
The shape of the probe allows mounting with a very small access bore. The cable connection has to be outside the cylinderhead, in an area free of oil mist. O-rings also permit mounting through coolant passages. The probe can be manufactured in custom lengths between 30 and 120 mm.

Application

The sensor Type 6053CC... is an excellent all-rounder. Its rugged construction makes it suitable for measurements at the knock limit as well as for thermodynamic investigations. This sensor is used mainly on multi-valve engines, motor cycle and other small engines and for combustion analysis.
This sensor should be used when there is insufficient mounting space available for the Type 6052C... .
At high speeds (vibrations), the Type 6053CC...U40 should be used. For applications mainly in the knocking range or at very high peak pressures, use of Type 6053CC...U20 with reinforced diaphragm (heavy duty version) is recommended.
The probe is supplied without a cable. See Accessories for the various cables available for different applications.

Technical Data

Measuring range	bar	0 ... 250
Calibrated sub-ranges	bar	0 ... 50, 0 ... 100, 0 ... 150, 0 ... 250
Overload	bar	300
Sensitivity	pC/bar	≈–20
Natural frequency, nominal	kHz	≈160
Linearity in all ranges (at 23 °C)	%/FSO	≤±0,3
Acceleration sensitivity		
axial	bar/g	<0,0002
radial	bar/g	<0,0005
Operating temperature range	°C	–20 ... 350
Temperature min./max	°C	–50 ... 400
Connector	°C	200

KISTLER
measure. analyze. innovate.

Technical Data (Continuation)

Sensitivity change		
200 °C ±50 °C	%	≈±0,5
23 ... 350 °C	%	≤±2
Thermal shock error		
(at 1 500 1/min Δp_{mi} = 9 bar)		
Δp_{mi} (short time drift)	bar	≤±0,5
Δp_{mi}	%	<±2
Δp_{max}	%	<±1
Insulation resistance		
at 23 °C	Ω	$>10^{13}$
Shock resistance	g	2 000
Tightening torque	N·m	1,5
Capacity		
Weight (Type 6053CC60)	g	10
Connector (PTFE)	–	KIAG 10-32

Type 6053CC...U20 (other specification as for Type 6053CC...)

Measuring range	bar	0 ... 300
Calibrated partial ranges	bar	0 ... 100, 0 ... 200, 0 ... 300
Overload	bar	350
Acceleration sensitivity		
axial	bar/g	<0,0005
radial	bar/g	<0,0005
Thermal shock error		
(at 1 500 1/min, p_{mi} = 9 bar)		
Δp (short time drift)	bar	≤±0,7
Δp_{mi}	%	≤±3
Δp_{max}	%	≤±1,5

Type 6053CC...U40 (other specification as for Type 6053C...)

Calibrated partial ranges	bar	0 ... 100, 0 ... 200, 0 ...250
Operating temperature range	°C	–20 ... 200
Temperature min./max.		–50 ... 200
Sensitivity shift		
23 ... 200 °C	%	≤±2

Mounting

Direct mounting:
Sensor Type 6053CC... can be mounted directly in the cylinder head, see Fig. 1. Machining of the bore must correspond exactly to the bore specifications shown in Fig. 2.

The Kistler tools:
Step drill Type 1300A53
Special tap Type 1357A and the
Finishing tool for bore Type 1300A79 or 1300A79Q01
must be used in order to comply with the tolerances required. The bore must be machined in one clamping. Before mounting the sensor, the sealing surface in particular must be checked; use of the finishing tool (reamer) Type 1300A79 is mandatory. When mounting the sensor, it is essential to comply with the tightening torque of 1,5 N·m. The sensor should therefore be mounted with the torque wrench Type 1300A17. You will find additional information for machining the bore and mounting in the instruction manual. Your Kistler distributor will provide you with information, for example concerning the preferred position of the indicating bore in the combustion chamber.
The shape of the probe and O-ring sealing allow mounting through coolant passages (see Figure 1). Reliable sealing requires a bore diameter of $6^{+0.03}_{+0.01}$, which can also be achieved with the drill Type 1300A53.

Mounting sleeve:
When space allows or if the water jacket of the cylinder head will be breached, a mounting sleeve Type 6525AQ... is recommended. Mounting sleeves are manufactured to customer requirements. An additional advantage of mounting sleeves is that the actual sensor bore in the sleeve can be very precisely machined. On request, Kistler will provide drawings for your particular mounting situation.

COMBUSTION EXPERIMENTAL PRESSURE SENSOR SPECIFICATION

GU22CK

TIGG1355A.01

★★ ★★ ★★

The GU22CK is an accurate and robust 6.2 mm plug-type sensor. It is based on a well established design concept that allows high accuracy. It has thermally optimized piezoelectric elements and no influence from the mounting bore on the pressure signal due to minimized mechanical contact between mounting bore and the sensor housing. A thermo protection can improve the cyclic drift down to ± 0.3 bar. The sensor is equipped with built in SID for SDM.

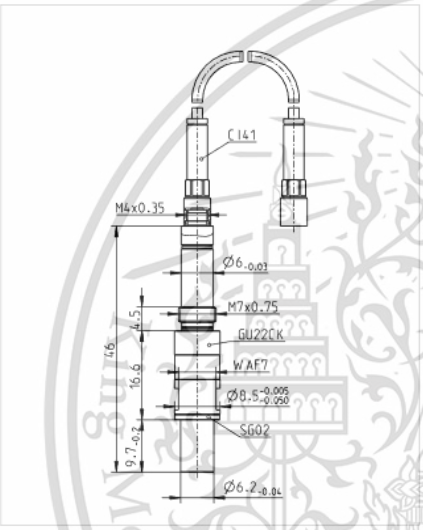

Scope of Supply

- Sensor GU22CK
- Piezo-input cable CI41-1
- Coupling CC41
- Gasket SG02
- Accessory kit (protection cap + 2 spare O-rings)
- Spare gasket SG02
- Calibration sheet
- Documentation

Specifications

Measuring range			0 ... 350 bar	
Overload			400 bar	
Sensitivity			34 pC/bar	nominal
Linearity	≤	±	0.3 %	FSO
Calibrated ranges			0 ... 80 bar 0 ... 150 bar 0 ... 300 bar	
Natural frequency			96 kHz	
Acceleration sensitivity	≤		0.001 bar/g	axial
Shock resistance	≥		2000 g	
Insulation resistance	≥		10^{13} Ω	
Capacitance			8 pF	
Operating temperature range (1)			- 40 ... 400°C	
Thermal sensitivity change	≤		1 %	20 ... 400 °C and 0 ... 300 bar
	≤	±	0.25 %	250 ± 100 °C and 0 ... 300 bar typ.
Load change drift			1.5 mbar/ms	max. gradient typ.
Cyclic temperature drift (2)	≤	±	0.6 bar	
Thermo shock error Δp (3)	≤	±	0.3 bar	typ.
Mounting bore			6.3 mm	shoulder sealed
Cable connection			M4 x 0.35	negative
Weight			12.5 grams	without cable
Mounting torque			10 Nm	

COMBUSTION EXPERIMENTAL HIGH SPEED VDO CAMERA

SPECIFICATION

Image Technology

the most experienced name in high speed cameras

MEMRECAM GX-1

High Speed Camera System

The Memrecam GX series: The workhorse family of ruggedized 1.3 Mega Pixel high speed camera systems.

Memrecam GX-1 FEATURES

CMOS Sensor: 1280 X 1024 — all Active Pixels

Bit Depth: 12/10/8-bit (customer selectable)

Electronic Shutter: OPEN to 1µsec

Variable Framing Profile: Test using a variety of frame rates, sequentially or in parallel.

Versatile Recording: Burst, multi-trigger and image trigger.

Multi-Camera Download: Download images from up to seven cameras simultaneously in same time it takes to download a single camera.

Hi-G Operation: Specifically designed to function effectively in Hi-G environments (to 100G shock).

Ultra-High Light Sensitivity

Ruggedized for Range Use: Sealed camera core, uses no fans.

NAC's Memrecam GX-1 boasts a 1.3 Mega Pixel sensor and the most light sensitive images in its class. The Memrecam GX-1 supports wide screen viewing of critical high-speed imaging events, keeping the subject in frame longer. The Memerecam GX-1 records brilliant color images or crisp monochrome images at full 1.3 Mega Pixel resolution at more than to 2,000 fps, 1 Mega Pixel resolution at more than 2,550 fps and 720p HD resolution at more than 2,780 fps.

The rugged Hi-G GX-1 is perfect for a variety of applications, including: Automotive Crash, Ballistics, Combustion, Materials Research, Machine Design, Microscopy, PIV, Flow Visualization, Spray Analysis, and many more...

When it comes to reliable, high-quality, high-speed camera systems, make the proven choice with NAC and you'll see the visible difference!

MEMRECAM GX-1
High Speed Camera System

Memrecam GX-1 Full Screen Mode		
Max Res (pixels)	1280 X 1024	
Optical Format	35.57 mm	
fps @ Max Res	2,078	
Gpix/ sec @ Max Res	2.72	
	Mono	Color
ISO Rating	20,000	5,000
Memory Options	2GB, 4GB, 8GB	
Max fps	245,098	

Imaging Formats	Max fps @ Full Res.
1 Mega Pixel	2,559
1280 X 720	2,789
XGA (1024 X 768)	3,293
768 X 768	4,359
768 X 576	5,477
VGA (640 X 480)	7,485
512 X 512	8,831
512 X 384	10,837
QVGA (320 X 240)	22,371
256 X 192	30,600
128 X 96	69,444
64 X 64	117,371
64 X 32	128,866

APPENDIX B

PUBLICATION SETC 2017

JSAE 20179094 / SAE 2017-32-0094

Impact of Biodiesel on Small CI Engine Combustion Behavior and Particle Emission Characteristic

Preechar Karin, Park Watanawongskorn, Jiramed Boonsakda
Eakkawut Saenkhumvong, Sippakorn Rungsritanapaisan, Settavit Srivarocha
Chinda Charoenphonphanich
King Mongkut's Institute of Technology Ladkrabang

Nuwong Chollacoop
National Science and Technology Development Agency

Katsunori Hanamura
Tokyo Institute of Technology

ABSTRACT

Diesel engines are high thermal efficiency because of high compression ratio but produce high concentration of particulate matter (PM) because of direct injection fuel diffusion combustion. PM must be removed from the exhaust gas to protect human health. This research describes biodiesel engine performance, efficiency and combustion behavior using combustion pressure analyzer. It was clearly observed that PM emitted from CI engines can be reduced by using renewable bio-oxygenated fuels. The morphology and nanostructure of fossil fuel and biofuel PMs were investigated by using a Scanning electron microscopy (SEM) and Transmission electron microscopy (TEM). The morphology of biodiesel and diesel doesn't have much different in the viewpoint of particulate matter trapping using DPF micro surface pores. The agglomerated ultrafine particles and primary nanoparticles sizes of diesel and biodiesel engine's PM are approximately 50-500 nm and 20-50 nm, respectively. The primary particle of biodiesel engine's PM is smaller than that of fossil diesel. The average of diesel and biodiesel PM's carbon platelets is in the range of 0.2-5.2 nm.

INTRODUCTION

Diesel engines are considered as one of the highest thermal efficiency engines among internal combustion engines (ICE) [1]. However, a major disadvantage is particulate matter (PM) emission which is harmful to human body and environment. Biofuels, such as biodiesel or ethanol, have been often discussed as alternatives for diesel fuel replacement since they are obtained from renewable sources and their benefits in emission reduction. Biodiesel consists of alkyl monoesters of fatty acids derived from vegetable oil or animal fats. Due to its similar physical properties to diesel fuel, there is no need to modify the engine when the engine is fueled with the blends [2-4]. In terms of engine performance and emission, many researchers have investigated effects of biodiesel fuel on diesel engines. M.M. Hasan *et al*. [5] investigated effects of biodiesel by blending with the maximum blend ratio of 30% biodiesel. Operated with a single-cylinder diesel engine, brake thermal efficiency of the blends was similar to diesel base fuel. There was a decrease of nitrogen oxides and smoke emission, while maximum heat release rate and maximum pressure for the blends at higher load were increased. Mohanad *et al*. [6-7] conducted investigations of a 4-cylinder diesel engine powered by rapeseed biodiesel blend. They showed that ignition delay increased for higher cetane number. Sakthivel *et al*. [8] studied performance, emission, and combustion characteristics of a diesel engine, injection timing is a major parameter that sensitively affects the engine performance, emission and durability. The brake thermal efficiency for B20 was higher compared to diesel in the entire load. The ignition delay and combustion duration were shorter for biodiesel than diesel which results in lower heat release rate, peak pressure and rate of pressure rise. Retardation of injection timing caused decrease in emission and combustion parameters like Oxides of Nitrogen (NO_x), Hydrocarbon (HC) and Carbon Monoxide (CO), peak pressure, ignition delay, combustion duration and heat release rate which increased with advancement in injection timing. An according research from Guven *et al*. [9] showed that biodiesel blends caused decrease in maximum pressure and heat release rate and retarded further far away from top dead center.

Diesel particulate matters consist of a solid fraction and a soluble organic fraction (SOF). Primary particles of the PMs, composed of carbon and metallic ash, are coated with SOF and sulfate. The mean diameter of primary particles is usually in the range of 20-80 nm. Agglomerated particles are an assembly of primary particles and surface area does not differ appreciable from the sum of specific surface areas of primary particles. Agglomerated particle size is normally 80-300 nm [10]. Scanning Electron Microscope (SEM) and Transmission Electron Microscope (TEM) observation of PMs have been conducted by several researchers [11]. A

primary soot particle has two distinct parts; an inner core and an outer shell [12-13]. Generally, a primary particle from ICE has only one core with concentric fringe pattern which is hard to be distinguished as inner core or outer shell [14]. Size distributions of diesel engine's PMs have been categorized as PM10, diameter (D) < 10 micron; fine particles, D < 2.5 micron; ultrafine particles, D < 0.1 micron; and nanoparticles, D < 0.05 micron or 50 nm. [15].

METHODOLOGY

Table 1. Engine specification.

Items	Details
Engine type	1-cylinder, Natural aspirated, Direct injection, Compression Ignition Engine
Bore x Stroke	97 mm x 96mm
Displacement	709 cm3
Compression ratio	18:1
Rated power	9.2 kW @ 2400 rpm
Injection timing	19° CA bTDC
Injection pressure	22 MPa

Table 2. Fuel properties.

Properties	Diesel	Biodiesel
Chemical formula	$C_{14.2}H_{28}$	$C_{14.9}H_{29.9}O_{1.9}$
Carbon (% mass)	85.1	74.5
Hydrogen (% mass)	14.0	12.5
Oxygen (% mass)	0.9	13.0
Auto ignition temp (°C)	288	294
Calorific value (kJ/kg)	46,180	39,525
Heat of vaporization (kJ/kg)	250	300
Viscosity @ 40°C (mm^2/s)	3.0	4.5
Density @ 25°C (kg/m^3)	844.8	875.3
Stoichiometric air fuel ratio	14.7	12.3
Distillation (°C)		
T10	214.3	336.2
T30	250.3	339.7
T50	281.5	341.4
T70	312.5	345.4
T90	352.3	351.2

The experiment was carried out on a 1-cylinder natural aspirated, direct injection, displacement of 709 cm3, compression ratio of 18:1, diesel engine. Fuel injection system was not modified (mechanical fuel injection system). Engine specification was represented in Table 1. The engine was coupled with an eddy-current dynamometer and a control system to adjust engine speed and engine load. Fuel supply system was set with a weight scale to measure fuel consumption. For parameter analysis in the combustion chamber, pressure versus crank angle data were measured by a piezoelectric sensor (Kistler 6052C31, 250Bar, sensitivity: ±0.5%) and a crank angle encoder (CA-RIE-360, resolution: 360 pulses/rev.). Signals of the cylinder pressure were recorded with one-degree resolution of crank angle. For further statistical analysis, two hundred engine cycles were recorded with three repeats. The pressure signals then were amplified with the data acquisition equipment (DEWESoft SIRIUSi-HS-CA) to obtain heat release rate.

The fuels used in this research include commercial diesel and biodiesel (B100). The commercial diesel contains approximately 5% biodiesel due to the regulation while the biodiesel was produced from palm-olein (B100-TIS2313-2549). Fuels properties are shown in Table 2. Biodiesel is more homogeneous molecules which shown by vaporize temperature. It is very narrow and very high around 610 to 620 Kelvin. This implies that biodiesel has higher heat of vaporization. Engine performance curve, brake specific fuel consumption (BSFC) and brake thermal efficiency (BTE) were measured to see overview effects of biodiesel compared with commercial diesel. In-cylinder pressure, net heat release rate, and accumulative heat release from selected engine operating conditions were then recorded to see combustion characteristics.

PM's quantity was measured by an opacity diesel smoke meter (OKUDA DSM-240, 0-100%, ±3% accuracy) which optically evaluate soot collected on paper filters by light reflection method. PM powder was collected by using an in-house metal-net particle collector to investigate morphology and nanostructures by using scanning electron microscopy (FE-SEM: Hitachi SU5000), and transmission electron microscopy (TEM: JEOL JEM-2100Plus)

RESULTS AND DISCUSSION

Combustion Characteristics

The engine performance curve of diesel and biodiesel is plotted in Fig. 1 (a). Engine load decreases as increasing engine speed for all fuels. Brake specific fuel consumption (BSFC) and Brake thermal efficiency (BTE) are shown in Fig. 1 (b) and (c), respectively. BSFC of the biodiesel are higher than that of diesel at all load conditions due mainly to the lower calorific value. Thus, the amount of fuel supply into the engine must be greater. The trend shows decrease in the BSFC as the engine load increase. It can be explained as; when the engine load increases, combustion temperature which is implied from the rise of Exhaust gas temperature (EGT) as shown in Fig. 1 (d) increases as well. Reactivity of fuel and oxygen activates conversion of combustion heat to mechanical work much more than amount of energy from the fuel input. That is why the BSFC decreases as the engine load increases. BTE plots show that as the engine load increases, the engine produces more thermal efficiency for both fuels. The BTE of biodiesel is higher than diesel at all load condition because the fuel properties such as more oxygen fraction could promote complete combustion which biodiesel could reach optimum BTE at less load compared with diesel.

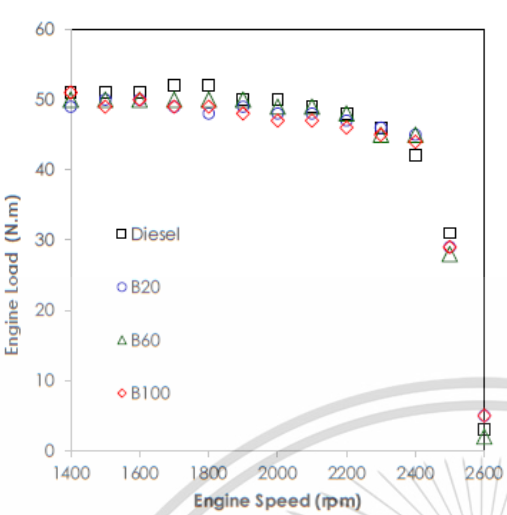

(a) Engine performance

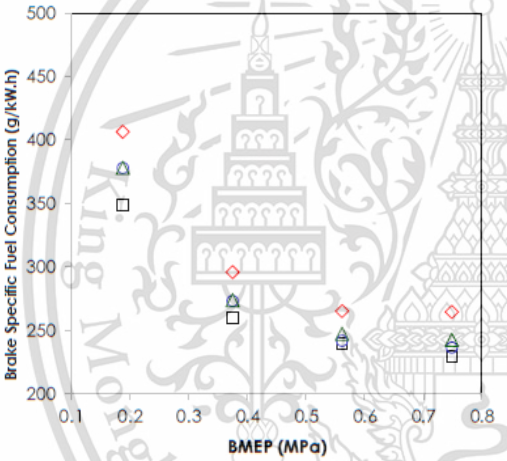

(b) Fuel consumption

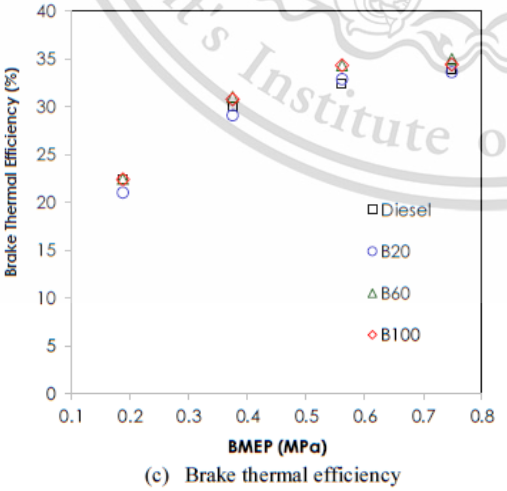

(c) Brake thermal efficiency

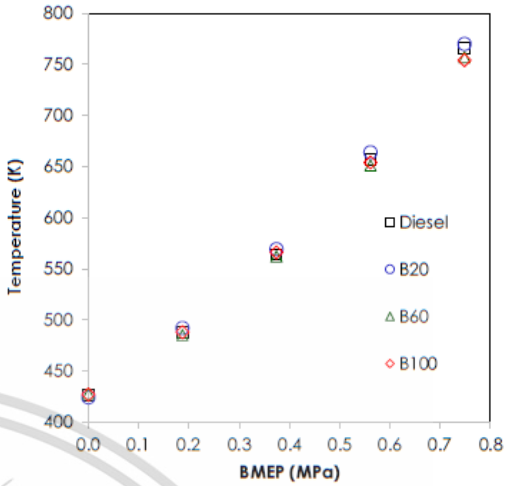

(d) Exhaust gas temperature

Figure 1. (a) Engine performance, (b) Brake specific fuel consumption (BSFC), (c) Brake thermal efficiency (BTE), and (d) Exhaust gas temperature (EGT) at the engine speed of 2000 rpm.

In-cylinder pressure variation with respect to crank angle is shown in Fig. 2, and heat release rate in Fig. 3. The engine load was varied in the range of 0.2 MPa, 0.4 MPa, and 0.6 MPa at constant engine speed of 2400 rpm. Peak pressures of all fuels increase with the increasing engine load. Considering the biodiesel at 0.2 MPa and 0.4 MPa BMEP load, the pressure rises of biodiesel before reaching peak pressure occurs prior to the diesel. This is the effect of higher oxygen fraction in fuel promote faster combustion. At higher engine load, the increase of combustion temperature cause better fuel vaporization for both fuels, so there is no significant in pressure rise with respect to crank angle.

Heat release rate plots show that combustion processes of all fuels start with ignition delay, premixed combustion phase, and followed by diffusion combustion phase. At same start of injection of 19° CA bTDC in the condition of 0.2 MPa and 0.4 MPa BMEP load, biodiesel has shorter ignition delay, while a higher peak of the heat release can be observed on diesel on all load conditions. From fuel properties of biodiesel, density and auto ignition temperature was negative impact with shorter ignition delay, so oxygen fraction is that mainly effects of shorter ignition delay than diesel fuel. The reason is that low temperature in the low load condition with higher oxygen fraction causes the biodiesel start combustion earlier. However, longer ignition delay in diesel causes enough fuel atomization and mixing with oxygen, so it produces higher peaks of heat release rate. In addition, it is also well-known that the high bulk modulus of the biodiesel makes the injection timing earlier in the case of mechanical injection system, which may advance the auto-ignition timing.

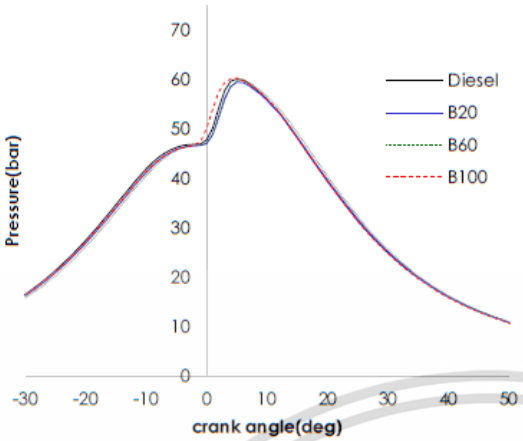

(a) 0.2 MPa BMEP

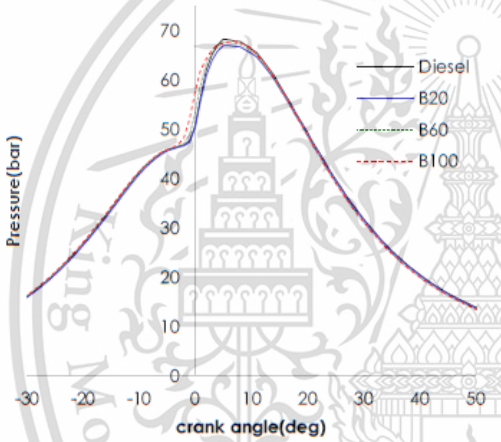

(b) 0.4 MPa BMEP

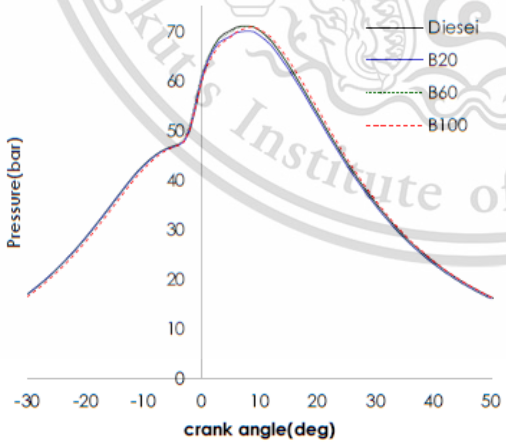

(c) 0.6 MPa BMEP

Figure 2. In-cylinder pressure versus crank angle at engine speed of 2400 rpm, (a) 0.2 MPa BMEP, (b) 0.4 MPa BMEP and (c) 0.6 MPa BMEP.

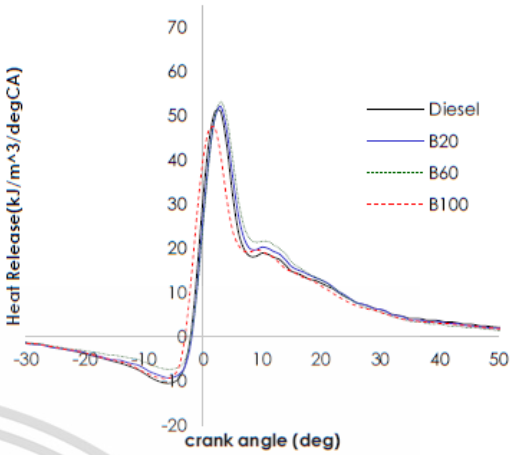

(a) 0.2 MPa BMEP

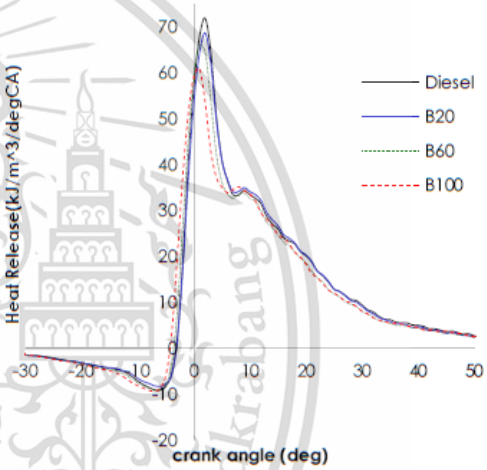

(b) 0.4 MPa BMEP

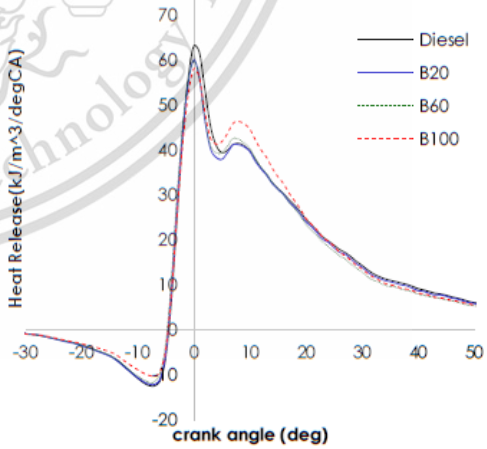

(c) 0.6 MPa BMEP

Figure 3. Heat release rate versus crank angle at engine speed of 2400 rpm, (a) 0.2 MPa BMEP, (b) 0.4 MPa BMEP and (c) 0.6 MPa BMEP.

SETC2017

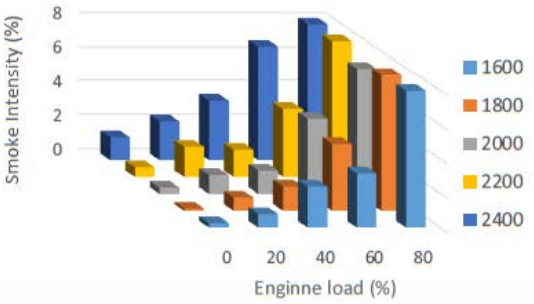

(a) Diesel engine's particulate matter

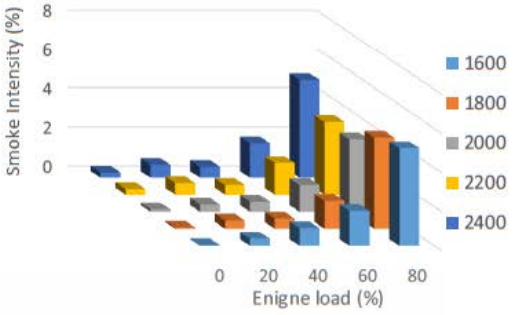

(d) B100 engine's particulate matter

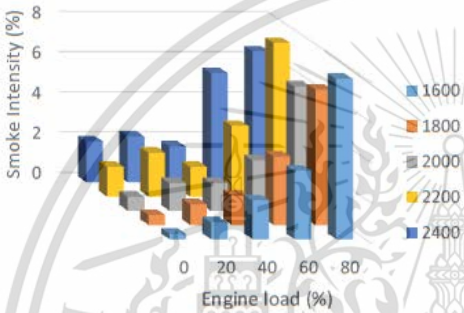

(b) B20 engine's particulate matter

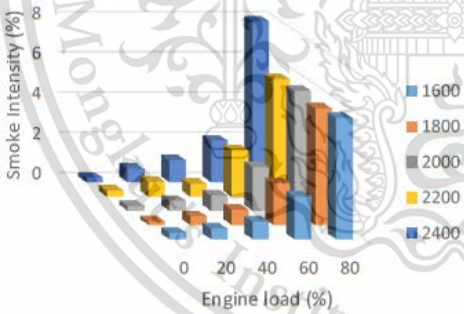

(c) B60 engine's particulate matter

Figure 4. Quantity of (a) diesel (b) B20 (c) B60 and (d) B100 engine's PM using opacity smoke meter in each engine load and engine speed operation condition.

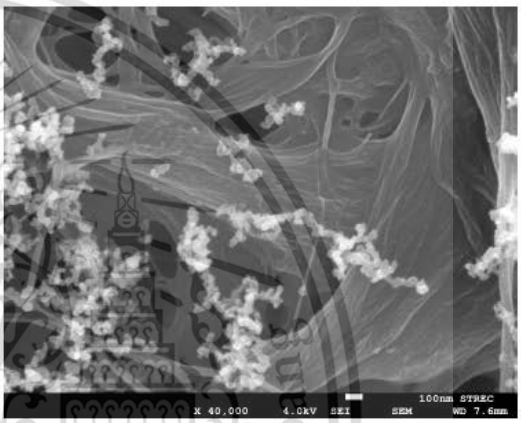

Figure 5. SEM image of diesel engine's fine particle emission in the condition of 80% load engine operation.

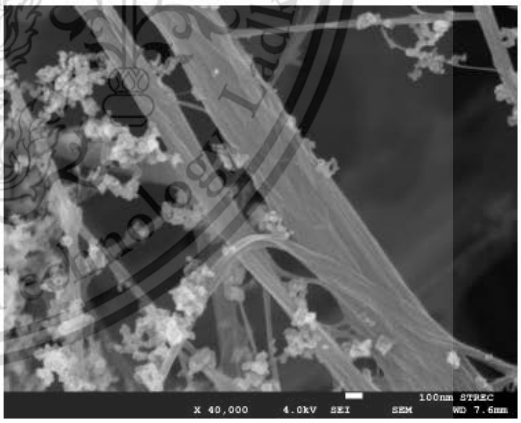

Figure 6. SEM image of B100 engine's fine particle emission in the condition of 80% load engine operation.

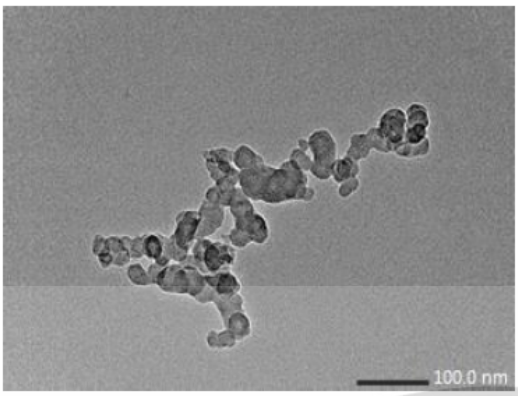

Figure 7. TEM image of diesel ultrafine particle emission in condition 80% load operation.

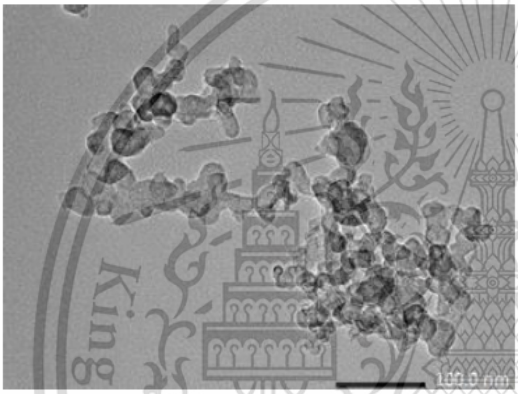

Figure 8. TEM image of B100 ultrafine particle emission in condition 80% load operation.

Particle Emission Characteristics

Figure 4 shows measurement results of smoke intensity which is an indirect method to estimate PM's quantity. The intensity is strongly dependent on the engine load. The more engine load, the greater smoke intensity due to more fuel supply for combustion. In this research, much amount of particle was used to determine the integrity of combustion process. The biodiesel produces less smoke than the diesel at almost all engine operating conditions because oxygenated fuel promote more complete combustion and better fuel-oxygen's reactivity.

Morphology and nanostructure of the PM were investigated by electron microscopy. Some PM's types were found on the paper filters such as fine particles and ultrafine particles. Ultrafine particles of diesel and biodiesel engine's PM consist of many single nanoparticles. Figure 5 and 6 show fine particle of diesel and biodiesel in the condition of 80% (engine torque of 38 Nm) load engine operation, respectively.

Agglomerated ultrafine particles of diesel and biodiesel engine's PM was also clearly observed using TEM as shown in Fig. 7 and 8, respectively. The average agglomerated ultrafine particle diameter size are in the range of 50-500 nm. Primary nanoparticles of diesel and biodiesel engines was also clearly observed using TEM as shown in Fig. 9 and 10, respectively. The average primary nanoparticle diameter size are in the range of 20-50 nm. Each carbon platelet in the inner core and outer shell of primary nanoparticle was also clearly observed by TEM.

Moreover, TEM image is used for numerate platelet number that aggregate layered in the particle. Each of platelet is consisted properly by carbon atom from incomplete combustion product. Figures 11, 12 and 13 are the images of original 10 nm^2 focused area, after post processing of two colors and after post processing of skeleton carbon platelet length estimation of diesel fuel. Figures14, 15 and 16 are the images of original 10 nm^2 focused area, after post processing of two colors and after post processing of skeleton carbon platelet length estimation of biodiesel, respectively. From the skeleton images, the carbon platelets inside the PM were measured by image processing program. The skeleton carbon platelets, which have 1-unit pixel width for each platelet, were measured for the white area in the image to be a carbon platelet length. The estimated of platelet sizes distribution in each condition are shown in Fig.17 and 18. The average of diesel and B100 PM carbon platelets is in the range of 0.2-5.2 nm.

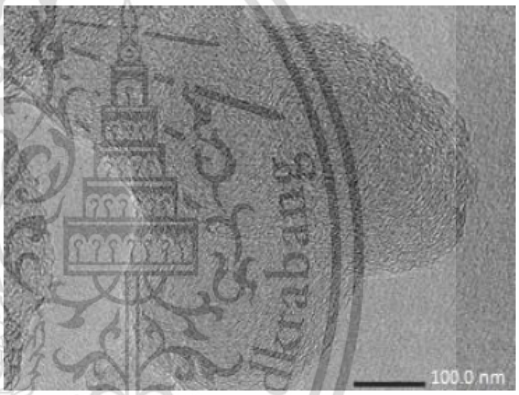

Figure 9. TEM image of diesel primary nanoparticle emission in condition 80% load operation.

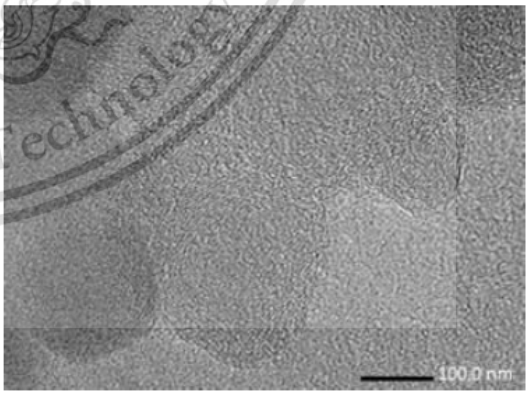

Figure 10. TEM image of B100 primary nanoparticle emission in condition 80% load operation.

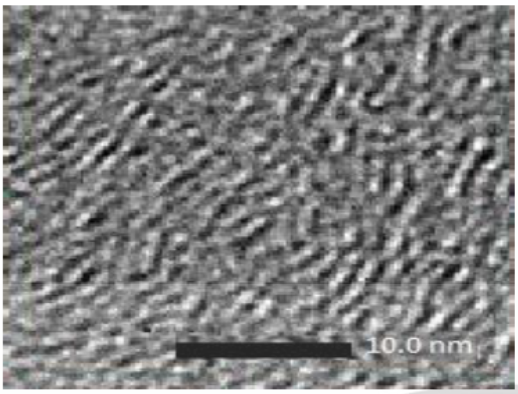

Figure 11. TEM images of engine 80% load operation diesel single PMs.

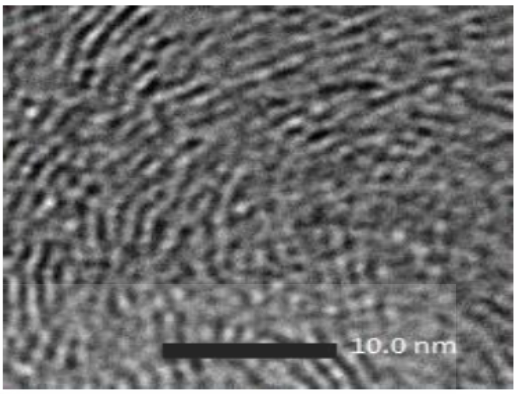

Figure 14. TEM images of engine 80% load operation B100 single PMs.

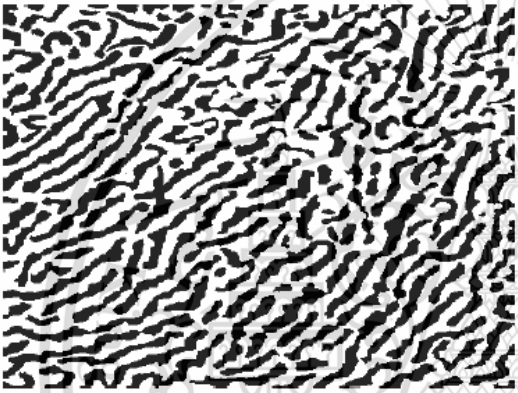

Figure 12. Two colors TEM images post process of engine 80% load operation diesel single PMs 10nm^2 focused area.

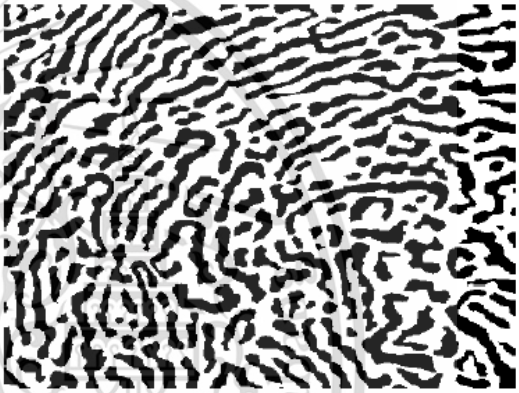

Figure 15. Two colors TEM images post process of engine 80% load operation B100 single PMs 10nm^2 focused area.

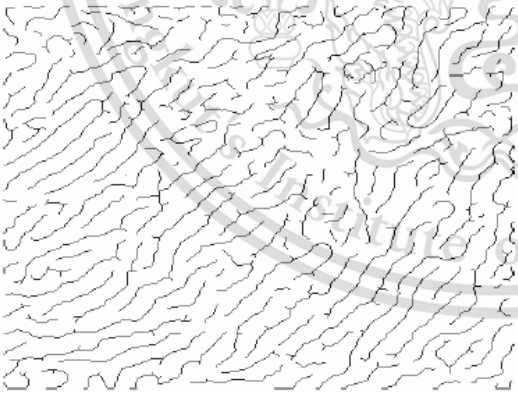

Figure 13. Skeleton TEM images post process of engine 80% load operation diesel single PMs 10nm^2 focused area.

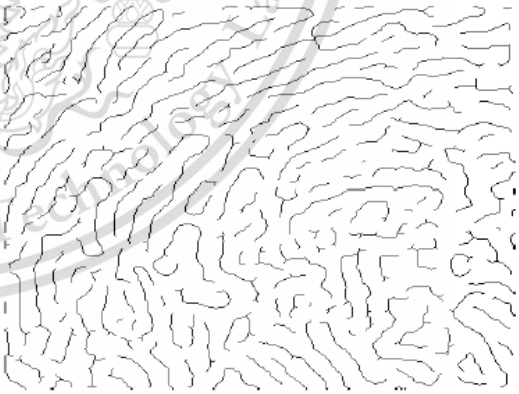

Figure 16. Skeleton TEM images post process of engine 80% load operation B100 single PMs 10nm^2 focused area.

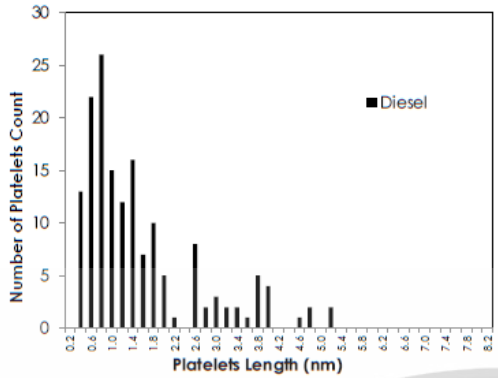

Figure 17. Platelet sizes distribution of diesel PM's carbon platelets.

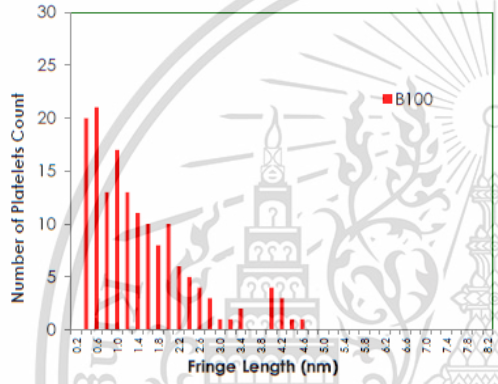

Figure 18. Platelet sizes distribution of B100 PM's carbon platelets.

CONCLUSIONS

The amount of particulate matter emitted from CI engine depend on several variables. The result shows the parameter which has the highest effect on PM quantity is engine load, concentration of biodiesel and engine speed respectively. When increase concentration of biodiesel in fuel, PM reduce because oxygen concentration in fuel increase. Higher concentration of oxygen makes more complete combustion and higher thermal efficiency. The quantities of particulate matter emitted from biodiesel engine are approximately a half of diesel engine's particulate matter. Morphology of CI engine's PM10, PM2.5, ultrafine particle and nanoparticle was characterized using SEM and TEM successfully. The morphology of biodiesel and conventional diesel doesn't have much different in the viewpoint of particulate matter trapping using DPF micro surface pores.

REFERENCES

1. J. B. Heywood, Internal Combustion Engine Fundamental, *McGraw-Hill series in mechanical engineering*, Singapore, (1998).

2. L. Zhu, C. Cheung, W. Zhang, and Z. Huang, Combustion, performance and emission characteristics of a DI diesel engine fueled with ethanol–biodiesel blends. *Fuel*, 90 (5), 1743-1750, (2011).

3. A. S. Ramadhas, S. Jayaraj and C. Muraleedharan, Use of vegetable oils as I.C. engine fuels – a review. *Renew Energy*, 29, 727–42, (2004).

4. M. S. Graboski and R. L. McCormick, Combustion of fat and vegetable oil derived fuels in diesel engines. *Prog Energy Combust Sci*, 24, 125–64, (1998).

5. M.M. Hasan and M.M. Rahman, Performance and emission characteristics of biodiesel–diesel blend and environmental and economic impacts of biodiesel production, *Renewable and Sustainable Energy Reviews*,74, 938–948, (2017).

6. M. Aldhaidhawi, R. Chiriac and V. Badescu, Ignition delay, combustion and emission characteristics of Diesel engine fueled with rapeseed biodiesel. *Renewable and Sustainable Energy Reviews,* 73, 178-186, (2017).

7. G.K. Prashant, D.B. Lata and P.C. Joshi, Investigations on the effect of ethanol blend on the combustion parameters of dual fuel diesel engine, *Applied Thermal Engineering*. 96, 623–631, (2016).

8. G. Sakthivel and N. Saravanan and M. Ilangkumaran, Influence of injection timing on performance, emission and combustion characteristics of a DI diesel engine running on fish oil biodiesel, *Energy*, 116, 1218-1229, (2016).

9. G. Gonca and E. Dobrucali, Theoretical and experimental study on the performance of a diesel engine fueled with diesel-biodiesel blends, *Renewable Energy*, 93, 658-666, (2016).

10. P. Karin, H. Oki, K. Hanamura and C. Charoenphonphanich, Nanostructures and Oxidation Kinetics of Diesel Particulate Matters, *Journal of Research and Applications in Mechanical Engineering*, 1(2), 3-8, (2012).

11. P. Karin, M. Borhanipour, Y. Songsaengchan, S. Laosuwan, C. Charoenphonphanich, N. Chollacoop and K. Hanamura, Oxidation kinetics of small CI engine's biodiesel particulate matter. *International Journal of Automotive Technology*, 16(2), 211-219, 2015.

12. P. Karin, J. Boonsakda, K. Siricholathum, E. Saenkhumvong, C. Charoenphonphanich and K. Hanamura, Morphology and oxidation kinetics of CI engine's biodiesel particulate matters on cordierite Diesel Particulate Filters using TGA. *International Journal of Automotive Technology*, 18(1), 31-40, (2017).

13. T. Ishiguro, Y. Takatori and K. Akihama, Microstructure of diesel soot particles probed by electron microscopy: First observation of inner core and outer shell. *Combustion and Flame* 108(1), 231−234, (1997).

14. R. L. Vander Wal, A. Yezerets, N. W. Currier, D. H. Kim and C. H. Wang, HRTEM study of diesel soot collected from diesel particulate filters, *Carbon,* 45(1), 70−77, (2007).

15. D. B. Kittelson, Engines and nanoparticles: A review. *J. Aerosol Science*, 29(5-6), 575−588, (1998).

ACKNOWLEDGMENTS

The authors gratefully acknowledge the support from Bangchak Corporation Public Co., Ltd., FOCUSLAB Ltd., Thailand Research Fund (TRF), KMITL and NSTDA.

PUBLICATION ICAE 2018

The 14th International Conference on Automotive Engineering
April 2-3, 2018,
Challenger, Impact, Muang Thong Thani, Bangkok, Thailand

TSAE-18IC-0101

Effect of Hydrotreated Vegetable Oil on Particle Emission Characteristics using Rapid Compression Expansion Machine and Electron Microscopy

Sippakorn Rungsritanapaisan[1*], Pop-Paul Ewphun[2], Preechar Karin[1], Susumu Sato[2], Hidenori Kosaka[2], and Nuwong Chollacoop[3]

1International College, King Mongkut's Institute of Technology Ladkrabang, Bangkok 10520, Thailand
2Department of Systems and Control Engineering, Tokyo Institute of Technology, Tokyo 179-0085, Japan
3 National Science and Technology Development Agency Pathum Thani 12120, Thailand

* E-mail: boom.e46@gmail.com

Abstract. This research investigates the effects of Hydrotreated vegetable oil-diesel blend to combustion characteristics under low temperature. Combustion characteristics were investigated using heat release rate analysis, two color method and soot concentration measurement. The experiments were carried out on a rapid compression expansion machine to simulate the ambient condition of a Compression ignition (CI) engines at Top dead center (TDC). With different ambient density and pressure at Bottom dead center (BDC) were used to simulate as different pressure condition in actual engine. A single hole injector was used with different fuels conventional commercial diesel and Hydrotreated vegetable oil (HVO). Particle emission were investigated by using scanning eletron microscope and investigated by image processing. The results showed that HVO has lower peak heat release rate curve compared to diesel in all test conditions due to a higher cetane number making ignition delay shorter. Soot concentration HVO was lower than diesel in all test conditions. This lead to a reduction in the unburned fractions.

1. Introduction

Currently, the world is faced with fossil fuel depletion and numerous environmental problems. Many researchers are trying to develop new, clean energy sources for vehicles such as electricity, fuel cell, etc. Unfortunately, it is difficult to replace conventional vehicles due to cost, energy sources, distance between refueling and vehicle performance. Internal combustion and hybrid engines will likely play a role in powering light-duty vehicles at least until 2050 [1].

Compression ignition (CI) engines provide higher thermal efficiency compared to other internal combustion engines. However, large amounts of NO_x and soot are produced during combustion.

Soot and NO_x emission can be reduced by using Hydrotreated vegetable oil (HVO) without the need of engine and control modification [2].

HVO is a second-generation biofuel that produce from vegetable oil by using hydrotreating process to remove oxygen from structure. HVO can be a candidate to replace diesel. It can be produced from various many kind of vegetable oil without compromising fuel quality, difference form FAME (fattycid

methyl ester) that can produce from limit feedstocks HVO has a similar viscosity, density and heating value as diesel [3]. The high cetane number of HVO decreases HC emissions and fuel consumption by increasing the advanced heat release rate and shortening ignition delay [4]. Other advantages of using HVO include advanced combustion phase, shortened combustion duration, and improved thermal efficiency [5].

2. Method

2.1. Heat Release Analysis

Heat release rate was calculated from pressure rise after fuel injection by theory of the first law of thermodynamics [6], as shown in Equation (1).

$$\frac{dQ}{dt} = \frac{\gamma}{\gamma - 1} \cdot P \cdot \frac{dV}{dt} + \frac{1}{\gamma - 1} \cdot V \cdot \frac{dP}{dt} \tag{1}$$

Where γ is ratio of specific heat, dV/dt is chamber volume change with time, dP/dt is in-chamber pressure change with time, P is in-chamber pressure, V is chamber volume.

2.2. Flame Temperatures

Flame temperatures were measured by the two colors method based on thermal radiation of soot particle in two different wave lengths [7]. Monochromatic radiation from non-black body, Base on Equation (2).

$$KL = -\lambda^a \ln\left[1 - exp\left\{\frac{C_2}{\lambda}\left(\frac{1}{T_a} - \frac{1}{T}\right)\right\}\right] \tag{2}$$

Before the two colors method can be applied to measure flame temperature, it is necessary to calibrate high speed camera for flame brightness measurement. Black body furnace and pyrometer are used to accurately determine the reference temperature. Distance between black body furnace and high-speed camera was set same as measurement distance used in the experiment. The visible light can be converted by CCD detector in the high-speed camera into three colors bands, red, green and blue. Any two of the three colors bands can be used for the calculation of temperature and KL factor. Two wavelengths that used in this experiment are blue (501 nm) and red (612 nm). Then flame temperature can be calculated by using MATLAB base on Equation (2).

3. Experimental Setup and Procedures

3.1. Experimental Setup

Experiments were done on a rapid compression expansion machine (RCEM) [8], shown in Figure 1. The RCEM combustion chamber has 86.0 mm bore with a 151.5 mm stroke. Ambient pressure was arrived at by mixing O and N in a mixing tank at 453 K, then filling synthetic gas into the combustion chamber until the setting pressure. It was then compressed by piston from BDC to TDC within 30 ms and kept at TDC for 150 ms to provide a constant volume condition. A single hole 0.2 mm diameter exit orifice was equipped with solenoid injector to inject test fuel with 100 MPa into the combustion chamber. A static pressure transducer was installed to measure ambient pressure at BDC. Pressure increase from combustion was measured by a piezoelectric dynamic pressure tranducer (Kistler 6125C01) and amplified by charge amplifier (Kistler 5011B). The pressure increase from the injected fuel was recorded by oscilloscope (YOKOGAWADL750) with a sampling rate of 1×10 sampling/sec. The flame image was captured by high speed camera (NAC GX-1) with lens (Nikkor 55 mm f/2.8) at 10,000 fps and 464 × 464 pixels. Soot concentration was measured by passing exhaust gas from

combustion to filter paper in order to collect soot emissions. It was then measured by smoke meter (SOKKEN GSM-3).

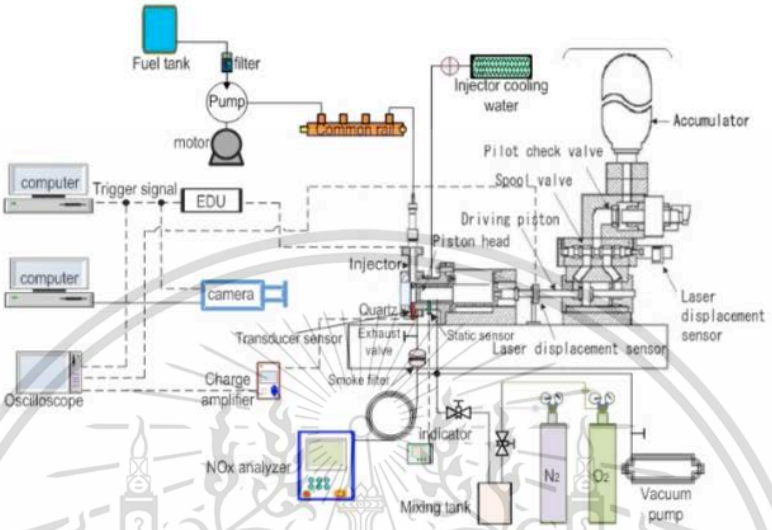

Figure. 1 Rapid compression expansion machine (RCEM).

3.2. Experimental Condition

Table 1. Experimental condition.

	Conditions
Test fuel	Diesel, HVO
Nozzle orifice diameter	Single hole 0.2mm
Energizing time	2.0 ms
Injection pressure	100 MPa
Ambient gas temperature	700 K
Oxygen concentration	21%
Ambient density	16 kg/m^3
Repeat	5 Times / Condition

Table 1 shows test conditions in this experiment. The experiment was conducted using two different fuels commercial HVO and conventional diesel. Other conditions were a nozzle exit orifice diameter of 0.2 mm solenoid injector 2.0 ms energizing time to reduce the effect of transient opening and closing 100 MPa injection pressure to avoid cavitation and vary ambient density were used to simulate the effect of supercharge under naturally aspirated conditions. For ambient temperature of 700 kelvin the effect was investigated of low temperature concentrations at ambient pressure under a constant equivalent ratio. All tests were repeated 5 times for each test condition.

3.3. Test Fuel

Table 2. Fuels properties

Properties	Standard	Diesel	HVO
Density @ 30°C (g/cm3)	ASTM D4052	0.824	0.778
Kinematic viscosity @40°C (mm2/s)	ASTM D445	3.24	2.64
Heating value (MJ/Kg)	ASTM D240	45.86	46.86
Surface tension (mN/m)	ASTM D1590	26.38	24.84
Carbon content (%)	ASTM D5291	85.73	84.24
Hydrogen content (%)	ASTM D5291	13.22	15.05
Oxygen content (%)	ASTM D5599	0.00	0.00
Distillation T10 (°C)	ASTM D86-11b	207.7	227.4
Distillation T50 (°C)	ASTM D86-11b	287.9	278.2
Distillation T90 (°C)	ASTM D86-11b	352.3	293.2
Derived cetane index	ASTM D4737	60.43	76.89

Comparison of diesel densities at 303 K to HVO showed decreases of 5.53%. Viscosity decreases at 40 C were recorded at 18.49%. Heating value increases were recorded 2.18%. Surface tension decreases were recorded at 5.84%. Distillation T10 increases were recorded at 9.49%. Distillation T50 decreases were recorded at 3.37%. Distillation T90 decreases were recorded at 16.76%. Derived cetane index increases were recorded at 27.24%. Mean increasing HVO blend percentage, density decrease, viscosity decrease, heating value increase, distillation T10 increase, distillation T50 decrease, distillation T90 decrease and derived cetane index increases as are shown in Table 2. From the physical and chemical property of HVO fuel tend to be good candidate to replace diesel.

4. Results and Discussions

In this experiment, combustion characteristics were investigated in terms of pressure, heat release rate, ignition delay, flame temperature, soot concentration and investigate morphology and nanostructures by using scanning electron microscopy (FE-SEM: Hitachi SU5000)

4.1. Pressure

From the experimental results, the pressure of Diesel and HVO are nearly identical to those of temperature 700 K. The strong pre-mixed combustion could increase the possibility of engine wear and combustion noise in CI engines, commonly referred to as diesel knocking [6]. However, pressure during the premixed combustion phase can be reduced by using HVO fuels with a shorter ignition delay and smaller pressure rise. The shorter ignition delays of 700 K. HVO fuel result in the earlier and longer mixing-controlled combustion phase as shown in figure 2.

4.2. Heat release rate

Figure 3 shows heat release rates of diesel and HVO as representative. Heat release rates are calculated from pressure rise after injected fuel by using Equation (1). In both after injection the evaporation of fuel into the hot environment causes a dramatically reduce to negative value in the heat release rates curves [6]. HVO shows a lower heat release rate curve compared to diesel in this test condition due to a higher cetane number making ignition delay shorter. HVO made more premixed combustion occurred in the chamber also had the effect of making the heat release rate more gradual. and lower peak heat release rate curve during lower ambient temperature condition compared to diesel fuel.

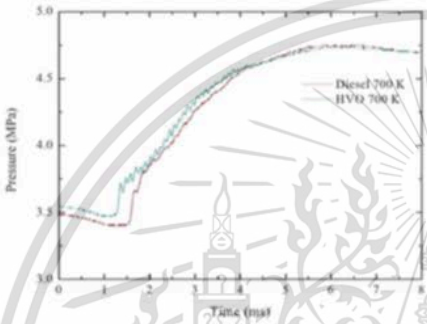

Figure. 2 Pressure of 700 K condition.

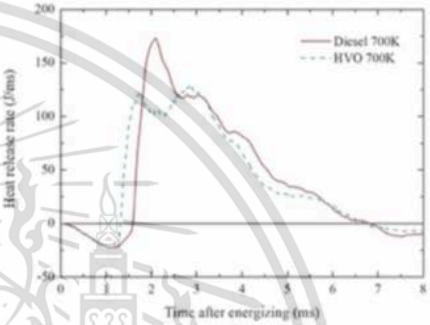

Figure. 3 Heat release rates of 700 K condition.

4.3. Flame Temperature

Figure 4 shows flame temperature image calculated by the two colors method of diesel and HVO as representative. HVO shows slightly lower flame temperature compared to diesel as show in figure 5. This is due to a higher cetane number. HVO shows slightly wider flame image This is due to a wider spray angle [9]. The lower viscosity of HVO increases turbulence at the nozzle exit making a wider spray angle [10]. Also contributing to making the flame image of HVO wider than diesel, is a lower distillation temperature which results in better vaporization and mixture formation at the flame border.

Ambient condition	Fuel	1.5 ms	2.0 ms	2.5 ms	3.5 ms	5.0 ms	7.0 ms
700 K 16 kg/m³	Diesel	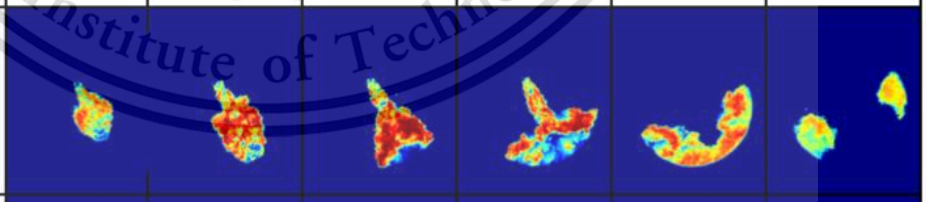					
	HVO	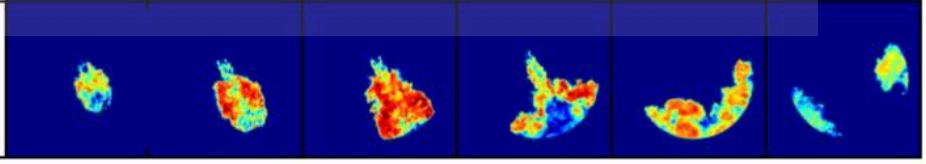					

Figure. 4 Flame Temperature Image of 700 K condition.

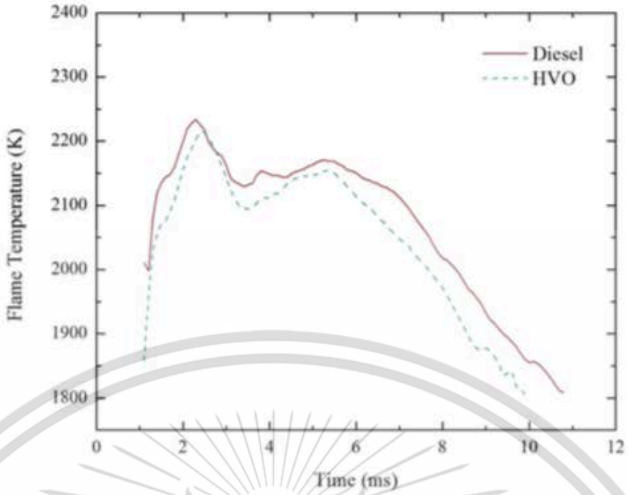

Figure. 5 Flame Temperature of 700 K condition.

4.4. Soot Morphology and Nanostructure

Morphology and nanostructure of the PM were investigated by electron microscopy. PM's types were found on the paper filters such as fine particles and ultrafine particles. Ultrafine particles of diesel and HVO particulate matter consist of many single nanoparticles. Figure 6, 7, 8 and 9 show fine particle of conventional diesel and HVO in the condition of 700 K with 16 kg/m^3 ambient density operation with 10^3 and 10^4 magnifications, respectively. Moreover, SEM image is used for numerate area of particulate matters from focused area, after post processing of two colors. From the two colors images, the area of the PM were measured by image processing program. were measured for the black area in the image to be a PM. The estimated of area of conventional diesel and HVO in 700 K condition are shown in Figure 10 and 11. The result shows that HVO fuel has lower average PM per focus area than conventional diesel fuel.

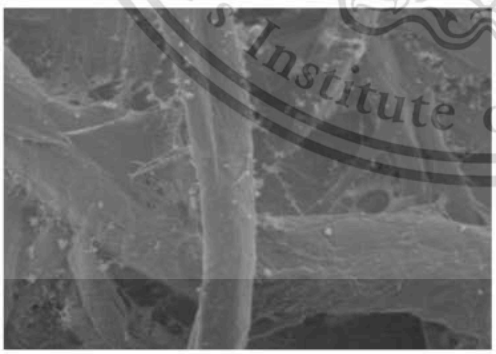

Figure. 6 SEM image of diesel pm

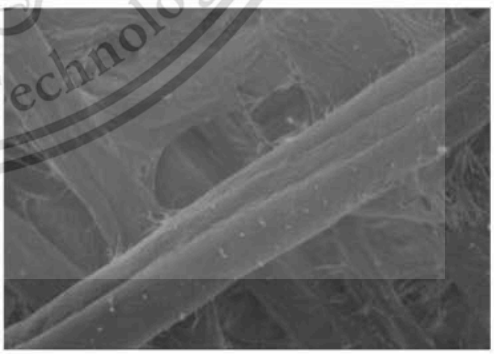

Figure. 7 SEM image of HVO pm

PUBLICATION JSAE 2018

講演番号	030

文献番号	20185030

Characterization of Hydro-treated Vegetable Oil Combustion Behavior and Particle Emission Nanostructure

Sippakorn Rungsritanapaisan [1], Pop-Paul Ewphun [2], Preechar Karin [1], Susumu Sato [2], Hidenori Kosaka [2] and Nuwong Chollacoop [3]

1) International College, King Mongkut's Institute of Technology Ladkrabang, Bangkok 10520, Thailand (E-mail: boom.e46@gmail.com)
2) Department of Systems and Control Engineering, Tokyo Institute of Technology, Tokyo 179-0085, Japan
3) National Science and Technology Development Agency Pathum Thani 12120, Thailand

ABSTRACT: This paper investigates the effects of Hydrotreated vegetable oil and diesel to combustion characteristics under low temperature and various ambient density conditions. Combustion characteristics were investigated by using heat release rate analysis, two color method and soot concentration measurement. The experiments were carried out on a rapid compression expansion machine to simulate the condition of a CI engines as compression stroke at TDC. Various temperature and ambient density at BDC were simulated as different pressure condition in actual engine. Particle emission were investigated by using scanning electron microscope and investigated by image processing. The results showed that HVO has lower peak heat release rate curve compared to diesel in all test conditions due to a higher cetane number making ignition delay shorter. Soot concentration HVO was lower than diesel in all test conditions. This lead to a reduction in the unburned fractions.

KEY WORDS: **Rapidcompression expansion machine, Hydrotreated vegetable oil, Low temperature, Particle emission**

1. INTRODUCTION

Nowadays, the shortage of energy is the one of main problem in the world. Many researchers are trying to develop new, clean energy sources for vehicles such as electricity, fuel cell, etc. However Diesel engines are considered as one of the highest thermal efficiency engines among internal combustion engines (ICE)[1]. Unfortunately disadvantage is particulate matter (PM) emission which is hazardous to human health and environment. Emission can reduce by using alternative fuel.

Biodiesel which is a first generation of biofuel can be produced by transesterification process. Biodiesel have been widely used, as it can be directly used or blending used with diesel in the engines without no modification. However it still have some disadvantages to the engines such as low heating value[2] and high density and viscosity that make larger droplet size distribution, poor fuel-air mixing processes and mixture formation[3,4]

Hydrotreated vegetable oil (HVO) is a second generation biofuel that produce from many kind of vegetable oil and have benefited in emission reduction. Using hydrotreating process its similar physical properties to diesel fuel[5]

HVO has a similar viscosity, density and heating value as diesel[6] using hydrotreating process to remove oxygen from structure. HVO can be a candidate to replace diesel. It can produced from various many kind of vegetable oil without compromising fuel quality, difference form FAME (fatty acid methyl ester) that can produce from limit feedstocks[5]. The high cetane number of HVO decreases HC emissions and fuel consumption by increasing the advanced heat release rate and shortening ignition delay[7]. Other advantages of using HVO include advanced combustion phase, shortened combustion duration, and improved thermal efficiency[8].

The objective of this paper is to study the effect of HVO under simulated low temperature conditions, specifically, observing combustion characteristics that have not been studied before.

This paper investigates the effects of HVO and diesel fuel to combustion characteristics under low temperature conditions using heat release rate analysis, two color method, soot concentration measurement and soot nanostructure analysis. A single hole injector was tested with different fuels-commercial diesel and HVO to investigate the effects of HVO on combustion characteristics. An analysis measuring heat release rate, ignition delay, heat release, flame temperature and soot concentration done. Testing was conducted on a rapid compression expansion machine (RCEM) with constant injection pressure and energizing time. Compression ratio were varied to simulate low temperature conditions. And soot nanostructure investigated by using scanning electron microscopy (SEM).

2018 JSAE Annual Congress (Spring) May 23 to 25, 2018
Issued on May 21, 2018
2018 JSAE Annual Congress Proceedings (Spring)

Diesel particulate matters consist of a solid fraction and a soluble organic fraction (SOF). Primary particles of the PMs, composed of carbon and metallic ash, are coated with SOF and sulfate. The mean diameter of primary particles is usually in the range of 20-80 nm. Agglomerated particles are an assembly of primary particles and aggregates whose total surface area does not differ appreciable from the sum of specific surface areas of primary particles. Agglomerated particle size is normally 80-300 nm[1,9].

Scanning Electron Microscope (SEM) observation of PMs have been conducted by several researchers[10]. A primary soot particle has two distinct parts; an inner core and an outer shell[11-12].

According to some recent researches about PM's quantity and morphology from biodiesel combustion, results showed that PM's quantity and average primary nanoparticle sizes have some relationships with temperature and pressure. Biodiesel's PMs emitted about half in quantity and a little smaller in primary particle size, compared with diesel's PMs[11]. As a result of diesel and HVO benefits mentioned as above, especially combustion characteristics, the aim of this research is to study effects of combustion characteristics on PM's quantity emission, morphology, and nanostructure, by using diesel and HVO fuel. The test was performed on a rapid compression expansion machine. PM quantity and morphology were investigated by an opacity smoke meter and electron microscopy for better understanding.

2. METHOD

2.1 Heat release analysis

Heat release rate was calculated from pressure rise after fuel injection by theory of the first law of thermodynamics[9], as shown in Equation (1).

$$\frac{dQ}{dt} = \frac{\gamma}{\gamma - 1} \cdot P \cdot \frac{dV}{dt} + \frac{1}{\gamma - 1} \cdot V \cdot \frac{dP}{dt} \quad (1)$$

Where γ is ratio of specific heat, dV/dt is chamber volume change with time, dP/dt is in-chamber pressure change with time, P is in-chamber pressure, V is chamber volume.

2.2 Flame temperatures

Flame temperatures were measured by the two color method based on thermal radiation of soot particle in two different wave lengths[13]. Monochromatic radiation from non-black body, base on Equation (2).

$$KL = -\lambda^{a} \ln\left[1 - exp\left\{\frac{C_2}{\lambda}\left(\frac{1}{T_a} - \frac{1}{T}\right)\right\}\right] \quad (2)$$

Before the two color method can be applied to measure flame temperature, it is necessary to calibrate high speed camera for flame brightness measurement. Black body furnace and pyrometer are used to accurately determine the reference temperature. Distance between black body furnace and high speed camera was set same as measurement distance used in the experiment. The visible light can be converted by CCD detector in the high speed camera into three color bands, red, green and blue. Any two of the three color bands can be used for the calculation of temperature and KL factor. Two wavelengths that used in this experiment are blue (501 nm) and red (612 nm). Then flame temperature can be calculated by using MATLAB base on Equation (2).

2.3 Ignition delay

The ignition delay is defined as the interval from start of injection (SOI) to the start of combustion (SOC) where heat release rate recover from the negative value due to heat absorption[9,14] as illustrated in Figure 1. Heat release is calculated by integration under the curve area of heat release rate from the start of combustion to the point at which the heat release rate decreases to a negative value.

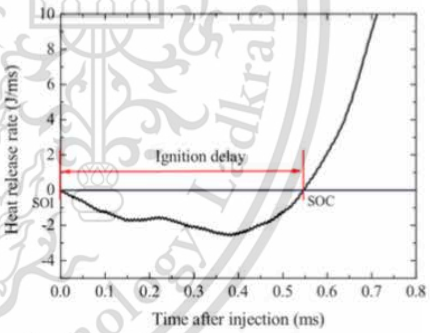

Fig. 1 The definition of the ignition delay

3. EXPERIMENTAL SETUP AND PROCEDURES

3.1 Experimental Setup

Experiments were done on a rapid compression expansion machine (RCEM)[15], shown in Figure 2. The RCEM combustion chamber has 86.0 mm bore with a 151.5 mm stroke. Ambient pressure was arrived at by mixing O and N in a mixing tank at 453 K, then filling synthetic gas into the combustion chamber until the setting pressure. It was then compressed by piston from BDC to

TDC within 30 ms and kept at TDC for 150 ms to provide a constant volume condition. A single hole 0.2 mm diameter exit orifice was equipped with solenoid injector to inject test fuel with 100 MPa into the combustion chamber. A static pressure transducer was installed to measure ambient pressure at BDC. Pressure increase from combustion was measured by a piezoelectric dynamic pressure tranducer (Kistler 6125C01) and amplified by charge amplifier (Kistler 5011B). The pressure increase from the injected fuel was recorded by oscilloscope (YOKOGAWADL750) with a sampling rate of 1×10 sampling/sec. The flame image was captured by high speed camera (NAC GX-1) with lens (Nikkor 55 mm f/2.8) at 10,000 fps and 464 × 464 pixels. Soot concentration was measured by passing exhaust gas from combustion to filter paper in order to collect soot emissions. It was then measured by smoke meter (SOKKEN GSM-3).

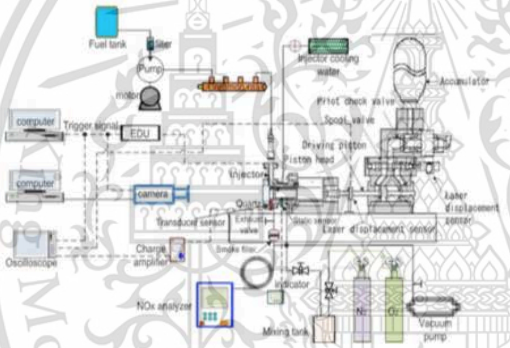

Fig. 2 Rapid compression expansion machine (RCEM)

3.2 Experimental condition

	Conditions
Test fuel	Diesel, HVO
Nozzle orifice diameter	Single hole 0.2mm
Energizing time	2.0 ms
Injection pressure	100 MPa
Ambient gas temperature	650, 700, 750 K
Oxygen concentration	21%
Ambient density	16 kg/m^3
Repeat	5 Times / Condition

Table 1. Experimental condition

Table 1 shows test conditions in this experiment. The experiment was conducted using two different fuels commercial HVO and conventional diesel. Other conditions were a nozzle exit orifice diameter of 0.2 mm solenoid injector 2.0 ms energizing time to reduce the effect of transient opening and closing 100 MPa injection pressure to avoid cavitation and vary ambient density were used to simulate the effect of supercharge under naturally aspirated conditions. For ambient temperature of 650, 700 and 750 kelvin the effect was investigated of low temperature concentrations at ambient pressure under a constant equivalent ratio. All tests were repeated 5 times for each test condition.

3.3 Test fuels

Properties	Standard	Diesel	HVO
Density @ 30°C (g/cm3)	ASTM D4052	0.824	0.778
Kinematic viscosity @40°C (mm2/s)	ASTM D445	3.24	2.64
Heating value (MJ/Kg)	ASTM D240	45.86	46.86
Surface tension (mN/m)	ASTM D1590	26.38	24.84
Carbon content (%)	ASTM D5291	85.73	84.24
Hydrogen content (%)	ASTM D5291	13.22	15.05
Oxygen content (%)	ASTM D5599	0.00	0.00
Distillation T10 (°C)	ASTM D86-11b	207.7	227.4
Distillation T50 (°C)	ASTM D86-11b	287.9	278.2
Distillation T90 (°C)	ASTM D86-11b	352.3	293.2
Derived cetane index	ASTM D4737	60.43	76.89

Table 2. Fuels properties

Comparison of diesel densities at 303 K to HVO showed decreases of 5.53%. Viscosity decreases at 40°C were recorded at 18.49%. Heating value increases were recorded 2.18%. Surface tension decreases were recorded at 5.84%. Distillation T10 increases were recorded at 9.49%. Distillation T50 decreases were recorded at 3.37%. Distillation T90 decreases were recorded at 16.76%. Derived cetane index increases were recorded at 27.24%. Mean increasing HVO blend percentage, density decrease, viscosity decrease, heating value increase, distillation T10 increase, distillation T50 decrease, distillation T90 decrease and

derived cetane index increases as are shown in Table 2. From the physical and chemical property of HVO fuel tend to be good candidate to replace diesel.

4. RESULTS AND DISCUSSIONS

In this experiment, combustion characteristics were investigated in terms of pressure, heat release rate, ignition delay, flame temperature, soot concentration and investigate morphology and nanostructures by using scanning electron microscopy (FE-SEM: Hitachi SU5000).

4.1 Pressure

From the experimental results, the pressure of Diesel and HVO are nearly identical to those of temperature 750K and 700K, while 650K shows a different results as shown in figure 3. At temperature 650K as shown in figure 3 (a) has the most rapid pressure rise because the longest ignition delay of this condition allows more time for the better fuel-air mixing leading to a strong pre-mixed combustion, the steep pressure rise and the large heat release during the premixed combustion phase then turned to premixed charge compression ignition (PCCI). The strong pre-mixed combustion could increase the possibility of engine wear and combustion noise in CI engines, commonly referred to as diesel knocking[9]. However, pressure during the premixed combustion phase can be reduced by using HVO fuels with a shorter ignition delay and smaller pressure rise. The shorter ignition delays of 750 K and 700 K of HVO fuel result in the earlier and longer mixing-controlled combustion phase as shown in figure 3 (b) and (c).

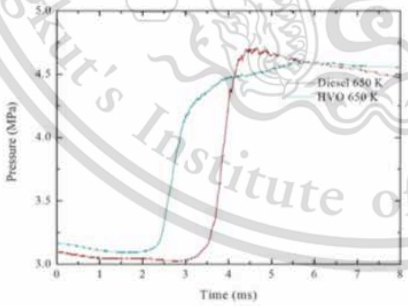

Fig. 3 (a) Pressure of 650 K condition.

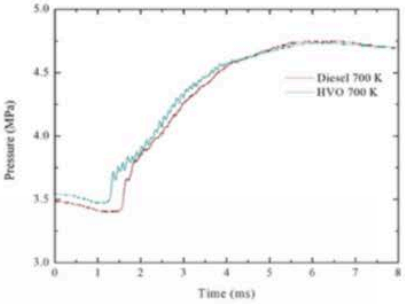

Fig. 3 (b) Pressure of 700 K condition.

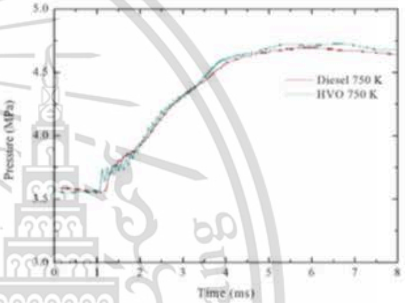

Fig. 3 (c) Pressure of 750 K condition.

4.2 Heat release rate

Figure 4 shows heat release rates of diesel and HVO as representative. Heat release rates are calculated from pressure rise after injected fuel by using Equation (1). In both after injection the evaporation of fuel into the hot environment causes a dramatically reduce to negative value in the heat release rates curves[9]. And the lowest ambient temperature 650 K condition in both fuels show effect of longer ignition delay making more premixed combustion occurred in the chamber and turned to premixed charge compression ignition (PCCI) also had the effect of making the heat release rate more higher compared to higher temperature.

Figure 4 (b) HVO shows a lower heat release rate curve compared to diesel in all test conditions due to a higher cetane number making ignition delay shorter. HVO made more premixed combustion occurred in the chamber also had the effect of making the heat release rate more gradual. and lower peak heat release rate curve during lower ambient temperature condition compared to diesel fuel.

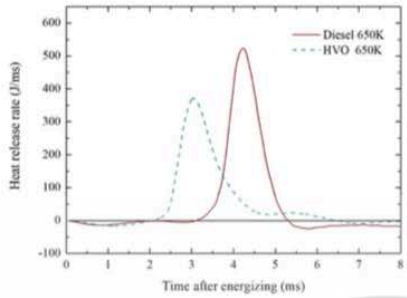

Fig. 4 (a) Heat release rate of 650 K condition.

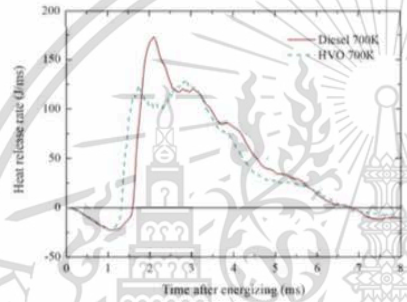

Fig. 4 (b) Heat release rate of 700 K condition.

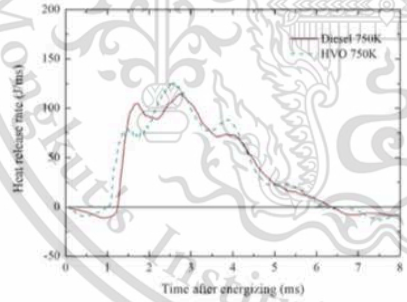

Fig. 4 (c) Heat release rate of 750 K condition.

4.3 Ignition delay

Figure 5 shows ignition delay. Ignition delay is mainly dependent on the fuel cetane number[16]. HVO shows shorter ignition delays compared to diesel at ambient density 16 kg/m^3 conditions

Figure 5 shows the effects of ambient temperature under constant ambient density on ignition delay. HVO also shows shorter ignition delays compared to diesel 20.69 % at an ambient temperature 750 K, 16.92 % at ambient temperature 700 K and 30.34 % at ambient temperature 650 K. The highest ambient temperature in both fuels show the shortest ignition delay compared to other cases. Increasing ambient temperature with constant ambient density improves mixture formation also decreases ignition delay. However, shorter ignition delay of HVO is the lower distillation temperature which make its faster evaporation with surrounding air in the chamber, and it might contribute to small droplet size distribution[14,17], which is related to a better mixture formation.

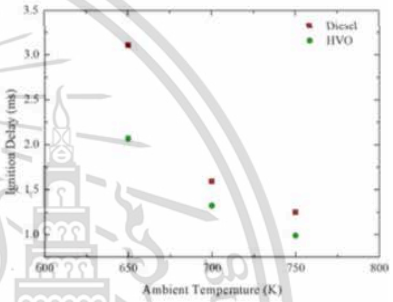

Fig. 5 Ignition delay of diesel and HVO fuel.

The conclusion in effects of HVO on the ignition delay is that decreasing in ignition delay so that combustion can be improved when compared with diesel fuel.

4.4 Flame temperature

Figure 6 shows flame temperature image calculated by the two colors method of diesel and HVO as representative. HVO shows slightly lower flame temperature compared to diesel. This is due to a higher cetane number. HVO shows slightly wider flame image This is due to a wider spray angle[18]. The lower viscosity of HVO increases turbulence at the nozzle exit making a wider spray angle[19]. Also contributing to making the flame image of HVO wider than diesel, is a lower distillation temperature which results in better vaporization and mixture formation at the flame border.

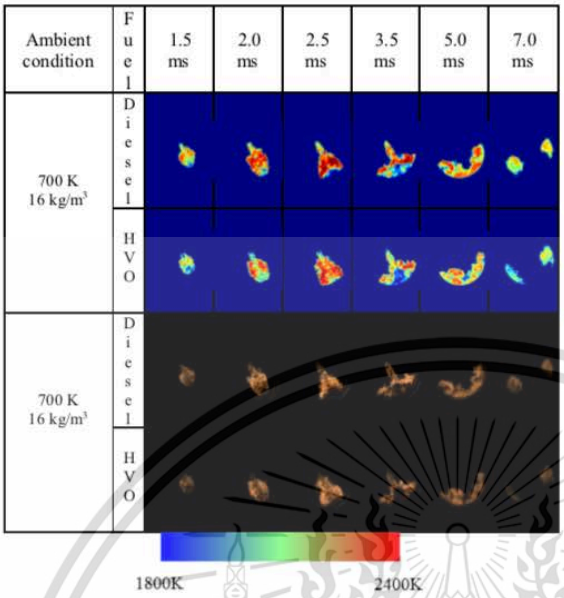

Fig. 6 Flame temperature image and Combustion image

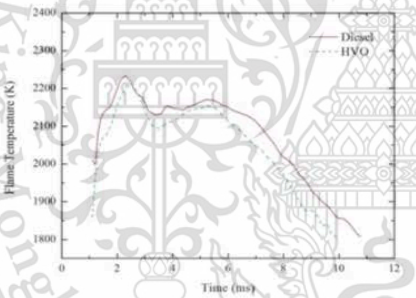

Fig. 7 Flame temperature of 700 K test condition.

4.5 Soot concentration

Figure 8 HVO shows lower soot concentration compared to diesel, with ambient condition O 21 % at ambient density 16 kg/m^3. HVO also higher the cetane number than diesel resulting in a reduction of the unburned fractions. Low distillation temperature of HVO improved fuel evaporation and mixing with surrounding gas[8].

Figure 8 shows the effects of ambient temperature under constant ambient density on soot concentrations. HVO also show lower soot concentrations compared to diesel 10.33 % at an ambient temperature 750 K, 16.32 % at ambient temperature 700 K and 27.55 % at ambient temperature 650 K. under oxygen concentrations of 21 %. Decreasing ambient temperature improves mixture formation and also longer ignition delay leading to soot reduction.

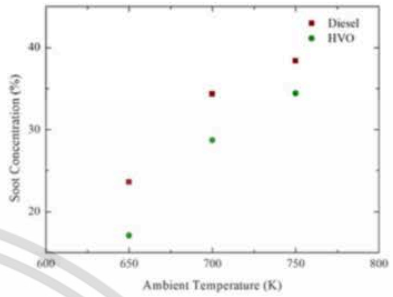

Fig. 8 Soot concentration of diesel and HVO fuel

4.6 Soot morphology and nanostructure

Morphology and nanostructure of the PM were investigated by electron microscopy. PM's types were found on the paper filters such as fine particles and ultrafine particles. Ultrafine particles of diesel and HVO particulate matter consist of many single nanoparticles. Figure 9 (a) and (c) show fine particle of conventional diesel and HVO in the condition of 700 K with 16 kg/m^3 ambient density operation, respectively.

Moreover, SEM image is used for numerate area of particulate matters from focused area, after post processing of two colors From the two colors images, the area of the PM were measured by image processing program. were measured for the black area in the image to be a PM. The estimated of area of conventional diesel and HVO in 700 K condition are shown in Figure 9 (b) and (d).

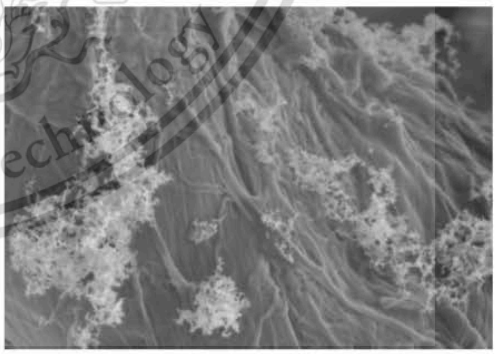

Fig. 9 (a) SEM image of conventional diesel ultrafine particle emission in 650 K condition.

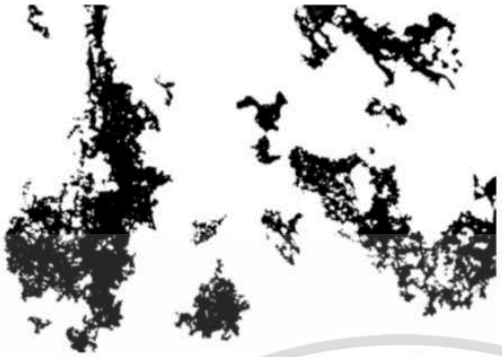

Fig. 9 (b) Two colors SEM images post process in 650 K condition of conventional diesel.

Fig. 9 (c) SEM image of HVO fuel ultrafine particle emission in 650 K condition.

Fig. 9 (d) Two colors SEM images post process in 650 K condition of HVO fuel.

The result shows that HVO fuel has lower average PM per focus area than conventional diesel fuel in all test condition as show in figure 9.

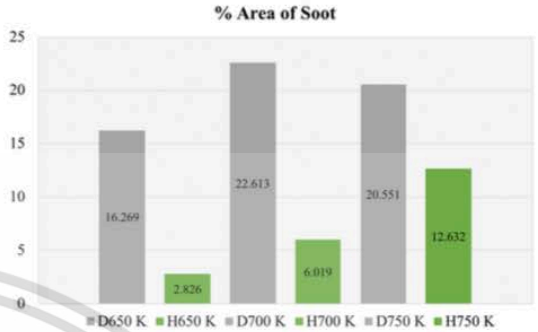

Fig. 9 Percent area of soot on focus area from SEM image.

5. CONCLUSION

The research started with a review of physical fuel properties in order to forecast combustion behavior of the conventional diesel and HVO. Then the rapid compression expansion machine (RCEM) test was conducted. Combustion analysis showed a considerable delayed combustion of the HVO fuel due to lower cetane index and more heat of evaporization. As a result of shorter ignition delay, HVO fuel have less preparation for atomization leading to longer premixed combustion also lower peak of heat release rate than diesel. Early finish in diffusion combustion phase also emphasizes the rapid combustion behavior of the HVO fuel. Combustion behaviors might effect on PM's quantity reduction. However, paper filter smoke meter is not the most accurate way to measure PM's quantity since some PM particles that covered by hydrocarbon cannot be detected by the smoke meter. PM's morphology and nanostructure were successfully investigated by SEM techniques. Amount nanostructure of agglomerated particles has significant difference among diesel and HVO fuel. These can be implied that HVO fuel has more potential in PM's oxidation reactivity.

6. ACKNOWLEDGEMENT

The authors would like to thank Thailand Advance Institute of Science and Technology, Tokyo Institute of Technology (TAIST-Tokyo Tech) and National Science and Technology Development Agency (NSTDA) and Science Technology Engineering and Mathematics (STEM) (Grant No. SAC-CO-2560-3603-TH) for providing full scholarship. Tokyo Institute of Technology, Advanced Thermo-Fluid Dynamics Laboratory (KosakaSatoLab), Bangchak Corporation, PTT Research & Technology Institute and Thailand Research Fund (TRF) for research funding, materials and facilities.

REFERENCES

(1) Preechar Karin, Hiroshi Oki, Katsunori Hanamura, Chinda Charoenphonphanich, Nanostructures and Oxidation Kinetics of Diesel Particulate Matters, The Second TSM International Conference on Mechanical Engineering, 19-21 October, 2011, Krabi

(2) Qi, D.H., Chen H., Geng L.M., and Bian, Y. ZH. (2010). Experimental studies on the combustion characteristics and performance of a direct injection engine fueled with biodiesel/diesel blends, Energy Conversion and Management, vol. 51, pp. 2985-2992.

(3) Gao, Y., Deng, J., Li, C., Dang F., Liao, Z., Wu, Z. and Li, L. (2009). Experimental study of the spray characteristics of biodiesel based on inedible oil, Biotechnology Advances, vol. 27, pp. 616-624.

(4) Mohan, B., Yang, W., Tay, K.L. and Yu, W. (2014). Experimental study of spray characteristics of biodiesel derived from waste cooking oil, Energy Conversion and Management, vol.88, pp. 622-632.

(5) Atola, H., Larmi, M., Sarjovaara, T. and Mikkonen, S. (2008). Hydrotreated vegetable oil (HVO) as a renewable diesel fuel: Trade-off between NO , particulate emission, and fuel consumption of a heavy duty engine. SAE Paper No. 2008-01-2500.

(6) Rantanen, L., Linnaila, R., Aakko, P. and Harju, T. (2005). Hydrotreated NExBTL-Biodiesel fuel of the second generation. SAE Paper No. 2005-01-3771.

(7) Sugiyama, K., Goto, I., Kitano, K., Mogi, K. and Honkanen, M. (2011). Effects of hydrotreated vegetable oil (HVO) as renewable diesel fuel on combustion and exhaust emissions in diesel engine. SAE Paper No. 2011-01-1954.

(8) Jaroonjitsathian, S., Saisirirat, P., Sivara, K., Tongroon, M. and Chollacoop, N. (2014). Effects of GTL and HVO blended fuels on combustion and exhaust emissions of a common-rail DI diesel technology. SAE Paper No. 2014-01-2763.

(9) Heywood, J. B. (1988). Internal combustion engine fundamentals. 2nd edn. McGraw-Hill. New York.

(10) Karin, P., Borhanipour, M., Songsaengchan, Y., Laosuwan, S., Charoenphonphanich, C., Chollacoop, N., & Hanamura, K. (2015). Oxidation kinetics of small CI engine's biodiesel particulate matter. International Journal of Automotive Technology, 16(2), 211-219. doi:10.1007/s12239-015-0023-4

(11) Karin, P., Boonsakda, J., Siricholathum, K., Saenkhumvong, E., Charoenphonphanich, C., & Hanamura, K. (2016). Morphology and oxidation kinetics of CI engine's biodiesel particulate matters on cordierite Diesel Particulate Filters using TGA. International Journal of Automotive Technology, 18(1), 31-40. doi:10.1007/s12239-017-0003-y

(12) Ishiguro, T., Takatori, Y. and Akihama, K. (1997). Microstructure of diesel soot particles probed by electron microscopy: First observation of inner core and outer shell. Combustion and Flame 108, 1, 231–234.

(13) Matsui, Y., Kamimoto, T. and Matsuoka, S. (1979). A study on the time and space resolved measurement of flame temperature and soot concentration in a D. I. diesel engine by the two-color method. SAE Paper No. 790491.

(14) Oo C.W., Shioji, M., Nakao, S., Dung, N.N., Reksowardojo, I., Roces, S.A. and Dugos, N.P. (2015). Ignition and combustion characteristics of various biodiesel fuels (BDFs), Fuel, vol. 158, pp. 279-287.

(15) Kobori, S. and Kamimoto, T. (1995). Development of a rapid compression-expansion machine simulating diesel combustion. SAE Paper No. 952514.

(16) Jung, S., Ishida, M., Yamamoto, S. and Sukaguchi, D. (2010). Enhancement of NO -PM trade-off in a diesel engine adopting bio-ethanol and EGR. Int. J. Automotive Technology 11, 5, 611–615.

(17) Nguyen, D.N., Ishida, H., and Shioji, M. (2010). Ignition and Combustion Characteristics of Gas-to-Liquid Fuels for Different Ambient Pressures.

(18) Hulkkonen, T., Hillamo, H., Sarjovaara, T., and Larmi, M. (2011). Experimental study of spray characteristics between hydrotreated vegetable oil (HVO) and crude oil based EN 590 diesel fuel. SAE Paper No. 2011-24-0042.

(19) Dernotte, J., Hespel, C., Houille, C., Foucher, F., and Mounaim-Rousselle, C., (2012) Influence of fuel properties on the diesel injection process in nonvaporizing conditions. Atomization and Spray. 22, 6, 461–492.

AUTHOR BIOGRAPHY

Author:	Mr. Sippakorn Rungsritanapaisan
Degree:	Master of Engineering
Date of Graduation:	15th August 2018
Date of Birth:	21st June 1990
Place of Birth:	Bangkok, Thailand

Undergraduate and Graduate Education:

Master of Engineering in Automotive Engineering,
King Mongkut's Institute of Technology Ladkrabang, Bangkok, 2018

Bachelor degree in Mechanical Engineering,
Chulalongkorn University, Bangkok, 2012

Major: Automotive Engineering

Presentations and Publications:

[1] Sippakorn Rungsritanapaisan, Pop-paul ewphun, Preechar Karin, and Hidenori Kosaka "Effect of Hydrotreated Vegetable Oil on Particle Emission Characteristics using Rapid Compression Expansion Machine and Electron Microscopy", 2018, The 14th ICAE International Conference on Automotive Engineering, April 2-3, 2018, Challenger, Impact Muang Thong Thani, Bangkok, Thailand.

[2] Sippakorn Rungsritanapaisan, Pop-paul ewphun, Preechar Karin, Susumu Sato and Hidenori Kosaka, "Characterization of Hydro-treated Vegetable Oil Combustion Behavior and Particle Emission Nanostructure", Technical Paper, 2018 JSAE Annual Spring Congress, 23-25 May 2018, Yokohama, Japan.